Paper-based Nucleic Acid Amplification Testing at the Point-of-Care for HIV Viral Load Monitoring

Benjamin P. Sullivan

A dissertation
submitted in partial fulfillment of the
requirements for the degree of

Doctor of Philosophy

University of Washington

2022

Reading Committee:

Jonathan D. Posner, Chair

Paul K. Drain

Nathan J. Sniadecki

Program Authorized to Offer Degree

Mechanical Engineering

University of Washington

Abstract

Paper-based Nucleic Acid Amplification Testing at the Point-of-Care for HIV Viral Load Monitoring

Benjamin P. Sullivan

Chair of Supervisory Committee:
Jonathan D. Posner
Department of Mechanical Engineering

Major advancements have been made in the past forty years to combat the HIV pandemic. Viral load testing, a type of nucleic acid amplification test (NAAT), is a crucial tool in early detection, monitoring antiretroviral therapy efficacy, and maintaining viral suppression. However, there is a significant lack in access to routine viral load testing, particularly in low- and middle-income countries where the burden of disease is often the highest. Current platforms are prohibitively expensive and require trained technicians, stable electricity, and established cold-chain logistics. These requirements limit traditional NAAT platforms to centralized laboratories, reducing access and delaying linkage to appropriate care. There is an urgent need to develop point-of-care (POC) NAAT devices for disseminated HIV viral load testing. In this dissertation, I describe novel technologies and advancements in various areas of the NAAT workflow for point-of-care implementation: sample preparation, amplification, and detection. While this work is focused primarily on HIV, many of the same processes can be applied to other bloodborne viruses, such as Hepatitis B, Hepatitis C, Zika virus, Ebola virus, or malaria.

I first describe a paper-and-plastic device that leverages isotachophoresis (ITP) for the electrokinetic extraction and purification of target DNA from a whole blood sample with minimal user steps. The device integrates on-chip high efficiency blood fractionation, proteolytic digestion of plasma proteins, and isotachophoretic extraction of nucleic acids with off-chip recombinase polymerase amplification (RPA). I detail steps towards modifying this device for extraction of viral HIV RNA. This requires the development and integration of lyophilized RNase inactivation chemistries onto paper membranes. I then discuss a novel method for the quantification of RPA reactions on paper membranes for point-of-care settings using amplification nucleation site analysis and show that this method can more accurately quantify extracted viral HIV RNA across subtypes compared to traditional tube-based reactions. The work presented in this dissertation describes advancements towards paper-based point-of-care platforms for low-cost disseminated viral load testing (and NAAT testing as a whole) with minimal user steps and cost.

Acknowledgements

While this dissertation reflects the work that I've completed during my doctoral training, this document also represents the countless people who have supported me throughout this process. Completing a PhD is a multi-year process of highs and lows; alternating between the elation of seeing manuscripts published, the depths of experiments inexplicably failing, and the joy after a fortuitous stroke of inspiration. As often is with life, it is the people that surround and see you through those various seasons that truly make experiences memorable and worthwhile. To my committee and lab mates, and everyone else who has taken part in my experience: thank you.

Dedication

To my wife, Nikki, who has been my biggest source of inspiration and encouragement.

Thank you for your unwavering patience, compassion, and love.

None of this would have come to be if not for you.

Table of Contents

List of Figures

List of Tables

List of Abbreviations

AIDS	Acquired Immunodeficiency Syndrome
ART	Antiretroviral Therapy
ddPCR	Digital Droplet Polymerase Chain Reaction
DNA	Deoxyribonucleic Acid
EOF	Electro-Osmotic Flow
dsDNA	Double Stranded Deoxyribonucleic Acid
DTT	Dithiothreitol
HDA	Helicase Dependent Amplification
HBV	Hepatitis B
HCl	Hydrochloric Acid
HCV	Hepatitis C
HIV	Human Immunodeficiency Virus
ITP	Isotachophoresis
LAMP	Loop-mediated Isothermal Amplification
LE	Leading Electrolyte
LoD	Limit of Detection
NA	Nucleic Acid(s)
NAAT	Nucleic Acid Amplification Test
PCR	Polymerase Chain Reaction
PEG	Polyethylene Glycol
PLHIV	People Living with HIV
POC	Point-of-Care
PVP	Polyvinylpyrrolidone
qPCR	Quantitative Polymerase Chain Reaction
RDT	Rapid Diagnostic Test
RNA	Ribonucleic Acid
RPA	Recombinase Polymerase Amplification
RT-PCR	Reverse Transcriptase Polymerase Chain Reaction
RT-RPA	Reverse Transcriptase Recombinase Polymerase Amplification
SDS	Sodium Dodecyl Sulfate
ssDNA	Single Stranded Deoxyribonucleic Acid
TE	Trailing Electrolyte
TPP	Target Product Profile

Chapter 1: Introduction

1.1 The HIV Pandemic

Since the first reports of acquired immunodeficiency syndrome (AIDS) caused by the human immunodeficiency virus (HIV) in 1981,[1] nearly 80 million individuals have been infected with HIV while over 36 million people have died as a result of AIDS-related illnesses.[2] Though major advancements in treatment and prevention have been developed in the past 40 years, the World Health Organization (WHO) estimates that at the end of 2020, there were 37.7 million people living with HIV (PLHIV) globally and 680,000 annual HIV-related deaths.[3] The majority of these individuals live in low- and middle-income countries, with Sub-Saharan Africa accounting for nearly 70% of global incidence.[4]

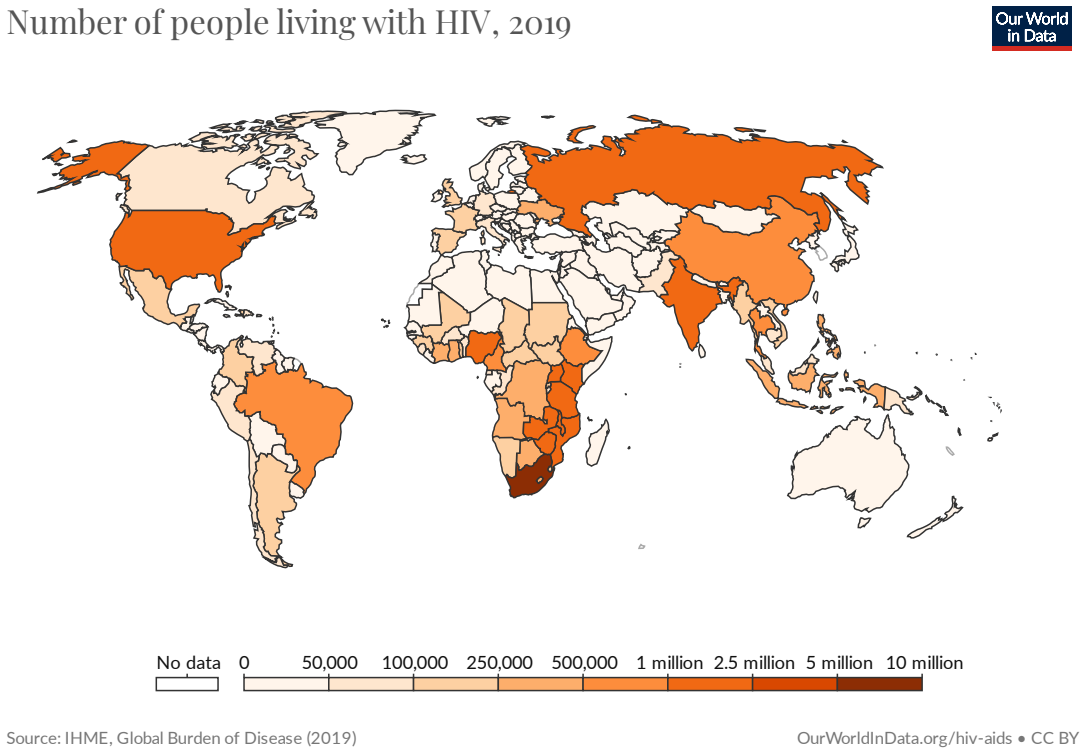

Figure 1-1: Number of people living with HIV by country.[5] The majority of people living with HIV are located in low- and middle-income countries, such as India and Sub-Saharan Africa.

HIV is classified as a bloodborne virus. though can also be transmitted via other bodily fluids, such as semen, vaginal fluids, and breast milk[6] It is an enveloped, single-stranded RNA virus, with a 9,749 base genome coding for 9 distinct viral proteins.[7] HIV preferentially targets and infects $CD4^+$ T-cells, eventually depleting an individual's white blood cell count and the reducing the immune system's ability to combat opportunistic infections.[8] Once the virus invades a $CD4^+$ T-cell, it reverse transcribes its RNA genome into proviral DNA through viral reverse transcriptase enzymes, and integrates the resulting DNA into the genome of the host cell, catalyzed by viral integrase enzymes.[9] The host cell then produces viral components from this proviral DNA, à la the central dogma of biology, budding new virions until eventual cell death.[10] The infection timeline of HIV is comparatively long, with serious symptoms often not presenting for years after initial infection, though individuals can still transmit the virus during this time frame.[11] As the reverse transcription step is comparatively error-prone, HIV is genetically diverse and has diverged into multiple groups and subtypes with differing genomes, shown in Figure 1-2. Group M (Major) represents the vast majority of global infections, and is further divided into nine different subtypes (A-D, F-H, J, and K).[12] The prevalence of each subtype is highly correlated to geography; Subtype B is dominant in North America and Europe, whereas subtype C is most prevalent in South Africa.[13] Groups O (Outlier) and N (non-M, non-O) are largely related to small geographic regions in central Africa.[14]

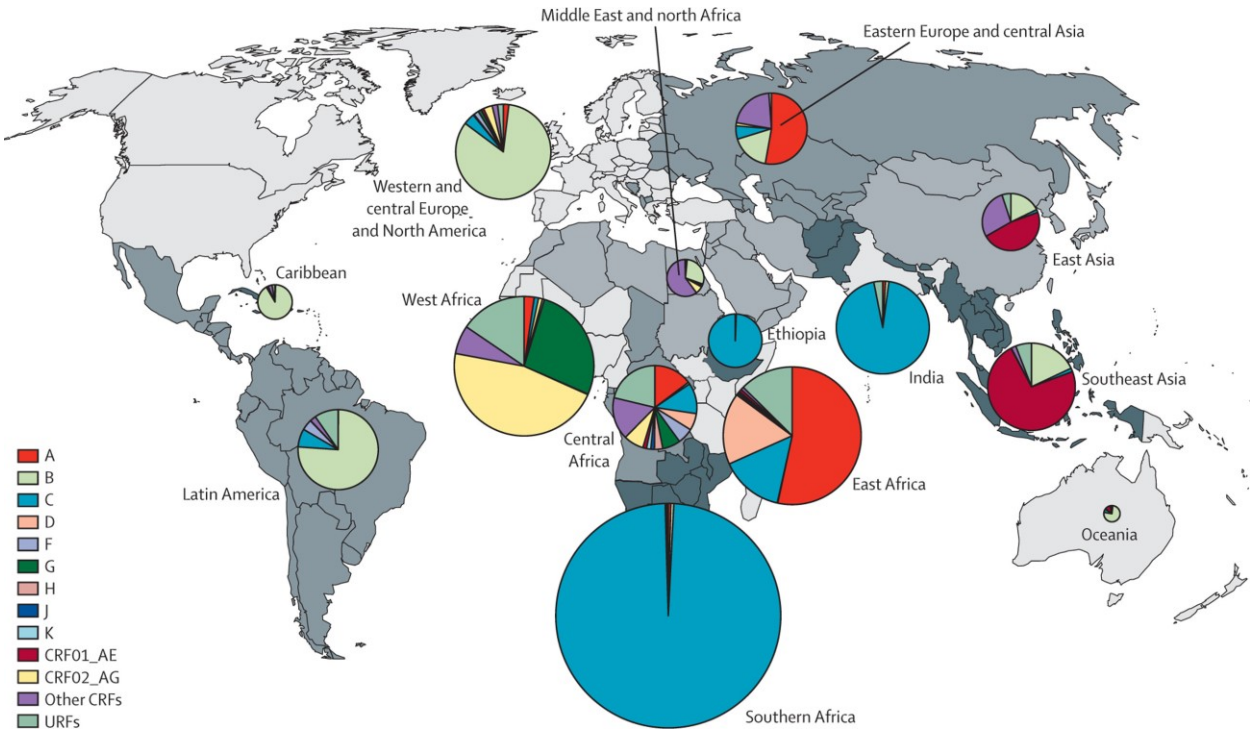

Figure 1-2: Global distributions of HIV subtypes.[15] While subtype C is most prevalent worldwide, specific regions are dominated by different subtypes. Reprinted from The Lancet, Vol. 19, Hemelaar et al., Global and regional molecular epidemiology of HIV-1, 1990-2015: a systematic review, global survey, and trend. Pages 143-155, Copyright 2019, with permission from Elsevier

One of the largest advancements in combating and controlling the HIV pandemic has been the development of antiretroviral therapies (ART). Antiretroviral therapies are drug regimens that inhibit the virus' ability to replicate within host cells by interfering with various steps and components of the replication process, suppressing viral infection. Examples of ART regimens include nucleotide reverse transcriptase inhibitors (e.g. tenofovir formulations), integrase inhibitors (e.g. bictegravir), and protease inhibitors (e.g. darunavir).[16–18] As of 2020, 27.5 million people living with HIV are receiving ART regimens.[19] As viral suppression is achieved, HIV-related mortality decreases[20] while sexual transmission risk is nearly eliminated.[21] Additionally, ART can be taken prophylactically by at-risk individuals, known as PrEP, significantly reducing the likelihood of contracting the virus.[22,23] However, the suppressive effects of ART can lapse due to lack of regimen adherence or antiretroviral resistance development.[23,24] In 2014,

the Joint United Nations Programme on HIV/AIDS (UNAIDS) developed the 90-90-90 targets as a global goal to address the HIV pandemic. These targets stated that by 2020: (1) 90% of PLHIV should know their status, (2) 90% of PLHIV who know their status should be receiving ART, and (3) of those receiving ART, 90% should be virally suppressed.[25] As of 2020, 81% of PLHIV knew their status, 79% of PLHIV who knew their status were on ART, and 92% of people on treatment were virally suppressed.[19] While these numbers represent significant achievement over the past several decades, only 59% of PLHIV were virally suppressed in 2020. More recent 95-95-95 targets state that by 2025, 95% of PLHIV should know their status, 95% of PLHIV who know their status should be receiving ART, and that 95% of those receiving ART should be virally suppressed. These recent targets also include goals of reducing societal and legal barriers to HIV care and prevention, specifically targeting the elimination of punitive laws, practices, and stigma that can hamper linking PLHIV with appropriate care and counseling.[26] Several countries have met or exceeded the 90-90-90 benchmarks, including Botswana and Eswatini (which has also met the 95-95-95 targets) in sub-Saharan Africa.[26] Bringing other countries and regions on track to meet the ambitious 95-95-95 targets by 2025 will take significant investments in novel research, development, and implementation strategies.

1.2 HIV Viral Load Monitoring

A crucial tool in controlling the HIV pandemic is routine viral load monitoring, which measures the concentration of HIV virus in a sample of plasma from whole blood. An individual's viral load is indicative of disease progression and ART efficacy, with individuals considered to be virally suppressed if they have a viral load of less than 1,000 copies of viral HIV RNA per mL of plasma. Those with a viral load of greater than 1,000 cps/mL are considered to be in viral rebound and are typically recommended for adherence counseling or second-line ART regimens.[27] It is suggested that individuals on ART receive a viral load test once every 3-12 months to assess disease status and treatment efficacy.[28] For PLHIV with undetectable viral load, transmission is virtually nonexistent, as publicized by the recent "Undetectable =

Untransmittable" campaign.[29] Viral load testing is also the most sensitive method for initial diagnosis of HIV infection and is able to detect HIV RNA as soon as 10 days after initial exposure. Other methods, such as antigen- and antibody-based diagnostics cannot detect infection for another 10 – 14 days (i.e. 20 – 24 days after initial exposure).[30–32] Despite its advantages, viral load testing is comparably expensive and is often limited to centralized laboratories due to the infrastructure, device, and training requirements to perform viral load testing.[33] Consequently, only 60% of PLHIV have regular access to viral load testing, with over 50 million viral load tests estimated to be required annually to meet the 90-90-90 targets.[34]

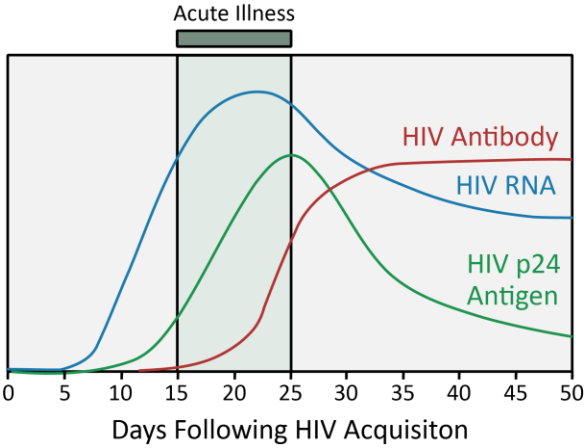

Figure 1-3: Relative levels of HIV RNA, p24 antigen, and HIV antibody after infection.[35] HIV RNA is the earliest detectable sign of HIV infection by 10+ days, followed by HIV p24 antigen, and HIV antibodies.

1.3 Nucleic Acid Amplification Tests (NAATs)

Viral load testing belongs to a larger family of assays known as nucleic acid amplification tests (NAATs). These assays target pathogenic nucleic acids (either RNA or DNA) and have become the gold standard for the diagnosis for many infectious diseases due to their unparalleled sensitivity and specificity.[36] The majority of NAATs are performed in centralized laboratories due to requirements of cold chain storage, sensitive instrumentation, reliable electrical power, proficient laboratory staff, and appropriate infrastructure (e.g. temperature and humidity controlled buildings) to host the required equipment. These

requirements limit wide-spread dissemination of NAAT testing, and further complicate pre- and post-test processes, such as specimen collection and transportation or return of results.[37] These requirements and the obstacles they pose are exacerbated in low- and middle-income countries, where a significant portion of disease burden lies.[38,39]

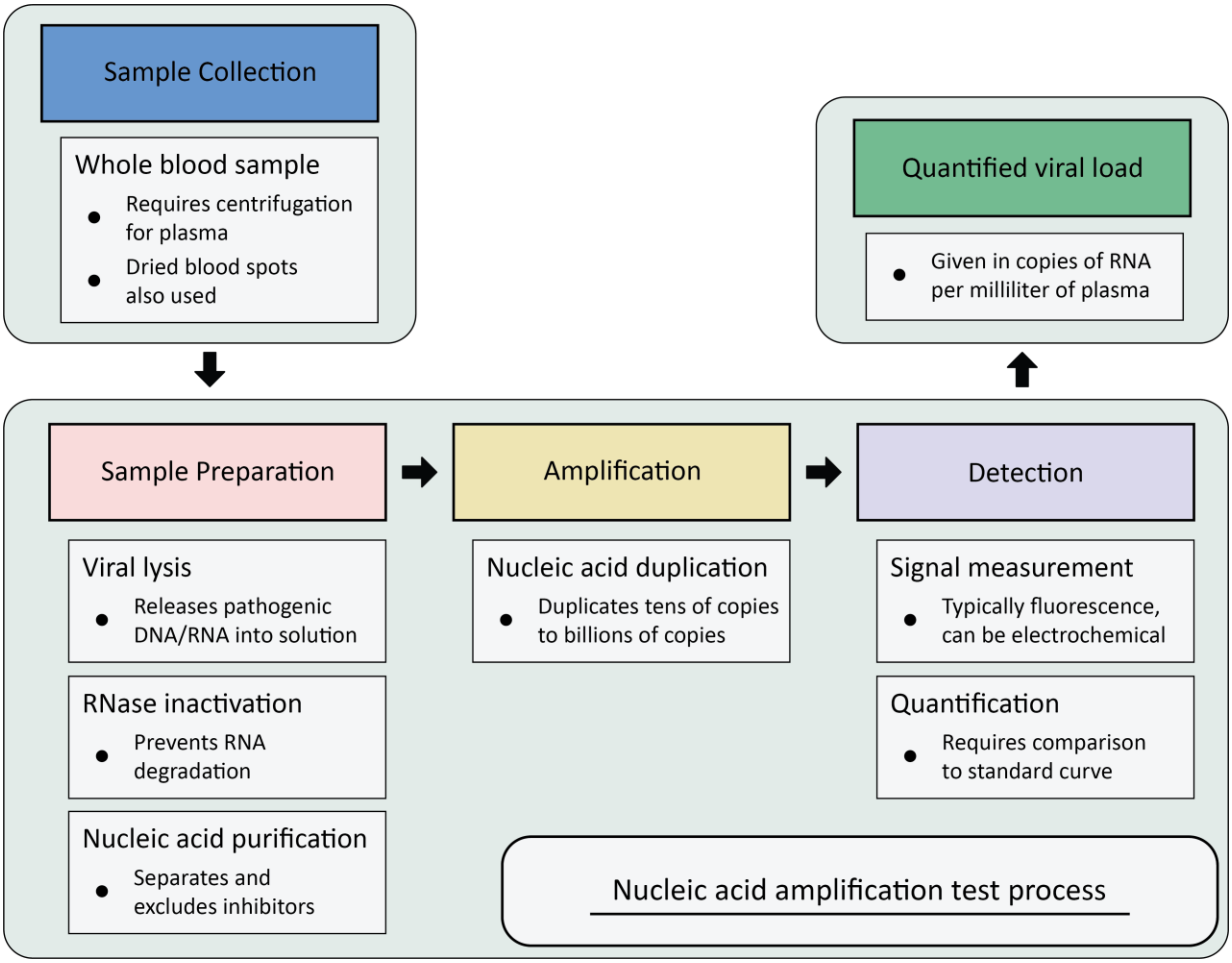

Figure 1-4: Viral load testing workflow. A whole blood sample is collected and then centrifuged to produce plasma. The plasma then is processed via sample preparation, in which viruses are lysed, endogenous RNases are inactivated, and nucleic acids are purified and separated from inhibitors present. The nucleic acids are then amplified and detected, with the output signal of the amplification assay (usually a fluorescent signal) used to quantify the input copy number relative to a known standard curve. This produces a quantified viral load measurement, guiding clinical decisions. Specific (e.g. lysis methods, amplification techniques, etc.) may vary for sample type and clinical needs.

The NAAT procedure is typically separated into three main steps: sample preparation, amplification, and detection. Sample preparation processes a raw biospecimen (e.g., blood, urine, saliva) to lyse pathogens and purify nucleic acids from inhibitors and other cellular debris present that would interfere with downstream processes. Amplification exponentially duplicates molecules of nucleic acids to billions of times their original concentrations through enzymatic reactions, which enables subsequent detection of these amplicons through a variety of means (e.g. fluorescence measurements, electrochemical detection, etc.)

In the context of viral load monitoring, the first step is typically the centrifugation or fractionation of a whole blood sample to produce plasma, excluding sources of proviral DNA (i.e. white blood cells). During sample preparation, the viral envelope and capsid of the virus is lysed, releasing genomic nucleic acids into solution. This can be accomplished through a number of methods, including chemical, mechanical, thermal, or enzymatic strategies.[40–42] Once in solution, nucleic acid purification is most often performed via solid phase extraction (SPE), which leverages silica columns, beads, or membranes to preferentially bind and release nucleic acids (e.g., Qiagen MiniPrep or RNeasy kits). SPE utilizes high-molarity chaotropic salts such as guanidine thiocyanate or guanidine hydrochloride (often also included in lysis buffers), as they help facilitate nucleic acid adsorption onto silica materials through various electrostatic shielding and hydrophobic interactions.[43–45] In most instances, these chaotropic buffers also serve to lyse virions and denature RNases and other inhibitory enzymes which can degrade nucleic acid targets.[46] Liquid-phase extraction, such as phenol-chloroform extraction, can also be used, though is less popular.[47] Both of these methods require multiple washes, centrifugations, and buffer exchanges, and can take up to an hour to perform. Figure 1-5 shows a typical solid-phase extraction protocol for RNA extraction from a plasma sample, requiring at least eight fluid manipulations and five centrifugation steps. This method is often referred to as Boom extraction.[43]

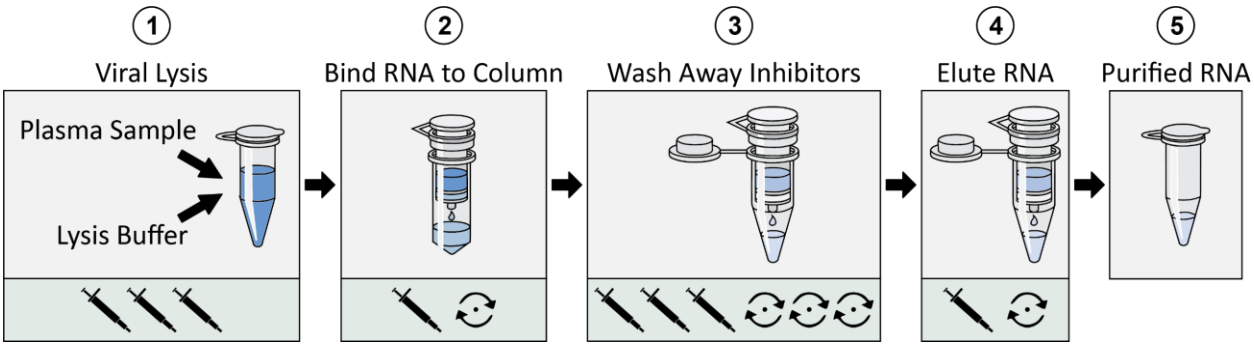

Figure 1-5: Qiagen RNeasy solid-phase extraction procedure for a plasma sample.[48] Each pipette and spin symbol represents a single fluid manipulation and centrifugation step, respectively, for a total of at least eight fluid manipulations and five centrifugation steps.

The resulting purified nucleic acids are then readily added to amplification assays, which duplicate the nucleic acids to detectable levels. Most commonly, polymerase chain reaction (PCR) or reverse-transcription polymerase chain reaction (RT-PCR) assays are used for amplification, due to the excellent sensitivity and specificity, though other methods exist (such as various isothermal methods, which are discussed later in more detail). In PCR, repeated thermal cycling is used to denature, anneal, and extend nucleic acid sequences.[49] PCR assays have been developed for a wide range of diseases, and can be multiplexed, targeting multiple sequences or pathogens in a single reaction.[50–52] In a typical PCR cycle, the reaction temperature is first raised to ~ 95 °C to denature double-stranded DNA (dsDNA) to single-stranded DNA (ssDNA). The temperature is then lowered (~ 55 °C) to anneal sequence specific primers, and then raised slightly (~ 75 °C), after which polymerase enzymes bind to the 5' end of the attached primers and extend towards the 3' end, creating a complimentary copy. After full extension, the cycle is repeated, and the resulting duplicated dsDNA is denatured, providing additional templates for further amplification. In this way, PCR doubles the amount of amplified DNA each cycle. This process is repeated for a total of 45+ cycles. The sensitivity (often less than 10 cps/rxn[53–55]) and specificity make PCR the gold-standard for amplification; however, the need for precise temperature control necessitates the use of expensive thermocyclers, and a typical PCR assay takes several hours to complete.

Detection of the amplified nucleic acids is often performed via fluorescence measurement, either through the use of intercalating dyes or fluorescent, sequence-specific probes, though other methods such as electrochemical measures or visual color change have also been used.[56–59] Detection can be done in real-time (i.e. during amplification) or as an endpoint measure (i.e. after amplification is completed).[60,61] Quantitative PCR (qPCR) detects the presence of and quantifies pathogenic nucleic acids.[62] In qPCR, real-time fluorescence monitoring of the reaction is used to calculate a cycle-threshold (Ct) value, defined as the number of thermal cycles required for the fluorescent signal to reach a specified intensity threshold. This is compared to calibration curves that are created with known target nucleic acid concentrations to establish the concentration of the "unknown" clinical sample, with lower nucleic acid concentrations having higher Ct values.[62] Digital droplet PCR (ddPCR) can also be used for absolute quantification of nucleic acids and does not require known comparison standards.[63] ddPCR instead uses thousands of discrete, droplet-sized PCR reactions in an oil-water immersion and leverages Poisson statistical distributions to determine the number of copies of target DNA or RNA present based on the number of "positive" droplets. This requires the use of complex droplet generators and separate readers with precise microfluidics and optics. HIV viral load monitoring typically uses qPCR, though qPCR is equally crucial in other diseases in which pathogen load can inform clinical treatment (e.g., SARS-CoV-2, Hepatitis B, Hepatitis C).[64–67]

These procedures can be performed manually, though due to the many laborious fluid manipulation, centrifugation, and thermal cycling steps, are often automated in large, high-throughput platforms, such as the Abbott *m2000*, Hologic *Panther*, or Roche *cobas* systems. These machines integrate sample preparation, amplification, and detection and can process 500-1,000 samples every 8 hours by leveraging complex hydraulics, electromechanical pathways, and robotics to replace the otherwise manual steps. However, the platforms cost upwards of $150,000 and require significant laboratory infrastructure (e.g., consistent electricity and temperature/humidity controlled environments), restricting their use to well-resourced centralized laboratories and limiting applicability in low- and middle-income settings.[68]

Figure 1-6: Automated, laboratory sample-to-answer platforms.(A) Hologic Panther Fusion (B) Abbott m2000 (C) Roche cobas

1.4 Point-of-Care NAATs

Point-of-care (POC) NAAT testing aims to inexpensively provide results at the time and place of patient care, alleviating many of the obstacles traditional methods face in more widespread access and dissemination (e.g., cost, sample transportation, difficulty in use, etc.).[38,69] To facilitate and guide the development of POC technologies, the World Health Organization has developed the ASSURED criteria (Affordable, Specific, Sensitive, User-friendly, Rapid and robust, Equipment-free, and Delivered) to describe the ideal point-of-care diagnostic.[70] Recently, the REASSURED criteria has been proposed, with the addition of "Real-time connectivity" and "Ease of specimen collection".[71]

Several POC NAAT platforms for HIV viral load monitoring have been commercialized, such as the Abbott *m-PIMA*, Diagnostics for the Real World *SAMBA II*, and the Cepheid *GeneXpert*. All of these platforms and devices aim to simplify user steps (to reduce specialized training requirements), with many receiving CLIA-waived status.[72] These platforms are cartridge-based, with the majority of the equipment (e.g. heaters, optics, robotics, etc.) enclosed in a reader unit, while sample is added to single-use, disposable cartridges that contain the necessary assay reagents. There has been success in disseminated testing with these platforms in low-tier laboratories, with many only requiring the additional step of centrifugation of blood samples to produce plasma.[73–75] The Cepheid *GeneXpert*, for instance, uses 1 mL plasma and is able to quantify HIV Group M, O, N, and P in 91 minutes with an impressive limit-of-quantification of 40

cps/mL.[76] The *GeneXpert* systems use a rotating piston to pump sample, lysis buffer (guanidinium thiocyanate), and elution buffer over silica-based solid-phase extraction beads, with purified nucleic acids then directed into a PCR manifold for RT-qPCR amplification, detection, and quantification. Cepheid offers a full catalogue of cartridges designed to different targets, including respiratory pathogens (e.g. influenza, RSV, SARS-CoV-2), bacterial targets (e.g. MRSA, tuberculosis), and even various genetic markers in the human genome (e.g. thrombosis risk factors).[77] The Abbott *m-PIMA* cartridge requires 50 μL of plasma and uses air pressure with multiple septums to control fluid movement within the fluidic pathways, with an analytical sensitivity of 800-1,000 cps/mL in the HIV-1/2 Viral Load Test.[78] It uses sequence-specific surface-hybridized capture oligos which bind HIV RNA present in a sample after pathogen lysis via chaotropic agents (guanidinium hydrochloride), with inhibitors subsequently washed away, similar to traditional solid-phase extraction. This is then followed by amplification of the viral RNA via RT-qPCR.[79] While not applicable to viral load monitoring, *m-PIMA* system also offers cartridges for qualitative detection of HIV, and uses a 25 μL sample of capillary blood (e.g. heel or finger prick); Cepheid also offers qualitative detection cartridges that can process whole blood samples. Despite their advantages, the costs of these systems are still often prohibitive for primary- and community-level testing, with platform costs of $10,000 – $25,000.[80,81] Similar to high-throughput platforms, these point-of-care platforms rely on mechanical and hydraulic complexities to automate user steps, driving platform costs upwards. Additionally, the majority of these devices require stable plug power and technician training (albeit significantly reduced from larger-scale platforms). Further innovation is still required to reduce testing and platform costs, reduce time-to-results, and simplify user steps and associated training for more widely disseminated NAAT testing, and will likely require significant deviations from traditional NAAT workflows.

Figure 1-7: Commercialized point-of-care NAATs for HIV viral load testing. (A) Abbott m-Pima (B) DRW Samba II (C) GeneXpert II

Recently, Drain *et al*. published a target product profile (TPP) describing an ideal point-of-care viral load test to guide assay and device development.[80] They describe a device that is able to return results in less than 30 minutes, uses small volumes of finger prick, capillary blood (< 200 µL), is small, portable, and robust, and has a limit-of-detection (LoD) of 200 cps/mL. A point-of-care device or system should be able to perform all of the steps in HIV viral load testing (sample collection and metering, plasma separation, viral lysis, RNA extraction, amplification and detection, and quantification) with minimal user steps or training required. While these are ambitious targets, this provides valuable metrics for researchers to work towards. Additional research gaps surrounding implementation are also identified; for instance, in terms of patient outcomes, what is the most impactful level of healthcare system to implement disseminated viral load testing (e.g. hospital, primary care clinic, community center, or in-home)? While the technological challenges remain significant barriers to point-of-care viral load testing, any development will also have to be paired with methodical research to understand the potential impact.

1.4.1 SARS-CoV-2 Point-of-care NAATs

While not a bloodborne disease, the global pandemic of COVID-19 (caused by the SARS-CoV-2 virus) resulted in a sudden and unprecedented need to develop point-of-care NAATs for rapid and sensitive

testing, accelerating many technologies into commercialization. Though laboratory-based PCR and self-administered rapid antigen tests account for the majority of diagnostic tests performed, several alternative point-of-care NAAT platforms have been developed that received FDA Emergency Use Authorization (EUA) approval.[82] These devices represent a major step forward towards disseminated NAAT testing, and include the first approved home-based NAAT, the Lucira *Check-It*. It is important to note that these systems are not directly applicable to HIV viral load testing, as blood samples contain significantly more inhibitors (both chemical and enzymatic) that must be addressed when compared to the nasal or saliva samples typically used for SARS-CoV-2 testing. The most prominent of these point-of-care systems include the Lucira *Check-It*, the Cue Health *Cue* system, and the Detect COVID-19 Test, shown Figure 1-8.

Figure 1-8: FDA EUA approved at-home SARS-CoV-2 NAAT tests. (A) Lucira Check-It (B) Cue Health Cue platform (C) Detect COVID-19 Test

The Lucira *Check-It* and Detect systems use self-administered nasal swabs that are eluted into a separate buffer tube. These buffers contain lytic agents to release viral RNA at room temperature.[83] The user then inserts the buffer tube into larger incubation and reader units which puncture the tubes and release the liquid (containing viral RNA), rehydrating lyophilized nucleic acid amplification reagents contained within the reader units. The Cue Health Cue system uses a proprietary swab system that is directly added to a separate cartridge that is inserted into a larger heater unit. The viral RNA is then amplified via

isothermal amplification (discussed in more detail in Section 1.5.2). Amplification reactions are monitored and read-out through electronic monitoring of color-changing reactions, electrochemical detection paired with an app, or lateral flow readout for the Check-It, Cue, and Detect, respectively. Results are produced in as little as 20 minutes. All three of these devices received FDA Emergency-Use Authorization,[82] with the only user-steps required being the sample self-collection and sample introduction. While initially focused on SARS-CoV-2, these platforms are being revised for detection of other respiratory viruses, such as influenza or RSV. Significant modifications are likely to occur in future iterations to make these devices more user- and cost-friendly, though they offer a foundation and pathway for future point-of-care NAAT testing.

1.5 Emerging Technologies

Significant research has been devoted to developing novel technologies to address aspects of the NAAT testing workflow (sample preparation, amplification, and detection) with the goal of faster, easier, and cheaper testing. Some works have addressed only one of the three steps, while others have focused on more integrated solutions, addressing multiple or all the necessary steps.

1.5.1 Sample Preparation

Sample preparation is often considered to be the primary bottleneck in nucleic acid testing.[84,85] Specific methods are inherently linked to the pathogen of interest and more importantly, the sample type used. In dilute samples with minimal amplification inhibitors, such as nasal swabs eluted into viral transport media for SARS-CoV-2 testing, samples can be directly added to amplification reactions without additional sample preparation.[86,87] Other sample types, such as blood or plasma, require significant sample preparation due to the high concentrations of amplification inhibitors and target-degrading enzymes (e.g. RNases) present.[88,89] Where significant sample preparation is required, e.g. HIV viral load testing, the majority of

previous works have used some form of solid-phase extraction where nucleic acids are bound to a substrate and interfering species are removed, with either novel solid-phase morphologies (e.g. beads, membranes, etc.) or fluid manipulation strategies to simplify the process. Since the fundamental mechanisms are the same as traditional solid-phase extraction (detailed in Section 1.3), there are similar requirements of repeated washing, elution, etc. Various research groups have leveraged microfluidics to pass sample, wash, and elution buffers past a stationary solid-phase isolation membrane or monolith to capture and purify nucleic acids.[90–93] These methods are amenable to further integration with amplification and detection, all on a single chip or device, yet still require the use of complex valving and hydraulic control and often use complicated and expensive manufacturing, such as lithography. Other research has focused on using magnetic beads that capture nucleic acids; often this involves manipulating the magnetic beads (and associated/bound nucleic acids) via an external magnet though several buffer reservoirs separated by immiscible fluids or air gaps.[94–97] These beads can be coated in silica (leveraging Boom extraction mechanisms) or conjugated with capture oligos designed to bind to specific target nucleic acids to retain the nucleic acids as inhibitors are removed with wash buffers. Other technologies use buffers with differing pH to modulate the surface charge of magnetic beads (e.g. Invitrogen ChargeSwitch technology), with nucleic acids binding to the beads under low pH conditions (as the beads are positively charged in this regime) while inhibitors are washed away, and then eluting into solution as higher pH elution buffer is added.[94] With bead manipulation via external magnetic fields, the nucleic acids are brought to and through the various wash and elution buffers (in contrast to traditional solid-phase extraction, where the buffers are brought to the capture media and nucleic acids in spin columns). All of these strategies can eliminate the necessity of centrifugation and manual buffer exchanges, though instead require robotics, pumps, and/or microfluidics to control fluid flow or external magnets, increasing platform complexity and costs.

Paper-based sample preparation methods have also been developed. One of the more popular commercial options is the Whatman FTA membrane, a cellulose-based membrane impregnated with propriety surface treatments that lyse pathogens and bind nucleic acids, releasing the DNA/RNA into

solution as an elution buffer is added.[39] These membranes have been integrated into origami-like devices such as that shown by Govindarajan *et al*.[98] to aid in useability, though this technology does require the use of wash and elution buffers that must be added separately and sequentially. A Whatman FTA membrane was integrated into paper-and-plastic devices by Connelly *et al*., in which a user would add a plasma sample to the FTA membrane, apply a wash buffer to the membrane, and then directly add LAMP reagents, amplifying the target (spiked *E. coli* cells) within the same membrane, with an intercalating dye finally added to the membrane for fluorescence detection. While this method simplified many aspects of the sample preparation process, it required a significant number of sequential fluid additions while the Whatman FTA membrane needed to be dried at an elevated temperature in between each step, necessitating the use of a 65 °C oven.[99] Jangam *et al*. used a similar approach, though used a Fusion 5 membrane onto which a sample of HIV+ blood as added followed by addition of NaOH to lyse cells and wash away hemoglobin (and other PCR inhibitors).[100] The small pad of Fusion 5 was then added directly to a PCR reaction, in which proviral HIV DNA was amplified and detected. It is unclear whether this method could be used for detection of viral RNA, as RNA is significantly more prone to degradation. Others have used reagents deposited onto paper membranes to selectively bind and elute nucleic acids, such as Byrnes *et al.,* who patterned chitosan onto glass-fiber membranes and selectively captured and eluted DNA by applying buffers with different pH (similar to ChargeSwitch technology).[101] All of these methods (among others) benefit from the low-cost and ease of manufacturing of paper-based devices.[102]

While many of these methods solve some of the practical issues surrounding complex sample preparation at the point-of-care, there is often some less-than-desirable tradeoff made. Virtually all of these methods still require some controlled movement/fluid manipulation, as multiple buffers must be sequentially introduced to the nucleic acids to bind, wash, and elute them into a clean system for downstream amplification (e.g. through the use of motorized external magnets or multiple manual buffer additions which increase platform costs or increase complexity, respectively), and consequently there is still a need to develop POC-amenable sample preparation methods.

1.5.1.1 Isotachophoresis

Isotachophoresis is an electrokinetic sample separation technique that has been applied to purification of nucleic acids from complex biological samples.[103–107] First recognized for its ability to separate and concentrate metal ions from organic solutions in the early 19th century,[108] isotachophoresis (ITP) is appealing for nucleic acid sample preparation as it uses simple, inexpensive buffers, and requires no moving parts or valving. ITP relies on a discontinuous buffer system containing a high electrophoretic mobility, high conductance leading electrolyte (LE) and a low mobility, low conductance trailing electrolyte (TE). As an electric field is applied to the system, a charged sample species with an intermediate mobility, such as nucleic acids in an appropriately designed system, focuses at the interface between the two electrolytes. A self-sharpening peak or plug of analyte forms, with species having higher or lower mobilities than the LE and TE, respectively, (e.g. inhibitory proteins) are excluded from the interface plug region, resulting in the purification and concentration of the analyte of interest (e.g. nucleic acids), often in less than 20 minutes.[109]

A typical isotachophoretic system is shown in Figure 1-9, where a sample is located between the LE and TE buffer. Note that this is an example of a finite injection scheme; semi-infinite schemes also exist, where the sample is mixed into the TE, though this typically results in lower extraction efficiencies at the benefit of reduced overall complexity.[110] Only finite injection schemes are used in this work, though the governing principles extend to semi-infinite schemes as well. A counter-ion is also used in isotachophoretic systems, which migrates in the opposite direction as the LE, TE, and analytes of interest, and helps regulate pH. Here, I will only consider anionic ITP, in which the LE, TE, and analytes are negatively charged (and thus migrate towards the positively charged cathode); cationic isotachophoresis also exists for the extraction and purification of positively charged analytes.[111]

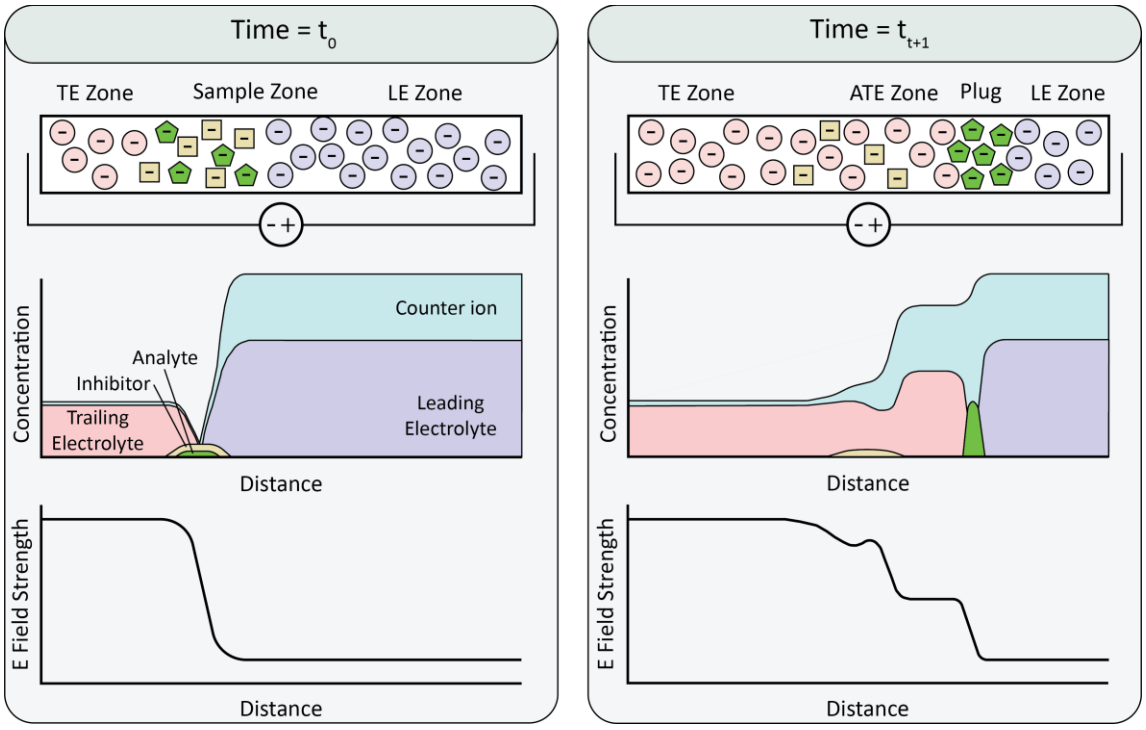

Figure 1-9: Finite injection anionic isotachophoresis at time t_0 and t_{t+1}. Initially the analyte is mixed with an inhibitor molecule, located between the TE zone and LE zone. As a potential is applied across the system, the negatively charged ions migrate towards the cathode, though the analyte (with its electrophoretic mobility in between that of the TE and LE) focuses at the TE/LE interface, while the inhibitor molecule with its lower electrophoretic mobility is left behind and excluded. As the ions migrate towards the cathode, the region in which TE ions displace LE ions is called the adjusted TE zone (ATE zone), and has slightly different characteristics (concentrations, field strength, etc.) than the original TE zone. Note that the various ions adjust their concentrations (and corresponding electric field strength) such that the ions migrate at the same speed. Concentration curves and electric field strength simulated in SPRESSO.[112]

The velocity of any given species within an isotachophoretic system is given by Equation 1, where μ_i is the electrophoretic mobility of the i^{th} species, E is the electric field strength, and V_i is that species velocity.

$$V_i = \mu_i * E \qquad \text{Eq. 1}$$

The electric field strength, E is determined by the current density (J) and the conductivity (σ) at that spatial point, given by Maxwell's current density equation: $E = J/\sigma$. The current density of the system is uniform (assuming constant cross-sectional area of the system), though as the conductivities of the LE and TE are significantly different, a non-linear electric field gradient forms across the length of the isotachophoretic system, shown in Figure 1-9. Chemical species present in the system will mutually separate themselves based on their electrophoretic mobilities, eventually forming distinct peaks or plateaus of species with migrating boundaries between them. The non-linear electric field gradient between these zones results in the self-sharpening boundary behavior that is indicative of isotachophoresis. As the analyte of interest electro-migrates towards the cathode, analytes molecules that diffuse forward into the LE zone suddenly experience a low electric field strength and the electrophoretic velocity of those molecules decreases (from Eq. 1). Conversely, if the molecules diffuse into the TE zone, the molecules experience a high electric field strength, and the electrophoretic velocity increases. In this way, a concentrated ITP plug is formed at the boundary of the LE and TE zones, concentrating analytes of interest by thousands or even millions of times their original concentrations.[113,114] As the LE and TE electrolytes are specifically chosen for a given analyte of interest, such that the two respectively electrophoretic mobilities bracket the analyte of interest's electrophoretic mobility ($\mu_{TE} < \mu_{analyte} < \mu_{LE}$), other species present of the system (e.g. various proteins or inhibitors) are excluded from the ITP "plug zone." These other, unwanted species either overspeed the plug zone into, and eventually in front of, the LE zone due to their higher electrophoretic mobilities or are very slow and are overtaken by the TE ions, being left behind. The concentrations of the LE, TE, and analyte adjust such that the velocities of all ions (on a bulk scale) are uniform; this is the origin of the term isotachophoresis, from the Greek roots "*ísos*" meaning equal and "*táchos*" meaning speed or velocity.

The theoretical framework for isotachophoretic dynamics was pioneered by Kohlrausch *et al.*[115] Everaerts *et al.*[116], and Bocek *et al.*[117]. Up until the early 2000's, ITP has primarily been used as a preconcentrating method for subsequent analytical techniques, such as capillary electrophoresis.[118] Since then, isotachophoresis has been used for purification of various bioanalytes[110] and the control and

acceleration of biochemical reactions.[119] A number of computational simulation tools have also been developed, such as SPRESSO and CAFES, to aid in the design of isotachophoretic systems.[112,120,121] Kondratova *et al*. were the first to show successful isotachophoretic extraction of nucleic acids from complex biological samples, including human plasma/serum and urine in agarose gel rods, though this required significant sample preparation, including overnight incubation with proteinase K/SDS and dialysis.[106,107] Since then, isotachophoresis has been demonstrated in microchannel and paper-based formats, and has been used to separate and purify nucleic acids from a range of biological samples, including urine, milk, and blood.[104,122–125]

Persat *et al*. were the first to extract and purify nucleic acids from diluted whole blood lysate using ITP.[104] They targeted genomic DNA with an estimated extraction efficiency of 30-70% and processed 2.5 nL of whole blood that had been diluted 10-fold with lysis buffer, for a total processed sample volume of 25 nL. Eid *et al.* extracted nucleic acids from *Listeria monocytogenes* cells in diluted whole blood via ITP and amplified using off-chip recombinase polymerase amplification, achieving a limit-of-detection (LoD) of $5x10^3$ cell-equivalents per mL when using purified genomic DNA and $2x10^4$ cells per mL when using *L. monocytogenes* cells.[126] In both experiments, 2.5 µL of whole blood was spiked with target and diluted 10-fold with lysis buffer and modified LE. Marshall *et al*. purified and detected genomic DNA from *P. falciparum* parasites using ITP, with a limit of detection reported as 500 parasites per µL blood.[127] In this work, 1 µL of whole blood was added to a 14 µL reservoir of TE and proteinase K, utilizing ITP with a semi-infinite sample injection scheme to separate the nucleic acids after pathogen lysis.

Previous implementations of ITP for the extraction and purification of nucleic acids from complex samples have been primarily performed in microchannel formats. As an alternative form factor, paper-based ITP separations have been leveraged for low-cost diagnostic applications. Moghadam *et al*. was the first to use paper substrates for ITP, showing a 900-fold concentration of fluorescent dye in a nitrocellulose membrane.[124] Later studies further expanded on paper-based ITP, such as that of Rosenfeld *et al.*[114] and Li *et al.*[125], though this work did not use complex samples. Bender *et al*. were the earliest to use complex

samples in paper-based ITP, extracting and simultaneously amplifying DNA (via recombinase polymerase amplification) from plasma samples.[105] Paper substrates are attractive for point-of-care diagnostics due to their low cost, ease of manufacture, large sample volumes, and loading simplicity. In later chapters, I describe advances made in developing an integrated ITP-based device for the extraction of nucleic acids from whole blood with minimal user steps.

1.5.2 Isothermal Amplification

One of the greatest impediments to more widespread use of PCR for amplification and detection is the requirement of expensive thermocyclers and long assay times.[128] As an alternative, isothermal amplification methods have been developed, such as loop-mediated isothermal amplification (LAMP), helicase-dependent amplification (HDA), isothermal strand-displacement amplification (iSDA), or recombinase polymerase amplification (RPA).[129–132]

Table 1-1: List of various isothermal amplification methods

Method	Temperature	Time
Loop-mediated isothermal amplification (LAMP)	65 °C	30-60 minutes
Helicase-dependent amplification (HDA)	65 °C	60 minutes
Isothermal strand displacement amplification (iSDA)	49 °C	20 minutes
Recombinase polymerase amplification (RPA)	39 °C	15 minutes
Nucleic acid based sequence amplification (NASBA)	40 °C	70 minutes

Instead of relying on thermocycling, isothermal amplification techniques leverage unique enzymes and/or primer design for nucleic acid replication, reducing the maximum operating temperature from ~95 °C (in the case of PCR) to 60 °C or below. LAMP is a highly explored amplification method that is performed at 60-65 °C for 30-60 minutes, and uses four to six primers for strand displacement and subsequent amplification.[129] Detection is typically done via fluorescent dyes, turbidity measurement, or halochromic visual indicators.[59,133,134] LAMP assays have been developed for many diseases, including

HIV, SARS-CoV-2, Hepatitis B, and Hepatitis C, though multiplexed detection can be difficult due to the complicated nature and structure of LAMP amplicons.[135–139]

RPA is a particularly attractive amplification method at the point-of-care because it is performed at a single low temperature (39 °C) and produces results in less than 20 minutes. RPA utilizes recombinase and single-strand binding proteins to facilitate primer insertion and amplification. Sequence-specific probes (similar to TaqMan probes used in PCR) are used for detection, allowing for multiplexed detection of pathogenic nucleic acids in a single reaction tube.[109,130,140,141] Figure 1-10 shows the mechanism of RPA. Briefly, recombinase proteins bind with the primers to form recombinase-primer complexes. These recombinase proteins facilitate the insertion of the primers into the homologous portion of the target genome, while single-stranded binding proteins stabilize the opposite, displaced strand. A strand-displacing polymerase (*Bsu* or *Sau* polymerase) then binds onto the inserted primers and extends the new strand in the 3' direction. This process then repeated with newly created strands, exponentially amplifying the targeted region between the forward and reverse primers. For fluorescence detection and monitoring of the reaction, a sequence-specific exo probe is included in the reaction. This oligo is complementary to a portion of the amplicon and consists of an internal fluorophore and quencher separated by an abasic site (i.e. tetrahydrofuran residue). The probe hybridizes with its complementary sequence, and an exonuclease (Exonuclease III) cleaves the abasic site, separating the quencher and fluorophore. The unquenched fluorophore and resulting fluorescence is then used to measure amplification progression. This cleavage only occurs if the probe is hybridized in double-stranded DNA, and consequently, this adds significant specificity to the reaction. The probe then acts as a primer, and exponential amplification of the region between the probe and either the forward or reverse primer occurs (which primer depends on which strand the probe is designed for). This process is shown in Figure 1-11.

The enzyme- and protein-intensive nature of RPA necessitates the use of significant concentrations of polyethylene glycol (PEG) as a crowding agent, resulting in highly viscous reaction chemistry that requires a manual agitation/mixing step to redistribute amplicons 4-5 minutes into a reaction.[142] RPA is also

unique in its reaction initiation mechanism; many, higher temperature amplification methods (e.g. PCR or LAMP) rely on WarmStart or HotStart enzymes to synchronize reaction initiation between tubes/experiments, a crucial aspect for most quantification or comparison schemes. In these assays, a temperature-sensitive antibody is conjugated to the polymerase, preventing polymerization of new strands of DNA until heated to a certain temperature, at which point the antibody dissociates and frees the polymerase, which then proceeds to amplify the target region.[143] As RPA is performed at relatively low temperatures (39 °C), this method of assay synchronization is not feasible; instead, magnesium acetate (a crucial cofactor for polymerase activity) is withheld until the start of the assay, and is typically pipetted into the tube cap such that when the reaction tubes are shaken, magnesium is introduced and initiates the reaction.[144]

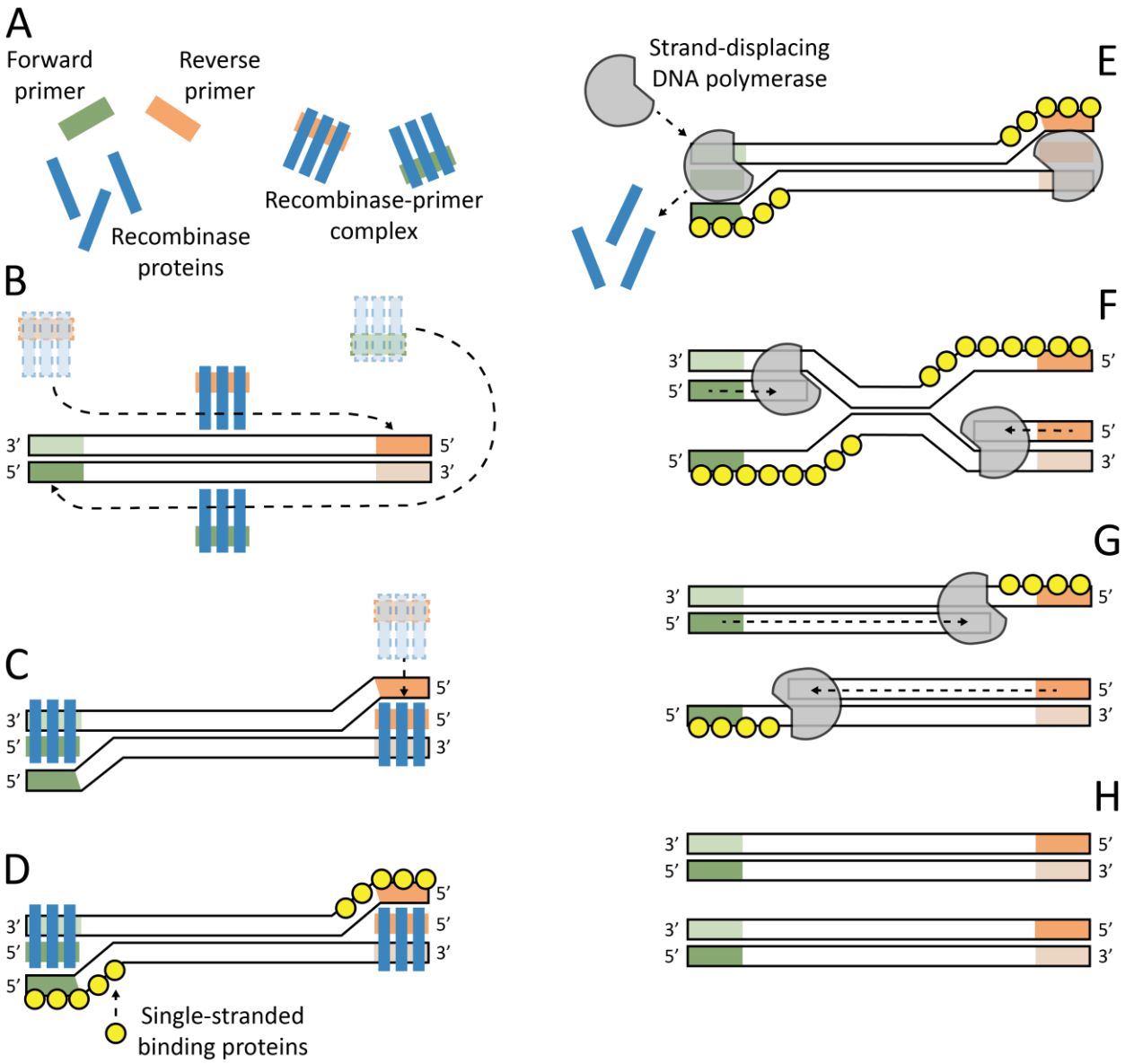

Figure 1-10: Recombinase polymerase amplification process.[144] (A) Recombinase proteins form recombinase-primer complexes or filaments with the target primers. (B,C) These complexes search for homologous sequences in target nucleic acids. The recombinase proteins promote primer insertion via strand invasion. (D) Single-stranded binding proteins stabilize the displaced nucleic acid strand. (E) A strand-displacing polymerase binds to the inserted primer as the recombinase-primer complex disassembles. (F-H) The polymerase elongates off the 3' end of the primer, producing a new complimentary strand. This process is continually repeated at 39 °C, resulting in exponential amplification. Adapted from Trends in Analytical Chemistry, Vol. 98, Lobato and Sullivan., Recombinase polymerase amplification: Basics, applications, and recent advances. Pages 19-35, Copyright 2018, with permission from Elsevier

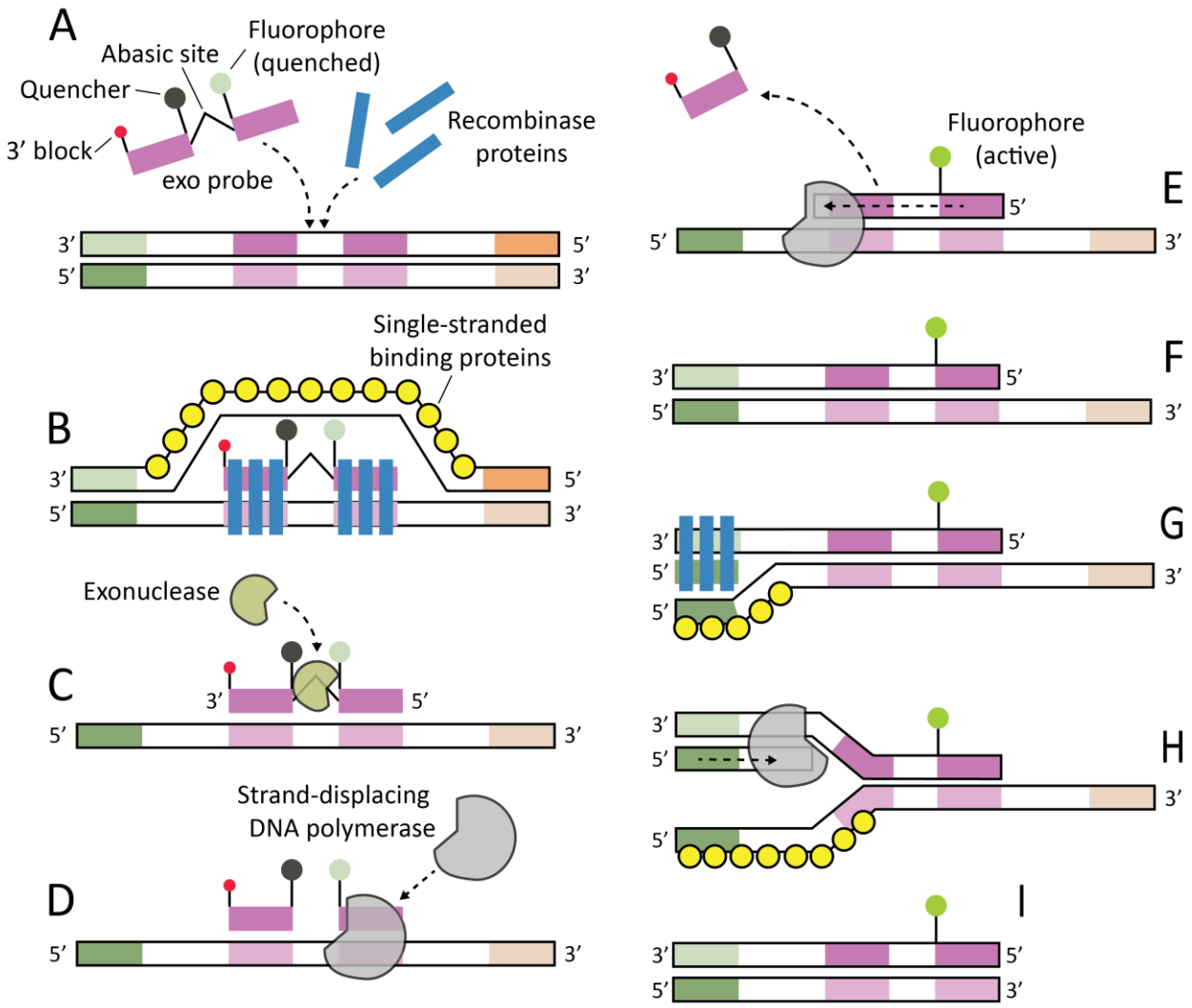

Figure 1-11: Recombinase polymerase amplification detection by exo probe. (A) Sequence-specific probes consist of a fluorophore and quencher separated by an abasic site (i.e. tetrahydrofuran residue). A blocking group (e.g. C3-spacer) is placed on the 3' side of the probe to prevent polymerase extension. (B) The probe hybridizes to its complementary sequence in the amplicon with insertion facilitated by recombinase proteins. (C) An exonuclease (Exonuclease III) cleaves the abasic site. This only occurs when the probe has hybridized with its complementary sequence to form double-stranded DNA. Note that the opposite strand is not shown here for clarity. (D,E) Strand-displacing polymerase binds to the 5' end of the probe and begins to extend in the 3' direction. This displaces the portion of the probe that contains the quencher, spatially separating it from the fluorophore, with the resulting fluorescence used to measure amplification progression. (F-I) This secondary amplicon can then be exponentially amplified between the probe region and one of the primers (depending on which strand the probe is designed to hybridize with).

Various form factors of RPA amplification have been investigated, including inexpensive paper-and-plastic devices for use at the point-of-care.[145–147] While isothermal amplification methods are much more easily implemented at the point of care, the lack of thermocycling also removes the inherent annealing/extension synchronization that gives qPCR its precise quantification capability, making sample quantification (crucial in HIV viral load monitoring) via isothermal amplification challenging.[148] Several groups have related various LAMP metrics, such as real-time reaction turbidity or end-point colorimetric indicator dyes to input nucleic acid copy numbers.[149,150] Most RPA assays use bulk fluorescence measurement (e.g. time-to-threshold) for nucleic acid quantification, though this approach lacks precision and calibrations can vary across target genotype/subtype.[151–154] Challenges in quantification by RPA have been attributed to desynchronized amplification, chemical initiation of the reaction, and high viscosity reaction chemistry.[148] Some efforts to use RPA for quantification, such as those shown by Crannell *et al*. and Bender *et al.* have had some success, though there are no careful studies showing that RPA has sufficient quantitative precision for a clinical application.[105,155]

While not necessarily an emerging technology, lateral flow assays (LFAs) can also be used to detect amplified nucleic acids as an endpoint measurement. These assays are attractive in point-of-care settings as they can be inexpensively mass manufactured, require very little training to perform, and can be readout visually with no external equipment necessary.[156] LFAs for nucleic acid detection work similarly to how antigen-based LFAs function. Briefly, amplified nucleic acids are applied and flow over a test line of pre-deposited capture molecules that are designed to specifically bind to certain molecular tags (such as biotin, FAM, or digoxigenin). Slight amplification assay modification is necessary for LFA applications through the conjugation of these tags to the forward primer, reverse primer, and/or probe, such that the resulting amplicon is tagged by two distinct conjugated molecules (e.g. biotin and FAM). As the tagged amplicons flow over the test line, one tag is bound by its complimentary capture molecule on a nitrocellulose substrate (e.g. streptavidin for biotin, anti-FAM for FAM, and anti-digoxigenin for digoxigenin). The other tag binds to its complementary capture molecule which is conjugated to a colorimetric particle (e.g. gold

nanoparticles or latex beads). In this way, a sandwich structure is formed, with the target of interest bridging the test line capture molecules and the colorimetric particles, forming a visually distinguishable test line. While LFAs have traditionally been limited to binary endpoint detection (presence vs absence of the target of interest – i.e., amplified nucleic acids), there have been reports of using the test line/band intensity as a quantitative measure, though this often requires the use of complex imaging or camera setups.[157–159] Recently, Hull *et al*., Mancuso *et al.*, and Rosenbohm *et al*. have shown quantitative lateral flow readout of RPA and HDA reactions, without complex imaging through the use of a duplexed competitive internal amplification control.[160–162] These amplification assays are designed such that when the target of interest is at a higher concentration than the designed internal control, the amplification reaction favors the target of interest and the target test line appears significantly stronger than the internal control test line in LFA readout. As the assay is multiplexed, the two reactions are competing over limited reagents (e.g. dNTPs, ATP, etc.) – if the target of interest starts at higher concentration, it will amplify first and faster, effectively starving the internal control reaction (or if the internal control is at a higher concentration, the target of interest reaction will be starved). In this way, a semi-quantitative "higher-than-or-lower-than" comparison against the internal amplification control can be achieved, though at the cost of increased assay complexity.

1.5.3 Technical Challenges in HIV Viral Load Testing

HIV viral load testing poses a particularly difficult target to work towards in POC NAAT development (though all bloodborne disease pose significant challenges in general). This is largely due to the inherent complexities of processing blood samples combined with the unique aspects of the HIV virus. The HIV virus replicates within $CD4^+$ T-cells, reverse transcribing its RNA into proviral DNA, and then inserting and integrating this proviral DNA within the cellular genome for viral component replication. This poses a challenge for viral load assays, as they cannot readily distinguish between viral RNA and proviral DNA, the latter of which can inflate viral load measurements even though it may not be indicative active viral replication.[163] Consequently, many viral load test require the use of plasma samples instead of whole

blood, as plasma excludes white blood cells (i.e. $CD4^+$ T-cells) which serve as a reservoir of proviral DNA. In this way, only virus (and viral RNA) is collected and measured in viral load testing, though this requires a separate centrifugation step. This same concern of proviral DNA carries over into point-of-care viral load testing, necessitating some form of integrated plasma generation, with significant research focused on the development of passive membrane-based plasma separators for similar use-cases.[164–166]

Blood is a particularly difficult sample to process due to its constituents. There are many inhibitors present, such as hemoglobin[89] that must be removed prior to amplification. Additionally, blood contains significant concentrations of RNases – ubiquitous nucleases that facilitate the degradation of RNA.[43,167] RNases are extremely hardy, resisting thermal deactivation and more common enzymatic deactivation protocols.[168] Reagents used in traditional solid phase extraction techniques entirely denature protein structures, including RNases, though the use of high molarity chaotropic agents. However, these reagents are inherently incompatible with subsequent amplification (as they would also denature the polymerase enzymes necessary for amplification), necessitating the many wash, centrifugation, and fluid manipulation steps that complicate traditional solid phase extraction. Previous studies have shown that over 99% of exogenous RNA added to human plasma becomes non-amplifiable via PCR after only 15 seconds of contact time.[167] Any point-of-care viral load test must actively and rapidly deactivate the RNases present in blood samples, as any extended contact time once the viral capsule is lysed will likely result in RNA degradation.

HIV is a relatively genetically diverse virus, which requires careful amplification assay design. As amplification assays rely on conserved genome sequences for primer and probe hybridization, nucleotide mutations or mismatches within these zones can significantly affect amplification efficiency. To accommodate the genetic diversity of HIV, many commercial amplification assays use multiple degenerate primers and/or probes with multiple gene targets. For instance, the Roche COBAS AmpliPrep/COBAS TaqMan HIV Test, version 2.0 qPCR assay targets both the LTR and *gag* genes, with three and four separate primers for each target, respectively.[169] The Hologic Aptima HIV Quant Dx Assay targets both the LTR and *pol* genes.[170] RPA is notable in that it can withstand multiple nucleotide mismatches in the primer and

probe sequences, allowing for cross-subtype detection with a single primer/probe pairing, though amplification efficiency can be affected.[154,171]

The relevant and necessary limits of detection in viral load monitoring are also extremely demanding. As an illustrative thought-experiment, consider a theoretical point-of-care device that were to use a finger prick blood sample with a volume a 50-100 μL, equating to roughly to 30-60 μL of plasma (assuming 40% hematocrit). At a viral load concentration of 1,000 copies per mL of plasma (the traditional cutoff for viral suppression), this results in only 30-60 copies of viral RNA to process, amplify, and detect. This is on the same order of magnitude as many amplification assay limits of detection,[154,172,173] leaving very little room for inefficiencies and losses throughout sample preparation and other manipulations.

In any successful point-of-care viral load test device, all these concerns and obstacles must be addressed simultaneously, which poses a significant challenge for any assay or device developer. New technologies are necessary to address the various steps in the viral load testing workflow in low-cost and low-complexity solutions.

1.6 Research Objectives

The previous sections have detailed the need and requirements of HIV viral load testing at the point-of-care. The objective of my dissertation is to develop novel techniques, technologies, and devices to address the various steps in the viral load testing process, including sample preparation, amplification, and detection in low-cost and disposable form factors. In order to address these objectives, I will detail the following works:

1. Nucleic acid sample preparation from whole blood in a paper-and-plastic microfluidic device using isotachophoresis and the integration of RNase inactivation chemistries
2. Development of amplification nucleation site analysis as a more accurate metric to quantify recombinase polymerase amplification (RPA) reactions across HIV subtypes

Chapter 2: Nucleic Acid Sample Preparation from Whole Blood using Isotachophoresis

2.1 Introduction

One of the key challenges facing more widely disseminated NAAT diagnostics is the complexities of current sample preparation techniques, which are often considered to be a primary bottleneck in nucleic acid testing.[84,85] Traditional sample preparation is performed via liquid phase extraction (LPE), such as phenol-chloroform extraction, or solid phase extraction (SPE) techniques, which preferentially bind and release nucleic acids to silica columns, beads, or membranes. These protocols utilize high-molarity toxic chaotropic salts such as guanidine thiocyanate or guanidine hydrochloride (often included in lysis buffers), which facilitate nucleic acid adsorption onto silica materials.[43,44] Both LPE and SPE result in purified nucleic acids that are readily added to amplification reactions. These protocols require numerous manual pipetting and centrifugation steps, can take more than an hour to perform, and can be difficult to implement in point-of-care settings due to their requirements for training, refrigerated reagent storage, and necessary associated equipment (e.g. centrifuges and pipettes).[39]

As described previously, isotachophoresis is a powerful separation method that has been used to extract and purify nucleic acids from biological samples with minimal user steps.[103–107] The majority of previous work that has focused on isotachophoretic nucleic acid extraction and purification has been performed in microchannel devices manufactured via traditional photolithography or injection molding.[174,175] These devices have a number of advantages, such as precisely defined geometries, minimal channel adhesion sample loss, and readily available mass manufacturing methods, though they suffer from complex LE/TE buffer loading procedures (often requiring vacuum assistance) and minimally constrained free-surface liquid reservoirs,[175] complicating potential applications at the point-of-care. Additionally, in microchannel based ITP, sample volumes have historically been relatively small (< 2.5 μL undiluted

sample), while recovering ITP-focused target analytes can prove challenging and cumbersome. Paper-based ITP systems are robust, extremely inexpensive to manufacture, and allow for larger sample volumes. Large scale paper-based ITP was originally used for laboratory separations of ions,[176,177] while more recent microfluidic-based paper devices have been developed for point-of-care applications.[124,125,178,179] Moghadam *et al*. were the first to demonstrate isotachophoretic preconcentration in a paper-based microfluidic device, using this to improve the limit of detection of rapid immunoassays by two orders of magnitude.[124,180] Rosenfeld and Bercovici created a paper-based ITP system by patterning wax onto a nitrocellulose membrane to constrain the LE/TE buffers and showed 20,000 fold sample focusing and amplification-free detection of target DNA in buffer.[179] Previously, Bender *et al.* extracted target DNA from human serum utilizing paper-based ITP and simultaneously amplified on-device via recombinase polymerase amplification with a limit of detection of 10^4 copies DNA per mL from an initial sample volume of 20 μL.[105] They also showed proof-of-concept data describing extraction and amplification of DNA from whole blood while using a significant concentration of target DNA.

While ITP represents an attractive solution for nucleic acid extraction and purification from complex samples such as whole blood, additional sample pretreatment steps such as off-chip sample dilution or protein digestion are often still necessary. Dilution is frequently required as the high salt and protein content of blood and plasma can make isotachophoretic extraction difficult due to effects on viscosity, ionic strength, pH, and conductivity of the system.[181] For applications that are primarily concerned with pathogen presence and binary diagnoses (i.e. where the concentrations of the target are relatively high), dilution may not be problematic. Dilution can be detrimental, however, for applications where low limits of detection are necessary, such as in HIV viral load monitoring.[80] In these application spaces, there is often only one (or less) target nucleic acids per microliter, necessitating large biological sample volumes to ensure sufficient target is present. In much of the previous work in which whole blood was used as a sample in ITP, the total processed sample volume was typically 10-25 microliters while the volume of blood processed was merely 1-2.5 microliters (i.e. 10x diluted). For this reason, there have been

several works that have focused on increasing ITP sample volume or biological sample concentration. For instance, van Kooten *et al.* focused DNA and *E. coli* bacteria diluted in 50 µL trailing electrolyte into a volume of 500 pL by carefully designing their microchannel-based system.[174] While this volume is impressive in an isotachophoretic system, complex biological samples were not tested. Bender *et al*. extracted nucleic acids from 20 µL of human serum, representing one of the largest volumes of undiluted complex sample used in isotachophoretic systems to date.[105] For bloodborne pathogen detection in the point-of-care setting, it is often necessary to process large volumes of blood to reach low limits of detection in downstream nucleic acid amplification assays. This requires an integrated approach that addresses many unique aspects of using whole blood as a sample, including leukocyte/erythrocyte depletion and endogenous protein digestion to successfully extract and purify target nucleic acids in an inexpensive, semi-automated manner with minimal user steps.

In this chapter, I present a paper-based, isotachophoretic nucleic acid sample preparation platform that extracts target DNA from undiluted human whole blood. This device directly processes relatively large volumes (33 µL) of whole blood, with no preliminary dilution or pretreatment steps required. I verify nucleic acid isotachophoretic extraction and purification by real-time imaging of fluorescently labeled DNA and off-device recombinase polymerase amplification (RPA). I show an optimized integrated plasma separation membrane for cell fractionation, as well as on-paper proteolytic digestion of endogenous plasma proteins via proteinase K to enable isotachophoretic extraction, verified using SDS-PAGE. I discuss design decisions in the development of a platform that reduces the number of user steps and potential sources of error, including the first integration of paper-based ITP buffer reservoirs. I then detail steps towards the integration of lyophilized RNase inactivation chemistries onto paper membranes for viral RNA extraction. The nucleic acid sample preparation platform presented here represents a step towards a simple, robust, low-cost sample preparation technique for point-of-care NAATs for bloodborne diseases, including HIV viral load monitoring.

2.2 Experimental Section

2.2.1 Device Construction

I use an integrated paper-based nucleic acid sample preparation device to extract target nucleic acids from whole human blood. Figure 2-1 shows the device constructed from different layers of inexpensive, readily available materials, including acrylic, paper-like membranes, PCR tape, and titanium foil. The acrylic body is fabricated into a 65 mm x 20 mm rectangle from 3 mm thick acrylic using a CO_2 laser cutter (M360, Universal Laser Systems, USA). Two 12.5 mm square ITP buffer reservoir wells are cut out of the acrylic near the ends. A 65 mm x 20 mm rectangle of PCR tape (TempPlate RT Select Optical Film, USA Scientific, USA) is cut via laser cutter, forming the bottom tape. Two rectangles of 20 mm x 6 mm x 0.12 mm titanium foil (LiteOutdoors, CAN) are cut by hand and placed in between the bottom tape and the acrylic body such that roughly 7.5 mm of the foil rectangles extend over the short edges of the device. Twelve 10 mm squares of glass fiber membrane (G041 Glass Fiber Conjugate Pad, Millipore Sigma, USA) are cut using a craft cutter (Silhouette Cameo 3, Silhouette America, USA), with six squares placed in each ITP buffer reservoir well, forming the paper-based ITP reservoirs. I use paper-based ITP reservoirs instead of traditional liquid reservoirs to minimize spills and leaks from the device during buffer loading and manipulation, as the entire liquid system is contained within a membrane matrix, a main benefit of paper-based devices. A Fusion 5 membrane (GE Healthcare Life Sciences, USA) is cut with the craft cutter as the ITP pad and placed such that the ends of the Fusion 5 are in contact with the glass fiber reservoirs. Towards one end of the Fusion 5 membrane is the sample pad which features a spade-like widening that is 9 mm at its widest extent. The remainder of the Fusion 5 membrane is 3 mm wide. I place the PCR cover tape over the Fusion 5 membrane and apply light pressure against the acrylic body to ensure a tight seal/bond. The cover tape has two small circular apertures that are located over the glass fiber reservoirs for buffer addition. The cover tape also has a rectangular opening that exposes a section of the narrower portion of the Fusion 5 membrane, identified as the eluate port, and another, separate spade-shaped cut-out,

called the sample port, that reveals the sample pad. Initially, a small rectangle of PCR tape (25 mm x 15 mm) covers the eluate port.

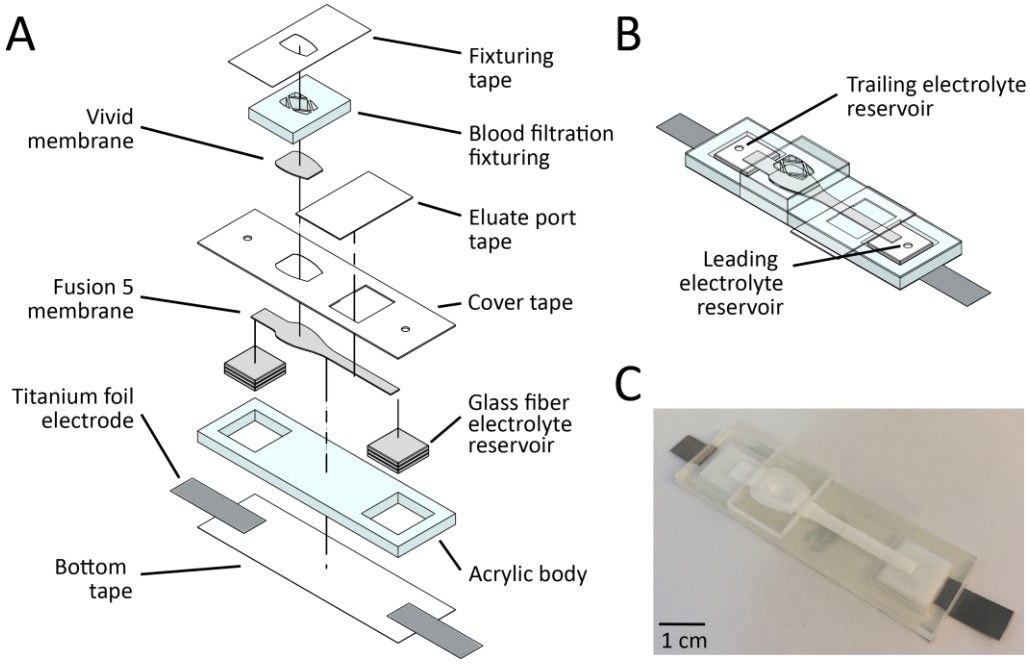

Figure 2-1: Device for extracting DNA from whole blood. (A) Device materials and construction. The device is constructed from various layers of acrylic, PCR tape, and several different paper membranes. The device is designed for an input sample volume of 33 µL of whole blood. (B) Schematic of assembled device, showing the glass fiber membrane reservoirs for ITP buffers. (C) Image of an assembled device.

I pipette 20 µL of proteinase K (P8107S, New England Biolabs, USA) onto the exposed Fusion 5 sample pad and desiccate the device for 20 minutes at room temperature to dry the membrane in a small laboratory desiccator. I then place a spade-shaped 0.765 cm^2 Vivid GR plasma separation membrane (Pall Corp., USA) into contact with the sample pad portion of the Fusion 5 ITP membrane. A separate piece of laser-cut acrylic (referred to as the blood filtration fixturing) is placed over the Vivid membrane. The blood filtration fixturing has several holes cut through for sample addition and a shallow laser-rastered relief on the downwards-facing side which provides an optimized compressive contact force with the Vivid

membrane. Lastly, a piece of PCR tape is placed over the blood filtration fixturing and is wrapped around and attached to the sides of the acrylic body to hold the fixturing in place.

2.2.2 Reagents and Chemistry

The ITP system leading electrolyte consists of 250 mM HCl (H1758, Sigma, USA) and 375 mM Tris (93362, Sigma, USA) at a calculated pH of 7.8. The trailing electrolyte consists of 25mM serine (84959, Sigma, USA) and 25mM Tris at a calculated pH of 8.7. Using these buffers, proteinase K is positively charged in the system due to its high isoelectric point (pH 8.9),[182] allowing the ITP system to separate it from the negatively charged nucleic acids as it will migrate in the opposite direction (towards the anode).[104] Isotachophoresis simulations were performed using SPRESSO to estimate local pH along the Fusion 5 membrane.[112] SPRESSO conditions and settings used are shown in Table 2-1.

Table 2-1: SPRESSO simulation inputs and parameters used to guide isotachophoresis system design.

Input/Parameter	Values	
Leading electrolyte composition	0.375 M Tris	Valence = 1, Mobility = 29.5e-9, pKa = 8.06
	0.250 M HCl	Valence = -1, Mobility = 7.91e-8, pKa = -2
Trailing electrolyte composition	0.025 M Tris	Valence = 1, Mobility = 29.5e-9, pKa = 8.06
	0.025 M Serine	Valence = -1, Mobility = 34.3e-9, pKa = 9.33
Analyte composition	0.010 M DNA	Valence = -1, Mobility = 40e-9, pKa = 6.8
Current	-2.5 µA	
Domain Length	30 mm	
Channel Shape	D Shape	
Dim. 1	20 mm	
Dim. 2	50 mm	
Injection point	15 mm	
Injection width	2.2 mm	

The target DNA is diluted to various concentrations in low-EDTA TE buffer (VWR, USA) and stored at -20 °C. The target DNA used is a synthetic strand (200 base pairs), detailed in Bender *et al*.[105] and

derived from the proviral HIV DNA *pol* gene. Primers and probes used were adopted from Boyle *et al.*[172] I use a 70 base pair oligonucleotide labeled with Alexa Fluor 488 to fluorescently monitor ITP plug location and progression. Full nucleotide sequences are listed in Table 2-2. All oligonucleotides were purchased from Integrated DNA Technologies (USA).

Table 2-2: Sequence information for abridged *pol* target and RPA primers, probe, and tracking DNA

Description	Sequence (5' – 3')
Abridged *pol* target dsDNA (200 bp)	AGGCTGAACATCTTAGGACAGCAGTACAAATGGCAGTATTCATTCAC AATTTTAAAAGAAAAGGGGGGATTGGGGGGTACAGAGCAGGGGAAA GAATAGTAGACATAATAGCAACAGACATACAAACTAGAGAACTAGGTT GAGAAATTAGAAAAGTTGAATATGTTAGGGTTTATTACAGGGACAGCA GAGATCCACTT
Forward primer (34 bp)	TGGCAGTATTCATTCACAATTTTAAAAGAAAAGG
Reverse primer (34 bp)	CCCTAACATATTCAACTTTTCTAATTTCTCAACC
Probe (48 bp)	TGCTATTATGTCTACTATTCTTTCCCC[T(FAM)]GC-[dSpacer]C-[T(BHQ 1)]GTACCCCCCAATCCCC-SpacerC3
Tracking dsDNA (70 bp)	[AF488]TCTATCTGGCATGGGTACCAGCACACAAAGGAATTGGAGGAAATG AACAAGTAGATAAATTAGTCAGTGC

I use off-device RPA to validate the presence of target DNA in the extracted sample after ITP. I use the TwistAmp exo kit from TwistDx (GBR) and follow standard operating procedures. The mastermix includes a lyophilized RPA-exo pellet, rehydration buffer, probe (120 nM), and primers (420 nM). Magnesium acetate (18 mM final concentration) is added to the reaction tube lid and introduced into the reaction via manual agitation immediately prior to incubation. A higher concentration of magnesium acetate than typically used (14 mM) is chosen to compensate for any residual EDTA that might be present in the ITP eluate (as the blood samples used contain K_2EDTA as an anticoagulant). The total RPA reaction volume is 50 µL. A T16-ISO instrument (TwistDx, GBR), set at 39 °C, amplifies and detects the DNA target via continuous fluorescence monitoring. After 4 minutes of incubation, I remove and agitate the tubes by hand to further mix reagents and then reinsert them back into the T16-ISO for an additional 16 minutes.

2.2.3 Data Collection

Real-time epifluorescence imaging of the ITP system is performed to determine the plug location and ITP progression, visualized by Alexa Fluor 488 labeled tracking DNA. An AZ100 microscope (Nikon, JPN) was used with a 0.5X objective, a 488 nm excitation and 518 nm emission filter cube set (Omega Optics, USA), and a 16-bit cooled CCD camera (Cascade 512B, Photometrics, USA). Grayscale images of the evolution of the ITP system are captured every 1 second for 20 minutes.

I quantify the extraction efficiency of the ITP system by comparing the bulk fluorescence of the fluorescently labeled tracking DNA to the plug region after extraction. The baseline value is established by pipetting 1 μL of 1 μM fluorescently labeled tracking DNA onto a region of Fusion 5 membrane and measuring the integrated fluorescence over that region via ImageJ. The fluorescence in the focused ITP plug is determined by integrating the fluorescence in a region of interest around the plug. The images are corrected for background by selecting a region of the Fusion 5 strip far from the tracking DNA to reduce any effects of autofluorescence of the membrane and/or PCR tape. I repeated this process for a total of 6 individual trials and the average experimental integrated fluorescence is divided by the average baseline integrated fluorescence to estimate the extraction efficiency of the system.

A T16-ISO instrument is used for RPA incubation and real-time fluorescent measurement. Real-time fluorescence values of the RPA reactions are recorded every 8-10 seconds. For comparison of the amplification reactions, I normalize fluorescence intensity values by subtracting the absolute intensity measured at 45 seconds, at which time fluorescence values have typically sufficiently stabilized.

2.2.4 Device Operation

Figure 2-2 shows the operation of the device. A freshly constructed device is used for each experiment. The undiluted whole blood sample is first pipetted onto the Vivid plasma separation membrane.

The sample consists of 33 µL human whole blood (K_2EDTA, BioIVT, USA), 1 µL target DNA at various concentrations, and 1 µL of 1 µM fluorescently labeled tracking DNA. This sample volume is chosen to comply with the Vivid membrane manufacturer's processing recommendation of 40-50 µL blood per square centimeter of membrane. Preliminary experiments showed that plasma extraction efficiency decreases rapidly as the sample volume applied deviates from this recommendation. Both the target DNA and fluorescently labeled tracking DNA are added to the whole blood sample immediately before sample loading onto the Vivid plasma separation membrane. After sample addition, I wait four minutes, allowing blood filtration and plasma separation to occur. During this process, plasma and the target/tracking DNA pass through the Vivid plasma separation membrane and into the underlying Fusion 5 membrane where it rehydrates the desiccated proteinase K. After four minutes, I remove the blood filtration fixturing along with the Vivid plasma separation membrane and cover the sample port with a small rectangle of PCR tape, ensuring a good seal near the sample pad to prevent evaporation and contamination. I find that it is necessary to remove the blood fractionation fixturing and Vivid membrane as if they are not removed, the red blood cells (or potentially hemoglobin) migrate laterally through the Vivid as the electric potential for ITP is applied to the system. The ITP buffers effectively saturate the Vivid membrane, allowing the red blood cells to move and migrate laterally through the upper, larger pores of the Vivid. The RBCs/hemoglobin eventually migrate out of the Vivid and onto the underlying ITP strip in the direction of the cathode, and are focused within the ITP plug. Initial experiments that aimed to prevent this lateral migration within the Vivid included heat-sealing/sintering the edge closest to the LE to completely close the pore structure of the polymer membrane through the application of heat and pressure, similar to that shown in Hin *et al.,*[183] though these efforts ultimately proved to be unsuccessful (shown in the Appendix A.1). It is likely that this method is feasible, though requires more precise application of heat and pressure parameters. I also investigated various methods of wax deposition to create hydrophobic barriers within the Vivid membrane, but found that standard methods of wax deposition (i.e. ColorQube wax printers) significantly affected the

Vivid membrane wicking properties, hypothesized to be due to contamination of the membrane by oil on the print drum (also detailed in the Appendix A.2).

The resulting plasma rehydrates the proteinase K that subsequently digests the endogenous plasma proteins. On-paper plasma protein digestion occurs for 15 minutes at various temperatures (22 °C, 37 °C, and 55 °C) on a hotplate. I then add 390 µL of leading electrolyte (LE) and 320 µL trailing electrolyte (TE) buffers to their respective glass fiber reservoirs through small holes in the cover tape. The liquid wicks into and saturates the glass fiber and the Fusion 5 membranes. A source meter (Model 2410, Keithley, USA) then applies 1.5 mA constant current via the titanium foil electrodes, initiating isotachophoresis.

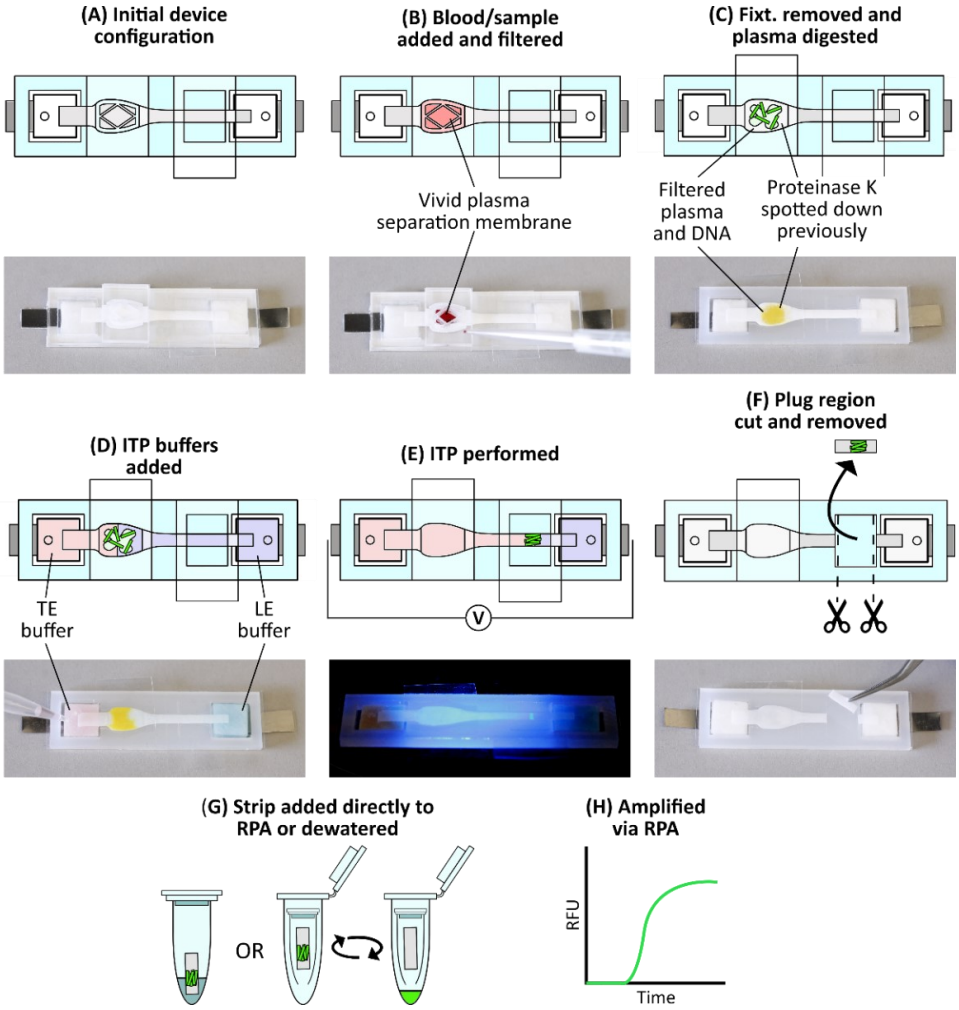

Figure 2-2: Device protocol to extract DNA from whole blood. (A) Initial device configuration. (B) A sample of 33 µL whole blood spiked with target DNA and fluorescently labeled tracking DNA is dispensed onto the Vivid membrane. Blood filtration occurs for 4 minutes, during which plasma and nucleic acids filter through to the Fusion 5 membrane. (C) After filtration, the blood filtration fixturing and Vivid are removed, and cover tape is applied to seal the sample port. Proteolysis then occurs for 15 minutes via the rehydrated proteinase K. (D) ITP buffers are added to their respective reservoirs. Colored zones are added for illustrative purposes: red represents trailing electrolyte buffer while blue represents leading electrolyte buffer. (E) ITP is initiated by the application of 1.5 mA constant current, focusing the DNA into a narrow plug which then migrates towards the leading electrolyte reservoir. This process is monitored in real-time via fluorescent microscopy. (F) Once the ITP plug reaches the eluate port, ITP is discontinued, and the eluate port tape is removed with the exposed portion of Fusion 5 membrane containing the ITP plug excised. Buffer colors here are removed for clarity. (G) The excised strip is either directly to an RPA reaction or first dewatered via centrifugation with the eluate added to an RPA reaction. (H) The RPA reactions are then incubated and recorded for 20 minutes.

As ITP progresses, both the target and tracking DNA are focused at the ITP plug interface of the LE and TE and migrate away from the digested plasma proteins. Once the ITP plug interface reaches the middle of the eluate port, the eluate port tape is removed and the 5 mm exposed section of the Fusion 5 membrane containing the ITP plug is excised with an X-Acto knife. This strip is then directly added into an RPA reaction tube immediately after the master mix has been added. The tube is then inverted several times to mix reagents, gently tapped on a surface to ensure the strip sits near the bottom of the reaction tube, and then placed into the T-16 ISO for amplification and fluorescence readout.

Alternatively, I dewater the strip via centrifugation and add the resulting eluate to the RPA reactions. In this procedure, a 10 mm section of Fusion 5 strip containing the ITP plug is cut out. After cutting the strip, I place this strip into a 0.5 mL micro-centrifuge tube that has a small opening at the bottom. This micro-centrifuge tube is then placed in a larger 1.5 mL micro-centrifuge tube and both tubes are placed in a centrifuge (5415D, Eppendorf, DEU) for 3 minutes at 6,000 rcf. The resulting eluate is collected at the bottom of the 1.5 mL micro-centrifuge tube. This typically results in 10 µL of eluate containing the target DNA and is split evenly between two RPA reactions, with 5 µL of the eluate added to each reaction. I find that splitting the eluate into two separate reactions results in more consistent amplification, likely due to trace inhibitor dilution. In all cases, the reaction with the poorer amplification (determined by time-to-threshold analysis) is discarded and is not used in further analysis. A list of complete user steps and their associated times are listed in Table 2-3.

Table 2-3: Order of user steps and operations

	Step description	Time required
1.	Add whole blood (33 µL) and target/tracking DNA sample to device	~15 seconds
2.	Blood filtration via Vivid plasma separation membrane occurs	4 minutes
3.	Remove blood filtration fixturing and Vivid plasma separation membrane, and place a rectangular piece of PCR tape over the sample port, ensuring a good seal	~30 seconds
4.	Plasma protein digestion occurs at room temperature.	15 minutes
5.	Add 390 µL LE buffer to the LE glass fiber reservoir. Immediately afterwards, add 320 µL TE buffer to the TE glass fiber reservoir.	~30 seconds
6.	Apply a constant current of 1.5 mA via the titanium electrodes, powering isotachophoresis.	10-15 minutes
7.	Once the ITP plug reaches the eluate port, remove the eluate port tape, and excise the exposed Fusion 5 membrane with an X-Acto knife.	~30 seconds
8a.	Add the cut-out Fusion 5 membrane directly to an RPA reaction, and perform RPA per the manufacturer's instructions.	~30 seconds
8b.	Add the cut-out Fusion 5 membrane into a 0.5 mL micro-centrifuge tube with a small hole in the bottom, placed into a larger 1.5 mL micro-centrifuge tube, and dewater the strip, collecting the eluate in the bottom of the 1.5 mL micro-centrifuge tube. Add the resulting eluate (~10 µL) to two separate RPA reactions (5 µL each) and perform RPA	4 minutes

2.2.5 Whole Blood Fractionation Optimization

I measured the plasma extraction efficiency of the target DNA through the Vivid membrane and into the underlying Fusion 5 during blood fractionation. To calculate the plasma extraction efficiency, I measured the mass of the underlying Fusion 5 membrane before and after blood fractionation. I define plasma extraction efficiency as plasma mass in the Fusion 5 membrane divided by the total plasma mass in the sample as, $\eta_{P.Extract} = (m_{P.F5}/\rho_P)/V_{blood} * (1 - HCT)$, where $m_{P.F5}$ is the mass of plasma residing in the underlying Fusion 5 membrane after fractionation, ρ_P is the density of human plasma, V_{blood} is the volume of blood applied to the Vivid plasma separation membrane, and HCT is the blood hematocrit value. I measured the blood hematocrit value using a Hb 201+ analyzer (HemoCue, USA). I also qualitatively investigated cell fractionation as well as quantified hemolysis. I visualized cell fractionation using a hemocytometer (Bright Line Hemacytometer 1492, Hausser Scientific, USA) with a TMS Inverted

Microscope (Nikon, JPN). Hemolysis was measured using the Harboe method[184,185] with plasma filtered by the device and a spectrophotometer (NanoDrop 2000, ThermoFisher Scientific, USA) and compared against plasma that had been separated via centrifugation.

2.2.6 SDS-PAGE

Sodium dodecyl sulfate polyacrylamide gel electrophoresis (SDS-PAGE) was performed to analyze and compare plasma protein digestion. I used 12% Mini-PROTEAN TGX precast protein gels (#4561045, Bio-Rad, USA) and Tris/Glycine/SDS running buffer (#1610732, Bio-Rad, USA). I used the same device as described previously, though without the blood fractionation fixturing (and without associated blood fractionation steps) to simplify the procedure. Pooled, sterile-filtered human serum (H4522, Sigma-Aldrich, USA) was first pipetted onto the Fusion 5 membrane sample pad region, onto which I had previously spotted and desiccated proteinase K. I used 20 µL of proteinase K and 20 µL of serum, which correspond to roughly the same volumes expected in the device. I then covered the sample pad region with PCR tape, as described previously. Three different digestion temperatures were tested: 22 °C, 37 °C, and 55 °C. For experiments not at room temperature (22 °C), I placed the device on a hotplate. I determined the proper hotplate setpoint such that the sample pad reaches the desired digestion temperature by inserting a Type-K thermocouple (9251T93, McMaster-Carr, USA) under the sample port tape, ensuring good contact with the sample pad. After 15 minutes, the PCR tape was removed, and the sample pad region of the Fusion 5 membrane was cut out and dewatered in a centrifuge. I also digested serum directly in tubes as a controlled comparison. In those experiments, I added proteinase K directly into human serum in a 1.5 mL tube and placed it into a water bath set at 55°C for 15 minutes. For both experiment types, I then diluted the resulting serum digest to 2.5 mg/mL of protein for a total volume of 20 µL, verified using a spectrophotometer (NanoDrop 2000, ThermoFisher Scientific, USA). The diluted proteins were added to 2x Laemmli sample buffer (S3401, Sigma-Aldrich, USA) on ice in a 1:1 ratio and immediately placed in a boiling water bath for 5 minutes. Then, 10 µL of the final solutions were added to the gel lanes. A protein

ladder (Precision Plus Protein Dual Color Standards #1610374, Bio-Rad, USA) was also added into the first gel lane for comparison. Electrophoresis was performed in a Mini-Protean Tetra cell (Bio-Rad, USA) at 200V for 45 minutes. I performed Coomassie Blue staining (Bio-Safe Coomassie G-250 #1610786, Bio-Rad, USA) after fixing the proteins in 40% ethanol and 10% acetic acid. A Perfection V370 scanner (Epson, JPN) was used for gel imaging.

2.3 Results and Discussion

This device is designed to simplify isotachophoretic sample preparation of nucleic acids from whole blood. For instance, paper-based reservoirs for ITP buffers are used to minimize the risk of spillage while loading the liquids and manipulating the device. By using an all-paper system, the sample and buffer liquids are fully contained within the membrane matrix, and simple loading procedures can be used. The only steps required by the user are the removal and application of various tapes and the initial dispensing of ITP buffers. The applied ITP buffer volumes are chosen such that the initial LE/TE interface is naturally located at the sample pad region, resembling a traditional finite injection ITP scheme without the need for carefully timed loading protocols. The paper-based architecture also allows for the integration of a plasma separation membrane (which functions via plasma wicking into the underlying membrane) and localized dispensing and desiccation of proteinase K, both of which would be difficult to implement in microchannel ITP formats. The device's processes are separated into three main areas: blood filtration/fractionation, on-paper plasma protein digestion, and nucleic acid extraction. Although integrated, on-device amplification has been shown by the Posner Research Group previously,[105] I chose to focus on integration and upstream sample preparation in this work, using off-device amplification for device validation.

Blood fractionation is important in many blood-based NAAT applications, particularly HIV viral load monitoring, to remove potent amplification inhibitors such as hemoglobin[88] and to remove sources of proviral DNA (e.g. white blood cells). Many current POC NAAT platforms use cell-free plasma sample

and require an initial blood centrifugation step.[80] In this device, erythrocytes and leukocytes are trapped by and remain in the integrated Vivid plasma separation membrane, resulting in cell-free plasma in the underlying membrane. Previous publications have shown Vivid membrane integration into various devices, with plasma extraction efficiencies ranging from 25-80%.[91,164,183,186–188] The manufacturer, Pall, reports >80% plasma extraction efficiency in their marketing materials. I achieve a plasma extraction efficiency of 72 ± 6.8 % (n=9) when I place the Vivid plasma separation membrane passively on top of the Fusion 5 membrane with no additional fixturing. I refer to this as the "standard configuration" or "unoptimized configuration" and illustrate this in Figure 2-3.

By adding the blood filtration fixturing which applies a compressive force between the separation membrane and the underlying Fusion 5, I achieve 88 ± 4.4 % (n=5) plasma extraction efficiency. Optimization of the rastered relief section is required in the blood fixturing design, as too little of a relief (i.e. more compressive force) results in increased hemolysis, while too much of a relief does not provide enough compressive force and overall extraction efficiency decreases (data not shown). Free hemoglobin in the filtered plasma was measured as 3.89 ± 0.86 mg/dL (n=4), well within normal reported plasma free hemoglobin levels.[189] Free hemoglobin in plasma obtained via centrifugation was measured as 1.86 ± 0.10 mg/dL (n=4). Hemocytometer images showing whole blood before and cell-free plasma after filtration are shown in Figure 2-4.

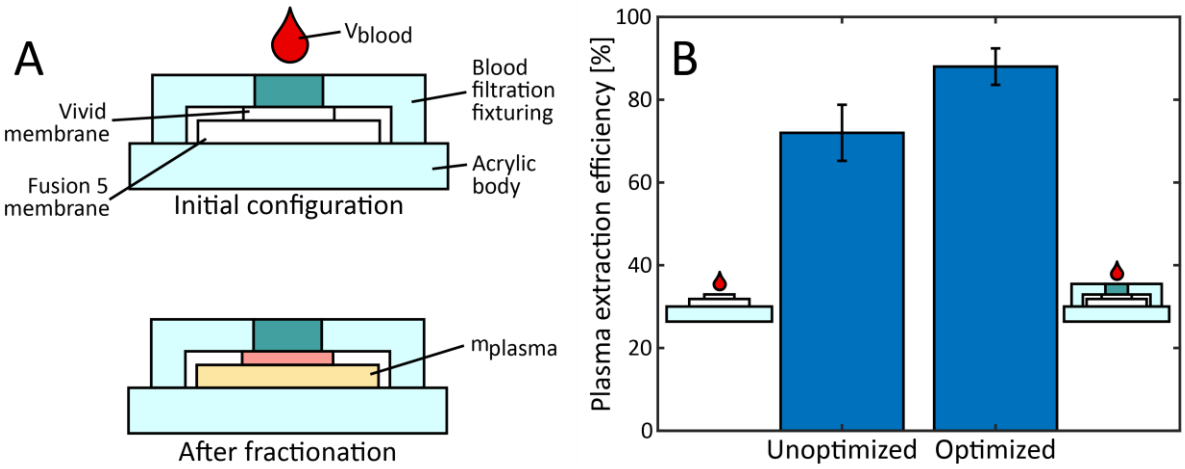

Figure 2-3: Schematic of blood fractionation/filtration process. The standard configuration represents an assembly in which the Vivid plasma separation membrane is simply placed on top of the Fusion 5 membrane underneath. I achieve a plasma separation efficiency of 72% (±6.8%, n=9) with this configuration. The optimized configuration represents an assembly in which an additional acrylic fixturing (blood filtration fixturing) is added on top of the Vivid membrane. This fixturing applies a compressive force to the Vivid, ensuring sufficient contact with the underlying Fusion 5 membrane. I achieve a plasma extraction efficiency of 88% (±4.4%, n=5) with this configuration.

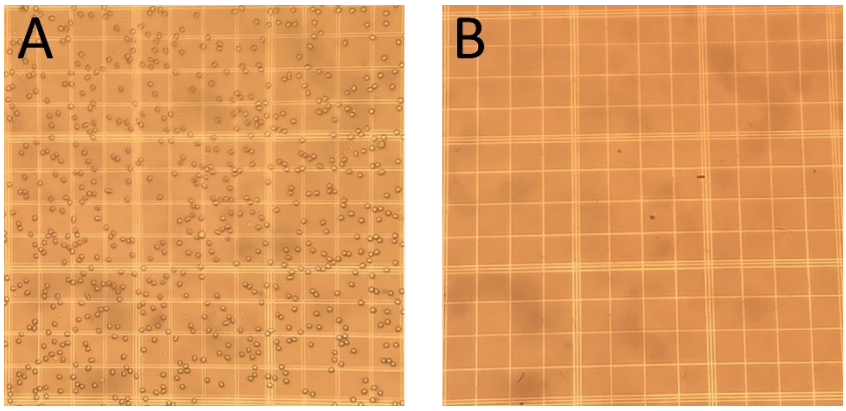

Figure 2-4: Hemocytometer images of whole human blood , before and after fractionation via the integrated Vivid plasma separation membrane. (A) Whole human blood that has been diluted 200 times with PBS. (B) Undiluted filtered plasma that has been centrifuged from the Fusion 5 membrane after filtration. No cells are visible.

I find that protein digestion is necessary for successful isotachophoretic extraction of nucleic acids from filtered plasma/serum samples. This is in agreement with other studies, which performed some form of protein digestion/degradation prior to extraction.[104,105,126,190,191] A common explanation for this requirement is that target nucleic acids and large proteins form complexes which modify the electrophoretic mobility of the nucleic acids, impeding migration and extraction. The majority of isotachophoretic extractions to date have used tube-based protein digestion as a pretreatment step prior to sample addition into the ITP system as a separate user step. Marshall *et al*. incorporated proteinase K into their trailing electrolyte to simplify their process.[190] Bender *et al.*, using a paper-based ITP system, spotted a small amount of proteinase K onto a glass fiber membrane before sample addition.[105] In this work, I employ a similar procedure in which proteinase K is dispensed onto a membrane prior to sample addition. To better understand this process, I performed sodium dodecyl-sulfate polyacrylamide gel electrophoresis (SDS-PAGE) to visualize protein digestion. Figure 2-5 shows several SDS-PAGE gels showing the results of this digestion process, at varying proteinase K concentrations and conditions.

While most traditional protein digests are performed over several hours, I chose to limit the digestion time to 15 minutes in order to reduce the overall protocol time, more consistent with point-of-care applications. In Figure 2-5, Lane 2 shows undigested human serum. The large band for albumin is visible between the 50 kDa and 75 kDa. Lane 3 represents a typical digestion buffer for DNA extraction (50 μg/mL proteinase K and 0.5% SDS) with the digestion performed in a tube in a water bath at 55 °C. The dark albumin band looks to be completely digested, with many digestion products visible between 37 kDa and 25 kDa.

If this same buffer (proteinase K and SDS) is used with the on-paper protocol in desiccated form, the digestion looks similar to (or even slightly worse than) on-paper digests performed with only proteinase K (detailed more in Figure 2-6A). Lanes 4-7 show digestions with various concentrations of proteinase K only, performed in a tube in a water bath at 55 °C. The completeness of digestion increases with proteinase K concentration, as to be expected. Lanes 8-11 are digests with the same proteinase K concentrations

performed using the on-paper digestion protocol at 55 °C. A similar concentration-digestion correlation is observed, though generally less overall digestion occurs compared to the tube-based digestions. I hypothesize that the reduced effectiveness of the on-paper digestion is due to some loss of proteinase K activity during the desiccation process. More sophisticated immobilization techniques, such as lyophilization, may reduce this effect. Lanes 13-16 show on-paper digestion performed at 37 °C. Lanes 17-20 are on-paper digests performed at room temperature (20 °C). I do not observe significant differences between the three temperature conditions when performing on-paper digestion. This is consistent with studies reporting proteinase K retains more than 80% of its activity between 20 °C and 60 °C.[192] Figure 2-5 represents a compilation of two different gels: Lanes 1-12 represent one gel, while Lanes 13-19 were performed on a separate gel due to gel size limitations. As such, there is some inter-gel variability due to staining/de-staining as well as inherent digestion variation, though I focus primarily on major differences between lane band structures.

I see a slight temperature dependency when in-tube digestion is performed, though only at high proteinase K concentrations (shown in Figure 2-6B).

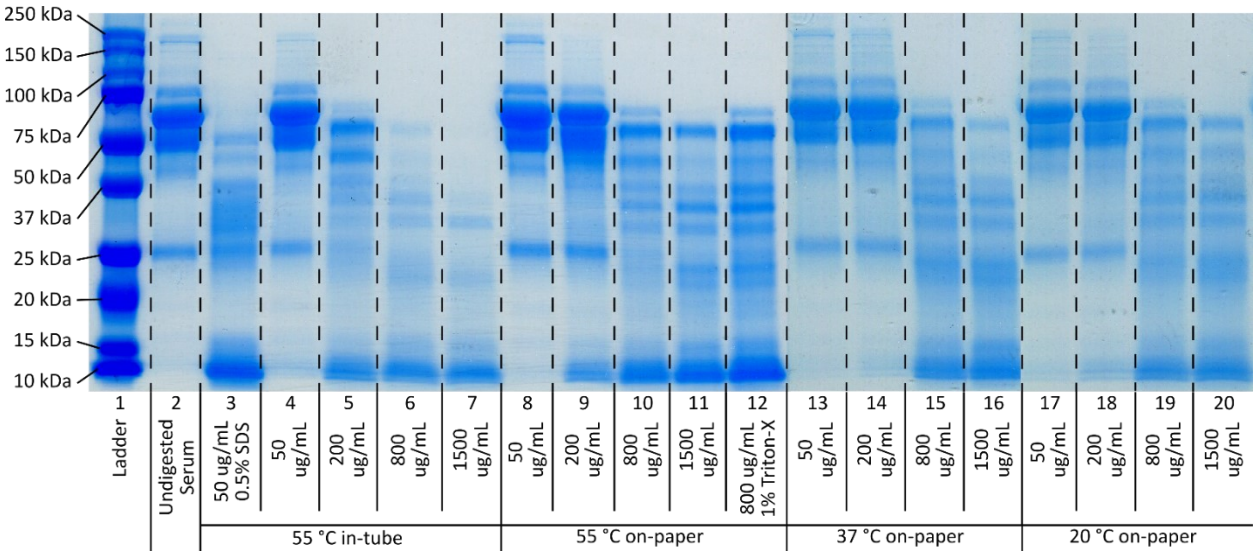

Figure 2-5: SDS-PAGE results of human serum protein digests via proteinase K. All digests were performed for 15 minutes to limit the overall protocol timespan. Lane 1 is a protein ladder (ranging from 250 kDa to 10 kDa) and lane 2 is undigested human serum. Lane 3 represents a commonly used digestion buffer for DNA extraction protocols, with 50 µg/mL proteinase K with 0.5% (w/v) SDS, digested in a microcentrifuge tube in a water bath at 55 °C. Lanes 4-7 show the effect of various proteinase K concentrations (50-1500 µg/mL) without SDS present, in a water bath at 55°C. Without SDS, the digestion is significantly diminished, though there is a clear relationship between digestion completion and proteinase K concentration. Lanes 8-11 show the same proteinase K concentration range using the on-paper digestion protocol at 55 °C. I see a lower digestion completion when compared to the in-tube protocol, though the same concentration dependent relationship is present. Lanes 13-16 and lanes 17-20 show the same proteinase K concentration range, using the on-paper digestion protocol at 37 °C and 20 °C, respectively. No significant difference is observed between the various temperature conditions.

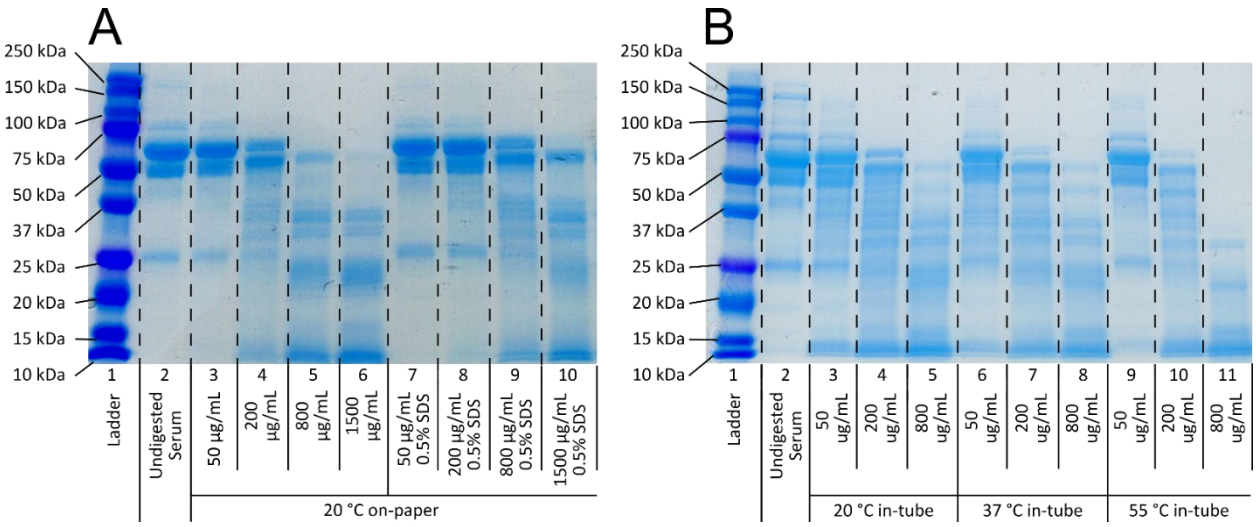

Figure 2-6: Additional SDS-PAGE results of various human serum digestions via Proteinase K. (A) All digests are performed for 15 minutes at room temperature (20 °C), using the on-paper digestion protocol described in the main text. Lane 2 shows undigested human serum. Lanes 3-6 show digests performed at varying concentrations of Proteinase K. Lanes 7-10 show digests performed at the same concentrations of Proteinase K, but with the addition of 0.5% SDS to the Proteinase K solution. Interestingly, these lanes show slightly less digestion when compared to Lanes 3-6. (B) SDS-PAGE results of human serum digestions via Proteinase K at various temperatures in-tube. Lane 2 shows undigested human serum. Lanes 3-5 show digests performed at 22 °C. Lanes 6-8 and Lanes 9-11 show digests performed at 37 °C and 55 °C, respectively. All digests are performed for 15 minutes in-tube. A slight dependency of digestion completeness on temperature is observed, with the most pronounced at higher Proteinase K concentrations (800 µg/mL).

I then evaluated the acceptability of the digestion in this system by the ability of ITP to successfully migrate and purify nucleic acid. Spatiotemporal maps of ITP extraction progression recorded via fluorescence microscopy while using various concentrations of proteinase K and on-paper digestion protocol are shown in Figure 2-7. When undigested serum is used (i.e. no proteinase K, Figure 2-7A), the labeled DNA forms a diffuse ITP plug and does not migrate downstream (from left-to-right in Figure 2-7).

When proteinase K partially digests the serum (i.e. 50 µg/mL and 200 µg/mL), the labeled DNA forms a marginally concentrated ITP plug, but still fails to migrate downstream (Figure 2-7B and Figure 2-7C).

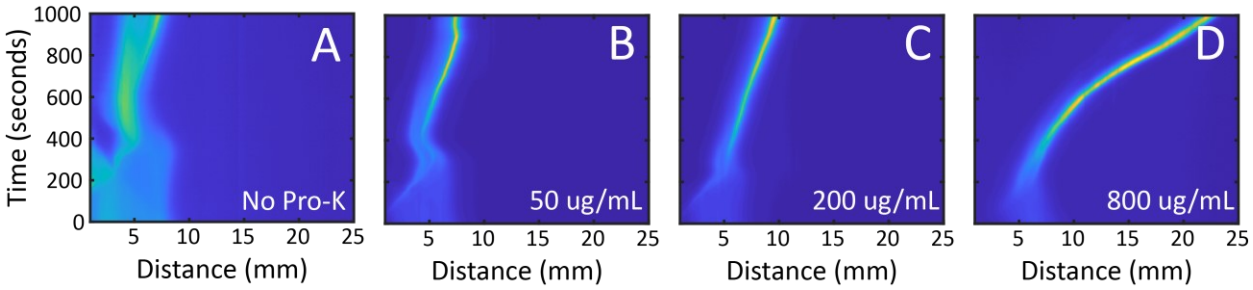

Figure 2-7: Spatiotemporal maps of representative ITP progression with varying concentrations of proteinase K, visualized via fluorescently-labeled tracking DNA with the on-paper paper digestion protocol. (A) When no proteinase K is used, the tracking DNA focuses into a diffuse region and does not migrate down the length of the Fusion 5 membrane. (B) and (C) When moderate concentrations of proteinase K are used, the fluorescently labeled DNA focuses into a concentrated plug, although the plug still does not migrate well downstream. (D) When 800 µg/mL proteinase K is used, the tracking DNA is focused into a concentrated plug and migrates down the length of the strip successfully.

Poor spatial migration is problematic because the target nucleic acids are not sufficiently concentrated or spatially separated from inhibitors present in the sample. Figure 2-7D shows the ITP migration when 800 µg/mL proteinase K is used. A highly concentrated ITP plug is formed and successfully migrates down the entirety of the Fusion 5 membrane. Similar behavior is seen when 1500 µg/mL proteinase K is used. The SDS-PAGE results show that large proteins are still present with proteinase K concentrations less than or equal to 200 µg/mL. I hypothesize that these large proteins play a large role in ITP dynamics by modifying the mobility of nucleic acids or binding to the porous membrane and increasing the system's electroosmotic flow. There likely lies a proteinase K concentration in this system and protocol between 200 µg/mL and 800 µg/mL that sufficiently digests the larger plasma proteins and allows for successful ITP migration and purification. I ultimately chose to use 800 µg/mL proteinase K with on-paper digestion protocols in subsequent experiments. A time series of successful ITP progression visualized by the fluorescently labeled tracking DNA in digested plasma is shown in Figure 2-8.

By comparing the integrated fluorescence density of the isotachophoretic plug region to the bulk fluorescence of the tracking DNA, I estimate that the extraction efficiency of my system is 21%. This is comparable to other isotachophoretic systems that perform nucleic acid extraction from complex samples.[110]

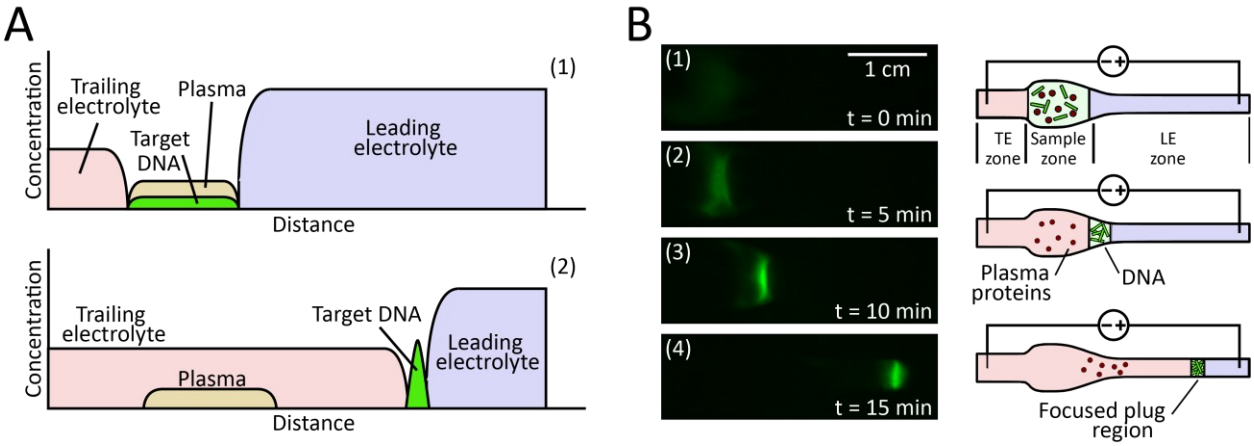

Figure 2-8: Images of ITP progression visualized via fluorescently labeled DNA. (A) Representation of species concentrations (1) before and (2) after ITP. (B) ITP progression visualized via fluorescently labeled DNA. (1) The sample is initially diffuse enough that no fluorescence is detected. (2-3) As ITP progresses, the sample concentrates into a distinctive ITP plug region. (4) The concentrated and purified plug region migrates down the length of the membrane until reaching the eluate port, at which point the membrane section containing the nucleic acids is cut and removed for amplification.

I present RPA amplification curves showing amplification of target DNA that has been extracted from whole blood, shown in Figure 2-9. I show amplification for input target DNA copy concentrations of $3x10^5$ copies/mL, $3x10^4$ copies/mL, and $3x10^3$ copies/mL in whole blood. These copy concentrations correlate to input copy numbers of 10,000 copies/trial, 1,000 copies/trial, and 100 copies/trial, respectively. I also performed RPA amplifications with target DNA diluted in whole blood directly added to RPA reactions without processing as a control, shown in Figure 2-9A. In these experiments, 5 µL of whole blood spiked with target DNA is added to a reaction, with the resulting amplification significantly inhibited,

consistent with previous studies that investigated the inhibitory effect of whole blood on RPA.[126,193] Figure 2-9B shows results using spun-out eluate, while Figure 2-9C shows the direct addition protocol, where the portion of Fusion 5 strip containing the ITP plug and target DNA is added directly to the RPA reaction tubes. In both protocols, all trials successfully amplified down to 100 cps DNA/trial ($3x10^3$ cps/mL whole blood). Trials below 100 cps DNA/trial did not consistently amplify. No template controls (NTC) did not amplify.

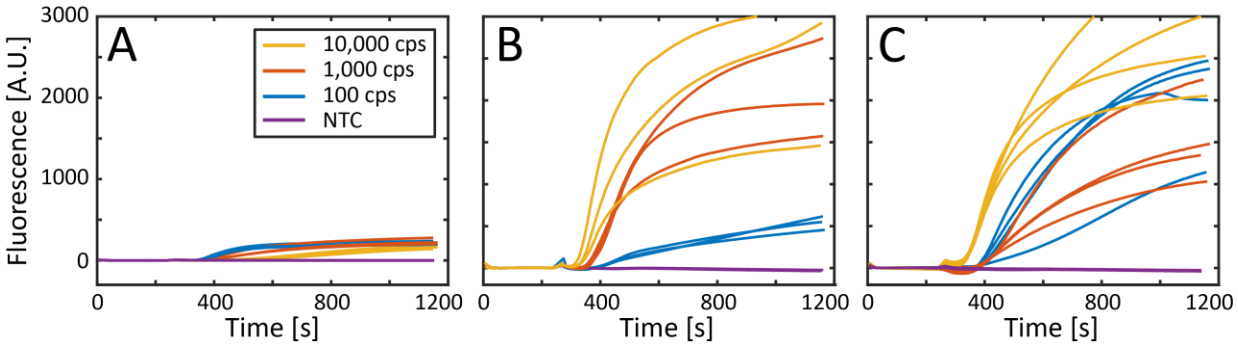

Figure 2-9: Recombinase polymerase amplification curves using DNA extracted from whole human blood. Input copy numbers of 10,000 cps/trial (yellow), 1,000 cps/trial (red), and 100 cps/trial (blue) correspond to input copy concentrations of $3x10^5$ cps/mL, $3x10^4$ cps/mL, and $3x10^3$ copies DNA per mL of input blood, respectively. NTC is a no template control. (A) Amplification of unextracted DNA in whole blood, with curves severely inhibited (B) Amplification curves using spun-out eluate (n=3 for all trials). (C) Amplification curves using the direct strip addition control (n=4 for all trials). All trials amplify down to 100 cps/trial ($3x10^3$ cps input DNA per mL of whole blood).

The direct addition trials' amplification slopes, endpoint fluorescence values, and time-to-threshold exhibit more variation than those of the spun-out eluates. I believe this is partially due to the effects the cut-out portion of Fusion 5 may have in the reaction tube, such as reduced mixing, nucleic acid or amplification enzyme loss due to non-specific binding with the membrane, or sensor/excitation beam obstruction of the T16-ISO. Strip effects are particularly apparent when the reaction tubes are removed, agitated, and placed back into the T16-ISO at the four-minute mark. Significant deviations in normalized fluorescence immediately after replacement of the tubes are observed, presumably due to the strip being repositioned

into or out of the excitation beam path during agitation and altering the measured fluorescence. This can be seen in several trials (e.g., 1,000 cps DNA in Figure 2-9C) where the normalized fluorescence is negative for a portion of time immediately after the tubes are returned to the readout machine. In preliminary experiments, I found that larger sections of Fusion 5 strip introduced into the RPA reactions had an even greater effect on fluorescence measurements, resulting in drastically different initial fluorescence values. I chose to use a 5 mm x 3 mm section of Fusion 5 to introduce the ITP plug and target DNA into the RPA reaction, though smaller strip areas may further mitigate strip-related interference. Other solutions may include removing the strip prior to amplification (i.e. dipping the strip into the reaction buffer) or a small insert that holds the strip away from the excitation beam path of the T16-ISO yet still in contact with the reaction volume. Other sources of variability (such inconsistent mixing, reagent degradation, inhibitor presence, etc.) may be controlled for by the inclusion of an internal positive control, similar to Rohrman *et al.*[194] or Gregory *et al.*[195]

2.4 Towards Integration of RNase Inactivation Chemistries for the Sample Preparation of Viral RNA

The described device represents a novel strategy and method for successful extraction and purification of target DNA from whole blood samples, while sample preparation for bloodborne RNA viruses, such as HIV, necessitates several additional considerations. The seemingly minor detail of RNA- vs. DNA-based targets significantly complicates sample preparation, as RNA molecules are significantly more prone to degradation compared to DNA. This susceptibility towards degradation can be primarily attributed to the hydroxyl group located at the 2' location on the ribose sugar in RNA. This hydroxyl group is reactive and can be easily hydrolyzed, ultimately breaking the phosphodiester bond in the sugar-phosphate backbone.[196] By contrast, DNA has a non-reactive hydrogen atom at this location. While this hydrolysis can occur passively (e.g. non-catalyzed), it is often facilitated by RNase enzymes: a family of

ubiquitous enzymes that degrade RNA molecules very efficiently. RNases are readily found in most environments and are the main reason for many laboratory precautions when working with RNA samples.[197] RNases are present in biological specimens and are at particularly high concentrations in blood-based samples including whole blood, serum, plasma, or derivatives.[43,167] Tsui *et al*. showed that over 99% of exogenous RNA added to human plasma becomes non-amplifiable via PCR after only 15 seconds of contact time, illustrating the high turnover efficiency of these enzymes.[167] RNases are also extremely hardy, resisting thermal deactivation and more common enzymatic deactivation protocols.[168] Chemicals used in traditional sample preparation (e.g. guanidinium thiocyanate, ß-mercaptoethanol, sodium dodecyl sulfate) completely denature protein structures, rendering RNases inert, though these chemicals are inherently incompatible with subsequent amplification, necessitating multiple wash and centrifugation steps. These chemical agents are also incompatible with ITP-based separations due to their high concentrations (typically 6M guanidinium hydrochloride 200-300 mM ß-mercaptoethanol, 0.5 – 0.1% sodium dodecyl sulfate) and similarity in electrophoretic mobility to nucleic acids.

Previous work has shown ITP-compatible RNase inactivation and subsequent ITP-based extraction of HIV RNA from HIV+ serum samples.[46,109] This work leveraged a wide-spectrum protease (proteinase K), detergent (SDS), and disulfide bond reducer (dithiothreitol) to denature and inactivate endogenous RNase enzymes in serum. These reagents also function as lytic agents, lysing virions and freeing the genomic RNA. In these works, tube-based incubations of serum samples with RNase inactivation chemistries for 15 minutes at 65 °C were performed to lyse virions and inactivate RNases prior to ITP-based extraction, requiring several pipetting steps to transfer and mix reagents and samples. In this section, I describe the development of dried and lyophilized RNase inactivation chemistries for integration onto paper membranes for eventual viral RNA extraction via the described ITP-based device.

In addition to the work described earlier in this chapter, several other works have shown the integration and drying of various chemical reagents into paper-like membranes for point-of-care diagnostic applications. These reagents have included amplification reagents and/or lytic agents.[147,198,199] This strategy

is advantageous as the reagents are often rehydrated by the sample itself when it is introduced to a device, removing any manual pipetting, mixing steps, or separate reagent storage. Methods for reagent deposition can range from simple air drying (leveraged previously in this chapter) to more complicated lyophilization procedures. The chosen drying/incorporation method is extremely reagent specific, particularly with enzymatic reagents. This is primarily due to the strong form-function relationship of enzymes. Many enzymatic structures are stabilized by hydrophilic and hydrophobic interactions between constituent amino acid groupings in aqueous environments, with more hydrophobic amino acids folding towards the center of the protein and more hydrophilic groups located on the exterior. In some cases, as the liquid phase is evaporated to dry reagents onto membranes, the resulting lack of hydrophilic/hydrophobic interactions leads to the unfolding of enzymes, effectively inactivating them.[200] Many enzymes (such as polymerases and reverse transcriptases) have been specifically designed to be more robust and are marketed as air-dryable. Additional excipients are often included in these mixes, such as various saccharides molecules which help thermodynamically stabilize the enzymes in dried form.[200] In these air-dryable systems, the reagents are simply deposited on the membranes with the water subsequently evaporated off (typically using an oven or desiccator). Lyophilization, or freeze-drying, is another common dehydration method. In these systems, the reagents are deposited and then frozen in the membrane, after which the ice is then sublimated away. Various sugars (e.g. sucrose, trehalose, mannitol, etc.) are almost always included for lyophilization as they form an amorphous glass-like solid that helps stabilize enzymes during the sublimation process.[201] Lyophilization is often considered the "gold-standard" method for reagent deposition as even the most sensitive enzymes can often be lyophilized into a stable powder form. However, the process requires large and expensive lyophilizers, as well as significant knowledge on appropriate excipient combinations/ratios and specific processing steps that are often considered to be closely-guarded trade secrets.

2.4.1 Lyophilization

Lyophilization is typically performed in three distinct stages: freezing, primary drying, and secondary drying.[202] The first stage, freezing, lowers the temperature of the sample until the water present in the sample has thoroughly solidified, undergoing ice nucleation and ice crystal growth. During primary drying, the pressure is reduced below the vapor pressure of ice with a small amount of heat then added to drive sublimation of ice into the vapor phase. After primary drying, small amount (10-20%) of residual water moisture often remains in the sample.[203] In secondary drying, the low pressure is maintained while the temperature is raised (usually between 10-50 °C) to drive off this final moisture, resulting in a thoroughly dry and stable lyophilized product.

The method and rate of freezing can have significant impacts on subsequent processing parameters and sample stability, and this stage greatly contributes to final sample characteristics. Freezing methods are usually described as slow-freezing (e.g. freezing the sample overnight in a -20 °C freezer) and flash- or fast-freezing (e.g. dipping the sample in liquid nitrogen). During slow-freezing processes, the kinetics of ice nucleation and crystal growth will favor larger, but fewer ice crystals, while flash-freezing produces many smaller ice crystals.[201] Larger crystals are often advantageous for primary drying, as this results in less tortuous paths for water vapor to escape. Smaller crystals result in more difficult path for water vapor to escape, significantly extending primary drying times which can be on the order of days.[204] This concern is more important in vial-based lyophilization, where there may be a significant thickness/height of initial solution and the ratio of free-surface area to volume of frozen sample is relatively small (e.g. vapor molecules from ice crystals at the bottom of a vial have large mean escape paths). This is likely less important when lyophilizing samples directly onto paper-like membranes, where the free-surface area to volume is relatively high (and water molecules have small mean escape paths). Slow-freezing methods extend the contact time between various sample species, some of which may react with each other. During the crystal growth stage of ice formation, solvent water is continually being removed from the system (as it is being “sequestered” within the solid ice being formed), resulting in the effective concentration of all

solutes present in the sample which may further increase reactivity.[204] It is important that the sample and all constituents are completely frozen prior to advancing to primary drying. Often, enzymes will be stored in some percentage of glycerol, which can prevent complete freezing. This typically necessitates the use of glycerol-free enzymes, which may or may not be readily available. Ultimately, the method, time, and temperature used in the freezing step is extremely sample and final form-factor dependent.

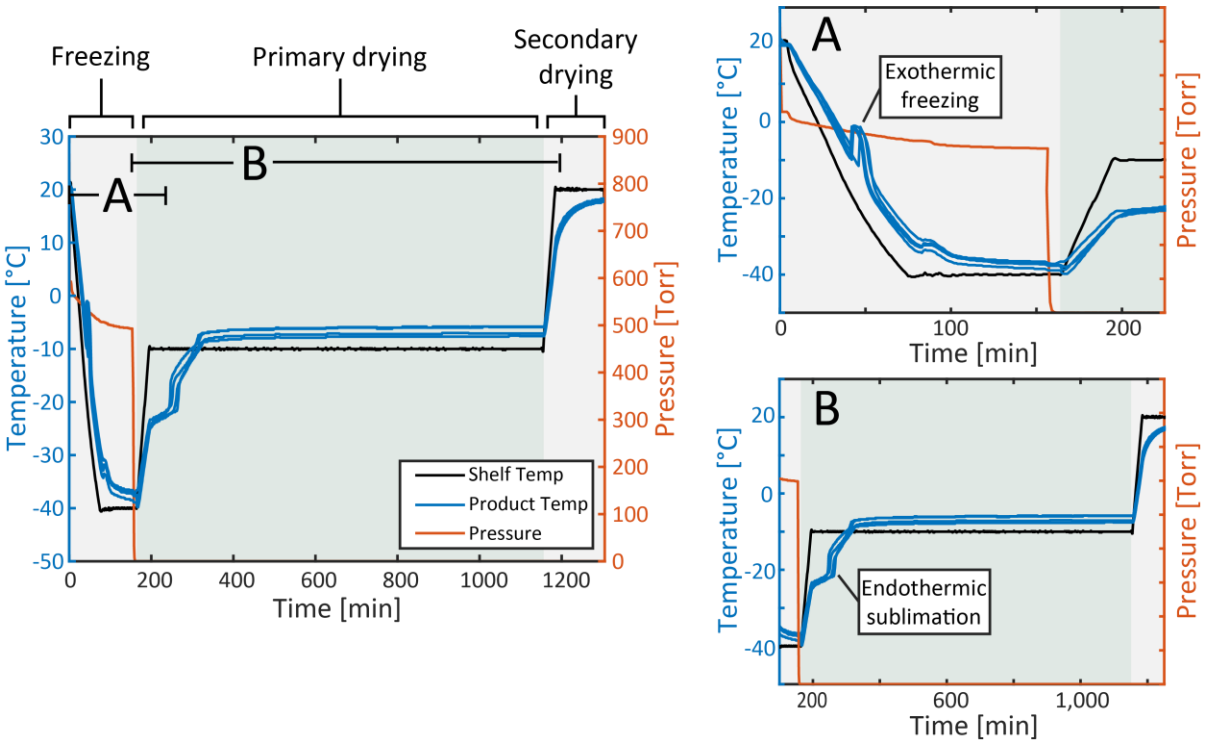

Figure 2-10: Temperature and pressure profiles from an investigatory lyophilization run**.** The product temperature is measured by several thermocouples placed in tubes containing reagents to be lyophilized. The three stages (freezing, primary drying, and secondary drying) are shown, with (A) freezing and (B) primary drying detailed. (A) During the freezing stage, the shelf temperature gradually decreases to the setpoint of -40 °C. The product temperature decreases as well, with the sharp increase in temperature near -10 °C indicative of exothermic product freezing. After complete freezing, the product temperature decreases until it reaches the shelf temperature. During primary drying in (B), the shelf setpoint is raised to -10 °C while the pressure is reduced below the vapor pressure of the ice. This increase in heat drives sublimation of the solid ice. As the shelf temperature increases, the product temperature increases as well, though the product temperature is lower than the shelf temperature due to endothermic sublimation. Once the majority of sublimation has occurred, the product temperature reaches the shelf temperature and primary drying is considered completed. Note that in this experiment, the primary drying phase extended far past what was likely required, though this extended primary drying should not adversely affect product quality. Finally, in secondary drying, the shelf temperature is increased to 20 °C while keeping the pressure low to further drive off any residual water content.

During primary drying, the pressure in the lyophilizer is lowered below the vapor pressure of ice, while the shelf temperature is raised to supply heat to drive ice sublimation. In manifold lyophilization, the ambient environment provides the necessary heat of sublimation. This stage requires the longest time and is often targeted for optimization to reduce lyophilization cycle runtimes. Typical pressures used are 50-200 mTorr, while the shelf temperature is dictated by the sample being lyophilized. It is advantageous to use as high of a shelf temperature as possible, as each 1 °C increase in temperature will reduce the amount of time required to complete primary drying by as much as 13%.[202] It is important to keep the shelf temperature below the product collapse temperature (T_c), which is the temperature at which the product loses mechanical stability and collapses, and is often very close to the eutectic or glass transition temperatures of the sample.[202] Determining the endpoint of primary drying can be challenging; the most accessible method is often to measure the temperature of the sample/product throughout the lyophilization run, though other methods, such as manometric temperature measurement, which measures the vapor pressure in the lyophilizer can also be used (though this requires additional equipment).[205] As sublimation is an endothermic reaction, the sample temperature will be lower than the shelf temperature as sublimation progresses; once the sample temperature reaches the shelf temperature, it is assumed that sublimation has finished.

When primary drying is completed, there is still significant residual moisture present in the sample. (10-20%).[202] To drive off this residual moisture, the shelf temperature is raised to 10-50 °C while keeping the chamber pressure low. The main purpose of this secondary drying is to further lower the residual moisture content of the sample to less than 1%. Determining the proper processing conditions (i.e. time and temperature) for secondary drying can be difficult, requiring repeated gravimetric measurements of the sample throughout the drying process.[206]

Production-scale lyophilization must also take into consideration the condenser capacity, as the sublimation of ice can overwhelm these systems if significant sample volumes are used, though in research scale runs this is rarely an issue. Various other preliminary investigatory processes, such as differential

scanning calorimetry, are often used to better understand the various critical temperatures of the sample (such as eutectic and glass transition temperatures). These temperatures then dictate temperatures used in the lyophilization process. Lyophilization success is often determined by visual appearance of the resulting cake (for tube- and vial-based formats), residual water content, and stability/effectiveness of the product after storage.[207]

In this sub-section, I show the integration and lyophilization of ITP-compatible RNase inactivation chemistries into paper-like analytical membranes. I detail the development of the lyophilization procedure and show that as serum is added to the paper membrane and incubated at 65 °C for 15 minutes, RNase inactivation chemistries are rehydrated, completely inactivating and eliminating the baseline RNase activity of serum. This is an important step towards an integrated point-of-care device for the isotachophoretic extraction of HIV RNA from HIV+ serum samples.

2.4.2 Air-Drying and Lyophilization Procedures

RNase inactivation chemistries included sodium dodecyl sulfate (71725, Sigma-Aldrich, USA), proteinase K (AM2546, Thermo Fisher Scientific, USA), and dithiothreitol (D9779, Sigma-Aldrich, USA). I tested trehalose (T0167, Sigma-Aldrich, USA), mannitol (M4125, Sigma-Aldrich, USA), and Lyophilization Reagent (2X) (OPS Diagnostics, USA) as lyoprotectants.

In all experiments, Fusion 5 (GE Healthcare Life Sciences, USA) is used as the primary membrane. I first block the membrane with 1% bovine serum albumin and 0.01% Triton-X 100 (Sigma, USA) for 15 minutes and then dry the membrane for 1 hour in a desiccator at room temperature. I then back the membranes with PCR tape (TempPlate RT Select Optical Film, USA Scientific, USA) and use a plotter-cutter (FCX4000-50ES, Graphtec America, Inc., USA) to cut the backed and blocked membranes to 18 mm diameter circles designed in AutoCAD (AutoDesk Inc., USA). This diameter of Fusion 5 corresponds with an absorption capacity of 100 μL.

The RNase inactivation chemistries are pipetted onto the blocked and backed Fusion 5 membrane. In air-drying experiments, the membrane is desiccated for 3 hours at room temperature. In lyophilization trials, various excipients are also added to the RNase inactivation chemistries before pipetting: trehalose, dextran, mannitol, and a proprietary mannitol-based lyophilization reagent (OPS Diagnostics, USA). In lyophilization screening experiments, 100 µL of RNase inactivation chemistry and excipients are added to the 18 mm diameter blocked and backed Fusion 5 membranes. I then place the membranes immediately into a -80 °C freezer to fast-freeze the reagents for 15 minutes, and then transfer them into a prechilled lyophilizer set at -40 °C (AdVantage Pro, SP Scientific, USA). The lyophilizer is programmed with the protocol shown in Figure 2-11.

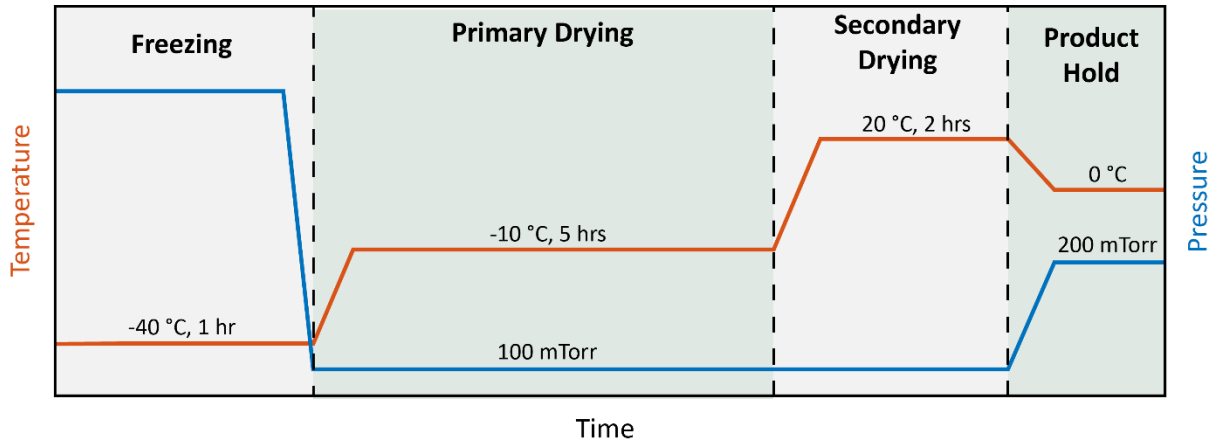

Figure 2-11: Lyophilization procedure for RNase inactivation reagents on Fusion 5 membranes. Membranes are flash-frozen in a -80 °C freezer before being placed in the lyophilizer (which is prechilled to -40 °C).

2.4.3 RNase Activity Assay

I use the RNase Alert Assay (Integrated DNA Technologies, USA) to measure the level of RNase activity of serum (and the efficacy of RNase inactivation chemistries). This assay uses short RNA oligonucleotides onto which a fluorophore and quencher are conjugated to opposite ends. While the oligo strand is intact, the fluorophore is quenched, and the assay does not fluoresce. When RNases are present in the assay, the RNA oligo stands are cleaved and the fluorophores produces measurable fluorescent signal,

recorded by a fluorometer in real-time with the rate of fluorescence increase proportional to RNase activity. The assay mechanism is shown in Figure 2-12.

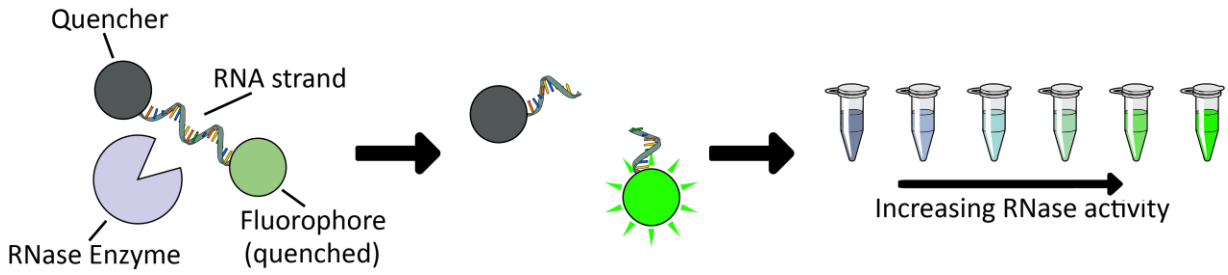

Figure 2-12: RNase Alert assay mechanism**.** The RNA oligonucleotide is initially intact, confining the conjugated fluorophore and quencher in near proximity to each other, resulting in no fluorescence. If RNase activity is present, the oligo is cleaved by an RNase molecule, and the quencher and fluorophore are free to drift, and the fluorophore is no longer quenched, producing a measurable fluorescent signal which is proportional to RNase activity.

First, 100 µL of pooled, sterile-filtered human serum (H4522, Sigma-Aldrich, USA) is pipetted onto an 18 mm diameter Fusion 5 membrane impregnated with various RNase inactivation chemistries (either air-dried or lyophilized). I seal the membrane against a glass slide with PCR tape and incubate it on a hotplate set at 65 °C for 15 minutes. The tape is then removed and the membrane placed into a 0.5 mL micro-centrifuge tube that has a small opening at the bottom. This micro-centrifuge tube is then placed in a larger 1.5 mL micro-centrifuge tube and both tubes are placed in a centrifuge (5415D, Eppendorf, DEU) for 3 minutes at 6,000 rcf to collect the treated serum eluate. I assemble the RNase Alert Assay in a lidded 96-well plate (3606, Corning Inc., USA). Briefly, 60 µL of chilled DEPC-treated water, 10 µL of each RNase Alert Buffer and RNase Alert Substrate, and 20 µL of spun-out treated serum eluate are added to each well. The plate is immediately lidded and placed into a plate reader (SpectraMax iD3, Molecular Devices, USA). The plate is incubated at 37 °C for 30 minutes with agitation, and the fluorescence is measured every 2 minutes. The excitation and emission wavelengths are set to 485 nm and 535 nm, respectively. Each condition is tested in 5 replicates. In each experiment, I include a negative control of DEPC-treated water, as well as a positive control of RNase A (2250G, Thermo Fisher Scientific, USA) at

a concentration of 1.5 U/L, with the maximum fluorescence of this positive control used to normalize the fluorescence values of each experiment. Often, a control of untreated serum is also included to illustrate the baseline RNase activity of the sample.

2.4.4 Results and Discussion

In screening tests of RNase inactivation chemistries and deposition methods, I used the ITP-compatible chemistries developed by Bender *et al*. as an initial starting point, with a solution of 0.5% SDS, 1 mg/mL proteinase K, and 10 mM DTT.[46,109] Fresh, liquid reagents mixed with serum, deposited onto a Fusion 5 membrane, and incubated at 65 °C for 15 minutes results in complete RNase inactivation, as shown in Figure 2-13A, given that no significant increase in fluorescence is observed in the RNase Alert Assay. This is in agreement with previous studies.[109] In contrast, untreated serum shows significant inherent RNase activity. Interestingly, air-drying these reagents onto Fusion 5 membranes via room-temperature desiccation results in significantly more RNase activity, even outpacing untreated serum. I hypothesize that this is due to the fact that while proteinase K can withstand 0.5-1% SDS, concentrations of the respective reagents increase significantly during air-drying as the solvent water is evaporated and removed, resulting in concentrations of SDS significantly above this threshold. Bender *et al*. have shown that serum in the presence of surfactants or detergents alone can increase endogenous RNase activity, likely due to disruption of semi-protective protein-RNA complexes.[46] As the proteinase K is likely denatured or inactivated during the air-drying process, this likely explains the poor result. Similar loss of proteinase K function is observed in SDS-PAGE gels of serum digested in membranes with desiccated proteinase K and SDS solutions in Figure 2-6A in Section 2.3 . While additional excipients may reduce this effect, lyophilization was investigated next.

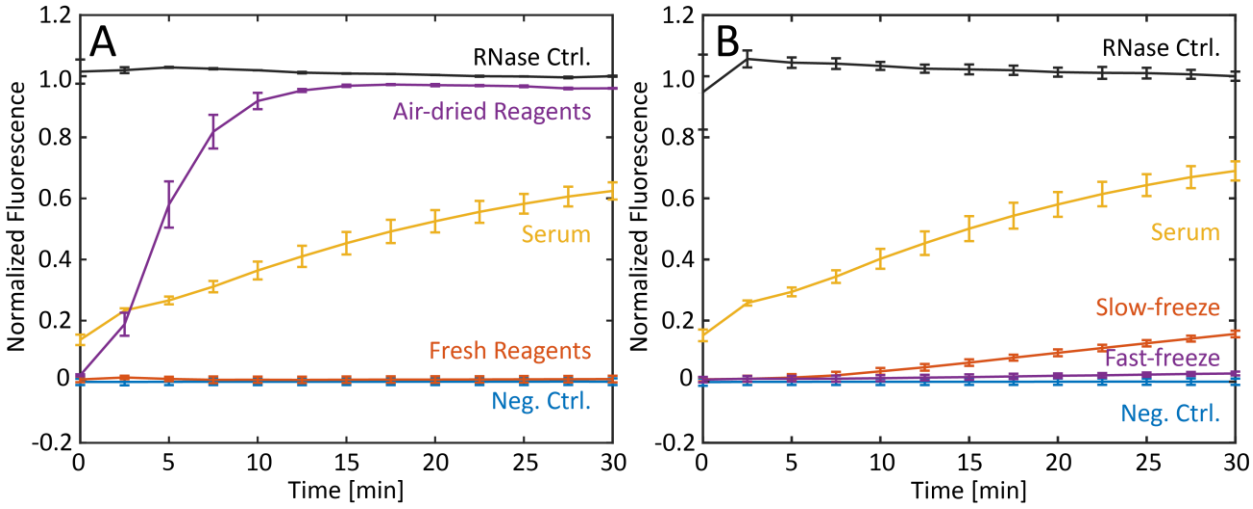

Figure 2-13: Initial screening of RNase inactivation chemistries via RNase Alert Assay. (A) Effect of air-drying RNase inactivation reagents (0.5% SDS, 1 mg/mL proteinase K, 10 mM DTT) onto Fusion 5 membranes on serum RNase activity. Untreated serum shows significant RNase activity, while liquid, fresh RNase inactivation reagents completely inhibit RNase activity in serum. Air-drying these reagents onto Fusion 5 membranes increases the RNase activity of the serum, likely due to proteinase K denaturation by increased SDS concentrations as solvent water is removed during drying. (B) Effects of lyophilized RNase inactivation reagents (0.5% SDS, 1 mg/mL proteinase K, 10 mM DTT, 10% trehalose) in tube format on serum RNase activity. Lyophilized reagents reduce the RNase activity of serum significantly after incubation. A difference between slow-frozen tubes vs. fast-frozen tubes is seen, with the fast-frozen tubes (immediately placed into a -80 °C freezer after mixing) inactivating RNases more completely. This result is hypothesized to be due to a similar SDS-proteinase K interaction as the air-drying results, where solvent water is slowly removed during slow-freezing, with the SDS concentrations increasing and denaturing the proteinase K with long contact times. Fast-freezing likely limits this contact time, preserving proteinase K efficacy.

Lyophilization in tube formats was used as an initial starting point. Solutions of 0.5% SDS, 1 mg/mL proteinase K, 10 mM DTT and 10% trehalose as a lyoprotectant (among other additives and lyoprotectants) were lyophilized. Good cake formation was observed for the majority of tubes/solutions tested, though several exhibited collapsed cakes (shown in Figure 2-14). Various processing parameters were altered and tested, including the freezing rate of the tubes. I observed a significant decrease in RNase activity with serum treated with tubes that were frozen slowly (i.e. ramped down from ambient to -40 °C over the course of 2 hours) and then lyophilized, though not to the extent of fresh reagents. When the RNase inactivation solution was fast-frozen (i.e. placed immediately into a -80 °C freezer) and then loyphilized,

the ability to completely inhibit RNases present in serum nearly matched that of fresh reagents. This is shown in Figure 2-13B. I hypothesize that some loss of proteinase K efficacy occurs via increasing concentrations of SDS in the slow-freeze tubes, as the solvent water is slowly sequestered into the solid ice being formed (in a similar mechanism to the hypothesized loss of proteinase K efficacy seen in air-dried experiments). By fast freezing the tubes, the SDS (and/or DTT) has little time to interact with the proteinase K, maintaining its potency.

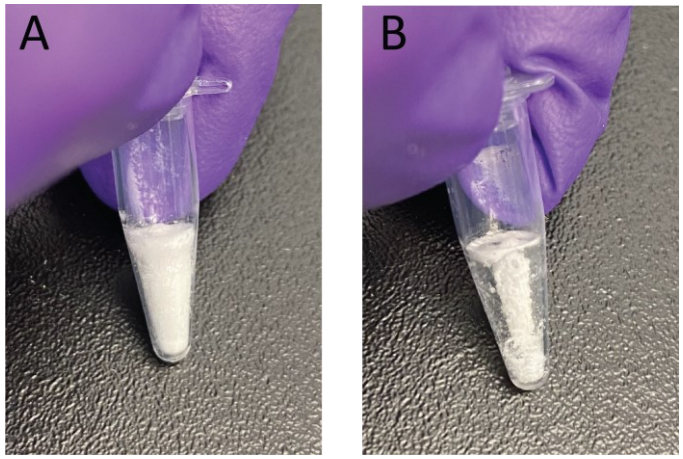

Figure 2-14: Example of lyophilized RNase inactivation chemistries in tubes as preliminary experiments. (A) 0.5% SDS, 1 mg/mL proteinase K, 50 mM DTT, with 10% trehalose as a lyoprotectant. A good cake is observed, typically indicative of successful lyophilization. (B) 0.5% SDS, 1 mg/mL proteinase K, 50 mM DTT with 10% trehalose and 2.5% mannitol as a lyoprotectant. The product is collapsed, likely due to exceeding the product's critical temperature during primary drying. Both tubes were processed identically, illustrating the importance of tuning lyophilization parameters to specific sample/product constituents.

I then used the fast-freezing protocol to lyophilize the RNase inactivation chemistries onto Fusion 5 membranes. When the RNase inactivation reagents are lyophilized onto bare, untreated Fusion 5 test circles (with 10% trehalose as a lyoprotectant), no reduction in the RNase activity of serum is observed (shown in Figure 2-15A). However, when the Fusion 5 is blocked (with 1% BSA and 0.01% Triton X-100) and backed with PCR tape, the RNase activity of treated serum is significantly reduced. This is likely explained by some reagents adsorbing to the glass fiber matrix in the untreated Fusion 5, while these sites

are blocked when the Fusion 5 is treated with BSA. Some residual RNase activity remains with these modifications. As the RNase inactivation chemistry concentrations are slightly increased to 0.7% SDS, 2 mg/mL proteinase K, and 50 mM DTT, RNase activity is completely eliminated (Figure 2-15). I find that choice of lyoprotectant does not have a significant effect on RNase inactivation, though minor differences and ease of use lead me to use the OPS Lyophilization Solution, a proprietary mannitol-based solution designed for lyophilization.

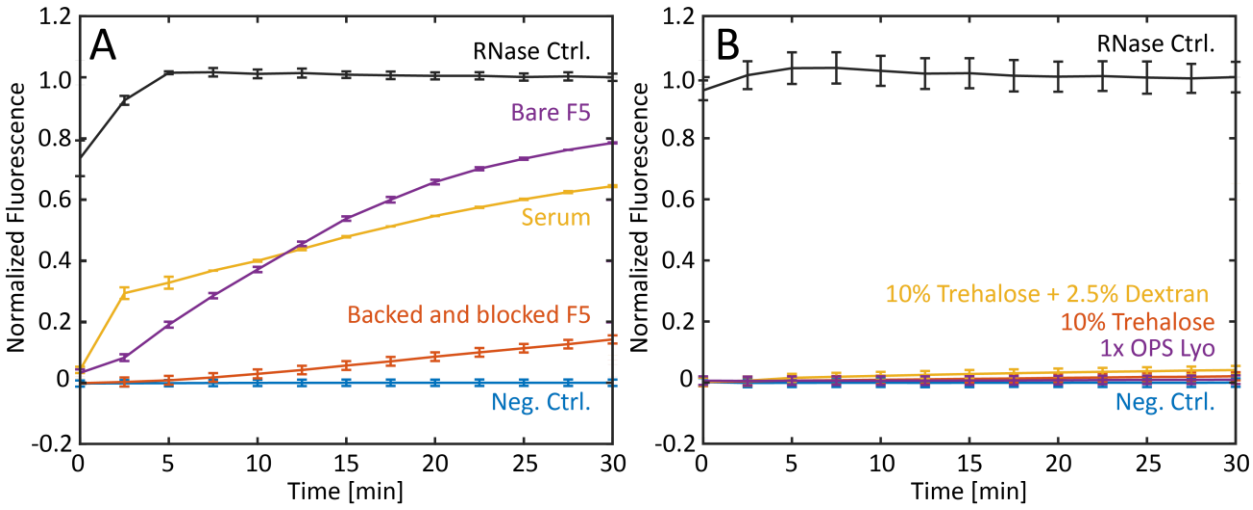

Figure 2-15: Efficacy of lyophilized RNase inactivation chemistries on Fusion 5 membrane on the RNase activity of serum. (A) Effects of backing and blocking Fusion 5 membranes prior to lyophilization of RNase inactivation reagents (0.5% SDS, 1 mg/mL proteinase K, 10 mM DTT, 10% trehalose). Lyophilizing these reagents onto untreated (bare) Fusion 5 does not reduce the RNase activity of serum. The RNase activity is significantly reduced when the Fusion 5 is blocked with 1% BSA and 0.01% Triton X-100 and backed with PCR tape prior to the addition and lyophilization of the RNase inactivation chemistry. (B) Effects on serum RNase activity of with increased concentrations of lyophilized RNase inactivation chemistry (0.7% SDS, 2 mg/mL proteinase K, 50 mM DTT) with various lyoprotectants onto blocked (with 1% BSA and 0.01% Triton X-100) and backed (with PCR tape) Fusion 5 membrane. The native RNase activity of serum is effectively eliminated after incubation for 15 minutes at 65 °C, with minimal difference between the various lyoprotectants tested.

This further integration of RNase inactivation chemistries onto paper membranes is an important step towards a comprehensive ITP-based nucleic acid amplification test device. These reagents are stable in dried format and can be rehydrated upon sample addition. The eventual goal of this work is further

integration into the previously described device, with the RNase reagents lyophilized onto the sample pad. This will require adjustment of the ITP system itself (LE, TE, applied voltage, etc.), as the additional BSA blocking and PCR tape backing affect isotachophoretic dynamics. As an example, in preliminary experiments, the addition of the BSA blocking resulted in significant reduction in electro-osmotic flow (EOF), leading to poor focusing and extraction of the target. It is common for ITP-based systems to require adjustment and recalibration as the sample characteristics change. Another area of necessary investigation is the interaction between the lyophilized RNase inactivation chemistries and the blood fractionation module/process. During early experiments of depositing alternative lysis chemistries (primarily proteinase K and Triton-X 100) onto the underlying Fusion 5 membrane, I found that these once these chemistries were rehydrated by the cell-free plasma, they would diffuse into the Vivid and lyse the trapped red blood cells, resulting in significant hemolysis and pass through of hemoglobin into the underlying membrane (shown in the Appendix A.3). It is unknown whether the RNase inactivation/lysis chemistries described here (i.e. proteinase K, SDS, and DTT) would have similar effects or if white blood cells (theoretically containing proviral DNA) would be affected, though this is an area of necessary investigation for further device integration.

2.5 Summary

In this chapter, I describe a paper-based nucleic acid amplification sample preparation device and protocol for the isotachophoretic extraction of target nucleic acids from whole human blood in under 30 minutes. A 33 μL volume of whole blood mixed with target nucleic acids is first fractionated and filtered via an integrated plasma separation membrane, achieving 88% plasma extraction efficiency. This device directly processes whole blood, thereby eliminating preliminary blood fractionation or dilution steps that are typically required for POC NAATs and ITP systems.[80] I process 33 μL of whole blood, a full order of magnitude larger volume than previous microfluidic ITP devices have reported.[104,175] Using large volumes of undiluted initial samples is important in applications in which low detection limits are required, such as

HIV viral load monitoring, as many devices are volume-limited and dilution significantly decreases the number of total target nucleic acids present in the device. On-paper plasma protein via proteinase K reduces the average size of the plasma proteins and allows for successful isotachophoretic extraction of the target nucleic acids. I use paper-based isotachophoresis to concentrate the target nucleic acids and separate them from amplification inhibitors present. The device presented here minimizes the number of user steps and sources of error by utilizing paper-based ITP buffer reservoirs and the self-filling characteristics of porous membranes, eliminating the need for more complex filling protocols. I then perform off-device RPA detection of the purified target nucleic acids by cutting out the portion of Fusion 5 membrane that contains the ITP plug and adding the membrane section directly to RPA reactions. Alternatively, I dewater the Fusion 5 membrane and add the resulting liquid eluate to RPA reactions. I show successful amplification of input copy concentrations as low as $3x10^3$ copies of DNA per mL of input blood, corresponding to 100 cps/trial. These concentrations are well within the clinical ranges of various bloodborne infections such as HIV, HCV, and HBV.[66,208,209] While this system and its current limit-of-detection are not relevant to all diseases or conditions (such as HIV+ individuals on successful antiretroviral treatment, who have viral loads of <1,000 cps/mL), there remains larger clinical relevancy for use in POC infectious disease testing. With respect to HIV, there remains a significant population who are either not on antiretroviral treatment or who have not achieved viral suppressed. Individuals with unsuppressed HIV infections may have viral loads as high as 10^7 cps/mL.[210] HCV viral loads can range near 10^5 cps/mL,[211,212] while HBV viral loads range from 300 to 10^6 cps/mL.[67] Here, I used target DNA as a step towards working with hardened targets, such as viral or bacterial infections. To move towards that goal, I also detail the development of lyophilized RNase inactivation reagents onto paper membranes for eventual incorporation into a point-of-care device In this work, I show that after several modifications and adjustments, a combination of proteinase K, sodium dodecyl sulfate, and dithiothreitol can be lyophilized onto Fusion 5 membrane and completely eliminate endogenous RNase activity of human serum when rehydrated after a short incubation. While these lyophilized reagents have not been further integrated into the described device yet, it is anticipated that they

will be able to be localized onto the sample pad. These aspects of device design and lyophilization protocol represent significant steps towards sample preparation methods for NAATs well-suited for POC bloodborne disease testing.

Chapter 3: Quantitative Isothermal Amplification through Amplification Nucleation Site Analysis

3.1 Introduction

Quantitative nucleic acid amplification tests (qNAATs) are critical tools in diagnosing infectious diseases and quantifying target nucleic acids concentrations in biological samples. In the context of HIV viral load testing, nucleic acid concentrations (i.e. viral load) are related to viral suppression and transmission risk; HIV-positive individuals with viral loads of less than 1,000 copies of viral RNA per mL of plasma have significantly better health outcomes and reduced risk of transmitting HIV to partners.[213–215] Recently, SARS-CoV-2 viral load measurements have been related to infectivity, with higher viral loads being strongly correlated to cultivable virus.[64,65] Quantification of pathogen load can be crucially important in triaging and determining appropriate clinical care for a range of diseases.

Quantitative PCR (qPCR) is the gold standard for quantifying nucleic acids and amplifies pathogenic nucleic acids using precise thermocycling for denaturation, annealing, and extension of duplicated DNA. qPCR provides quantification over nine orders of magnitude relative to known quantities of DNA in a standard calibration curve. Digital droplet PCR (ddPCR) has emerged as the most precise method for absolute NA quantification. It leverages Poisson statistics with thousands of discrete PCR amplification reactions to provide absolute sample quantification.[63,216] ddPCR typically has lower dynamic range than qPCR (five orders of magnitude for commercial systems such as the BioRad QX200[217]) due to signal saturation, requires separate droplet generation prior to amplification cycling, and can suffer from false positives resulting from inappropriate thresholding.[218] Both qPCR and ddPCR are traditionally restricted to well-instrumented laboratories or hospitals due to cold chain dependent reagents, delicate instrumentation, reliable electrical power, proficient laboratory staff, and appropriate infrastructure to host required equipment.[38]

HIV viral load testing using traditional qNAATS in outpatient or low- and middle-income country clinics is challenging due to the logistics around specimen collection, transport, batched testing, and the return of results to clinicians and patients (in addition to the aforementioned restriction to centralized laboratories).[78] In outpatient clinics, this can result in delayed diagnoses that prevent immediate linkage to appropriate treatment or lead to loss-to-follow-up.[219,220] Consequently, there is an unmet need to develop inexpensive point-of-care (POC) qNAATs, particularly in low- and middle-income countries (LMIC).[38,78] Isothermal amplification methods are emerging as an alternative to PCR, as they require significantly less instrumentation and produce results much more quickly than PCR. As described in Section 1.5.2 , isothermal amplification techniques use novel primer designs and various enzymes for nucleic acid replication at a single temperature of 60 °C or below without the need for thermocycling. While this significantly reduces the necessary equipment for amplification, this also eliminates the cycle-based amplification synchronization that allows qPCR to precisely quantify samples. This complicates sample quantification via isothermal amplification methods.[148]

In recombinase polymerase amplification assays, time-to-threshold analysis is commonly used to approximate nucleic acid concentrations. This analysis uses the time it takes a reaction to reach a specified fluorescence intensity threshold, similar to cycle threshold in qPCR assays. However, calibration curves are highly dependent on target and/or subtype.[151–154] For instance, Abd El Wahed *et al*. developed an RT-RPA assay for Dengue fever detection, and while quantification was not a goal of this work, they showed time-to-threshold data across target concentrations with very little differentiation between 10^3 and 10^7 copies per reaction as all reactions amplified between 4.5 and 5.5 minutes.[151] Lillis *et al.* showed time-to-threshold results of an RT-RPA developed for cross-subtype detection of HIV.[154] There was a general correlation between time-to-threshold and input copy number, though various subtypes had significantly different amplification behaviors, with an estimated 20 copies per reaction of subtype A RNA amplifying at nearly the same time as an estimated 9,000 copies per reaction of subtype D RNA. Quantification via RPA is complicated by the manual chemical initiation of reactions and a highly viscous reaction chemistry

that is sensitive to small pertubations.[148] There are currently no careful studies showing that RPA is sufficiently quantitative for clinical applications.[105,155]

Isothermal amplification has also been used in digital amplification schemes using individual droplets or wells in microfluidic devices for absolute quantification of nucleic acids.[221,222] For instance, Li *et al*. were able to precisely quantify *Listeria monocytogenes* DNA from concentrations of 1.3E4 to 2.9E6 cps/mL using a microfluidic device with 27,000 picoliter-sized reaction wells.[223] Similar to ddPCR, these digital methods use binary determination of amplification in each individual well or droplet combined with Poisson distribution statistics. This approach requires that individual small aqueous reaction volumes be generated, for example, using a microfluidic device for droplet generation in a immiscible oil carrier phase,[224] or sliding chip that compartmentalizes small volumes in wells, such as the SlipChip.[221,225] These digital isothermal amplification methods demonstrate repeatable outputs with precise and accurate quantification, though they all require specialized chips, emulsion generators, and/or complex loading procedures that potentially increase costs and complicate POC applications.

Paper-based POC NAATs devices have leveraged isothermal amplification within commercially available porous substrates.[105,145,147,199,226] This approach has been developed with the goal of reducing test cost and complexity as well as increasing their robustness. Much of this paper-based work has focused on qualitative tests; however some effort has been made to extract quantitative or semi-quantitative information about input nucleic acid concentration.[105,198,199,227] Lateral-flow readout has been used with some success for order-of-magnitude semi-quantitative isothermal nucleic acid amplification. A range of isothermal chemistries (RPA,[157,160,161] LAMP,[228,229] and HDA[162]) have been amplified in tubes[160,161,228] or in membranes[229,230] and then read out using lateral flow strips, with line intensity (or some ratio of line intensities) being used to provide quantification. Very recently, tunable competitive internal controls have been added into amplification reactions to further improve quantification, such as those shown by Hull *et al*., Mancuso *et al.*, and Rosenbohm *et al*,[160–162] discussed further in Section 1.5.2 . These methods demonstrate quantification across several orders of magnitude (the competitive internal control can be tuned

to extend this range if multiple parallel reactions are used), though at the cost of increased assay complexity and user steps.

Fluorescence-based assays with various isothermal amplification chemistries have also been used in paper-based NAATs, with bulk fluorescent signals related to sample concentration, similar to traditional tube-based assays.[90,105,147,226,231,232] These previous works have used both liquid and lyophilized isothermal amplification chemistries, and show correlations between bulk endpoint fluorescence and input copy number across 4-6 orders of magnitude; however there is typically significant variation in output signal that makes precise quantification challenging, even across orders of magnitude. As others have pointed out, this is likely due to the sensitivity of isothermal amplification to various random perturbations and effects of non-specific amplification products.[161] Collectively, these previous strategies fail to show adequately precise quantification of isothermal amplification methods in low-cost paper-based devices that can be used at the point-of-care, and warrant investigation into other, novel strategies for quantification.

In this chapter, I report a paper-based, isothermal nucleic acid amplification test that quantifies input HIV RNA and DNA by leveraging distinct regions of fluorescent amplification products. I show that RPA reactions in paper membranes produce discrete amplification nucleation sites and that the number of amplification sites correlates to input NA concentrations. I develop and use image analysis algorithms to quantify RNA and DNA in the range of 67-3,000 copies per reaction in less than 20 minutes at a constant 39 °C. I show that this method can more precisely quantify RPA reactions across HIV subtypes than traditional tube-based time-to-threshold analysis. I demonstrate a mobile phone-based image capture system with onboard image processing using a custom Android app, showing that this method may be well suited for point-of-care settings, including HIV viral load applications.

3.2 Experimental Section

3.2.1 Amplification on Membranes

RPA and RT-RPA reactions are performed on a variety of commercially available porous membranes (Millipore GF041, Whatman GF/DVA, Whatman Fusion 5, and Millipore PES GPWP04700). I first cut the membranes with a flatbed plotter-cutter (FCX4000-50ES, Graphtec America, Inc., USA) into squares to accommodate a 50 μL RPA reaction volume. Dimensions of the squares differed with respect to each membrane's respective water absorbency, with side lengths of 11.2 mm, 7.2 mm, 12.7 mm, and 13.4 mm, for the GF041, GF/DVA, Fusion 5, and PES membranes, respectively.

The Millipore PES GPWP04700 membrane tears when cut by the flatbed plotter-cutter, so these membranes are cut with a CO_2 laser (PLS6.150D, Universal Laser Systems, USA). The low water absorbency of the PES membrane necessitates a square pad with a 25 μL capacity to prevent an excessively large imaging area.

Amplification pads are placed into a 60 x 15 mm polystyrene Petri dish (25384-092, VWR, USA), and a 50 μL RPA reaction (mastermix and target) is pipetted evenly onto the pad (25 μL in the case of PES). The amplification pad is then covered with PCR tape (TempPlate RT Select Optical Film, USA Scientific, USA), ensuring good sealing adhesion between the PCR tape and the Petri dish. I lid the Petri dish and seal along its edges with Parafilm M (Millipore Sigma, USA) to prevent contamination via aerosolized amplification products. The Petri dish is placed on a resistive heater (Mr. Coffee, USA) that is set to 39 °C using an external PID temperature controller with a Type-K thermocouple attached to the heating surface. The reaction is imaged for 20 minutes and then the Petri dish is sealed in a plastic bag and disposed of. The experimental process is shown in Figure 3-1.

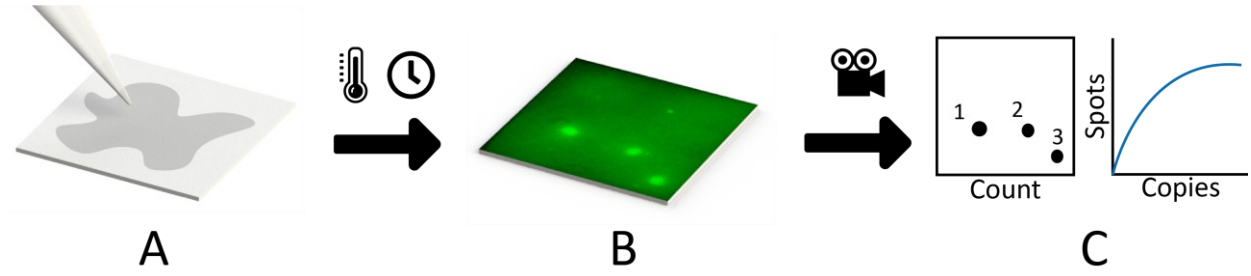

Figure 3-1: Process flow for amplification nucleation site quantification and analysis. (A) Recombinase polymerase amplification mastermix and target are dispensed onto paper membrane. The membrane is covered with PCR tape and heated to 39 °C for 20 minutes. (B) Discrete amplification nucleation sites begin to form and are recorded via fluorescent microscopy. (C) The resulting images are analyzed via an image analysis algorithm which quantifies the number of amplification nucleation sites. This value can then be related to the original sample target concentration.

3.2.2 RPA, RT-RPA, and qPCR Conditions

In RPA experiments, I targeted synthetic DNA (gBlocks Gene Fragments, Integrated DNA Technologies, USA) that contains 1,000 base pairs of the HIV genome (Group M, Subtype A). For RT-RPA experiments, I targeted purified HIV RNA from HIV supernatant, prepared as described in Lillis *et al.*[154] The majority of following experiments used HIV supernatant (Group M, Subtype A, NCBI accession number: JX140650) that was received from the External Quality Assurance Program Oversight Laboratory at Duke University,[233] and extracted using QIAamp Viral RNA Mini Kits (Qiagen, DEU). The resulting viral RNA was quantified via quantitative real-time PCR. Both target types were diluted with DEPC-treated water to create dilution series used in establishing quantifiable ranges for amplification nucleation site analysis. To compare the quantitative power of amplification nucleation site analysis across HIV subtypes, I used two additional HIV supernatants: subtype B (Group M, NCBI accession number: KC59066) and subtype D (Group M, NCBI accession number: KF716503). Viral RNA was similarly extracted with QIAmp Viral RNA Mini Kits and quantified via real-time PCR, following the protocol shown in Rouet *et al.*[234] qPCR standards were created from 500 bp gBlocks (Integrated DNA Technologies, USA) containing the LTR gene. RNA transcripts were created from these LTR gBlocks using the MEGAscript and

MEGAclear kits (ThermoFisher Scientific, USA), following the standard manual procedures. The resulting transcripts were quantified via NanoDrop UV-vis spectrophotometer (ThermoFisher Scientific, USA) and diluted in DEPC water to create standard curves.

In both RPA and RT-RPA, I use primers and probe developed by Lillis *et al*. for cross-subtype HIV detection.[154] The amplification mastermix consists of a TwistAmp exo kit lyophilized pellet (TwistDx, GBR), 29.5 μL rehydration buffer, 14 mM magnesium acetate, 540 nM forward and reverse primer (Integrated DNA Technologies, USA), and 120 nM exo-probe (LGC Biosearch Technologies, GBR). In the case of RT-RPA experiments, 0.08 U/μL reverse transcriptase is added (OmniScript, Qiagen, DEU). The TwistAmp exo kit instructions are otherwise followed up until incubation. Briefly, the mastermix of rehydration buffer, primers, probe, and RT (in the case of RT-RPA) is added to a lyophilized exo-kit RPA pellet, rehydrating it. I then add the target (DNA or RNA) to the mastermix and add 2.5 μL MgOAc (280 mM) to the cap lid of the tube. The tube is then closed and shaken manually for ~30 seconds to start the reaction and ensure homogenous distribution of reactants. I then immediately open the tube and pipette the 50 μL reaction volume evenly onto an amplification pad. In the case of tube-based experiments, the tubes are placed into a T16-ISO instrument (Axxin, USA), which incubates the tubes at 39 °C and records fluorescence for 20 minutes, with a manual mixing step at 4 minutes. To test for the presence of proviral DNA in the extracted viral RNA, I performed tube-based RPA experiments using the viral RNA in which reverse transcriptase was purposefully excluded; these experiments did not amplify.

3.2.3 Imaging and Data Analysis

An epifluorescence fluorescence microscope (AZ100, Nikon, JPN) with 0.5x objective and illumination system (X-Cite exacte, Excelitas Technologies, USA) images the RPA nucleation site evolution in the pad. The 0.5x objective used has a field of view diameter of 43 mm. I use an epifluorescence

filter cube set (XF100-2, Omega Optical, LLC., USA) and capture grayscale images every second for 20 minutes using a CMOS camera (Prime BSI Express, Teledyne Photometrics, USA).

A custom image analysis algorithm (MATLAB, MathWorks, USA) counts the number of amplification nucleation sites over the full 1,200 frame image-stack. The algorithm first resamples the image-stack, effectively doubling the pixel density, then averages the pixel intensity over every 10 frames to reduce image noise. It applies background subtraction to the entire image-stack by averaging the frames in the first 2 minutes and subtracting this resulting average frame from all subsequent frames on a pixel-by-pixel basis to eliminate any artifacts caused by auto-fluorescence of the amplification membranes, PCR tape, or Petri dish. A circle-finding function (based on a Circular Hough Transform algorithm) identifies discrete amplification nucleation sites for each frame. A moving-mean smoothing function averages the number of amplification nucleation sites over time using a 5-frame window, as inherent pixel noise can result in deviations in number of identified sites from frame to frame. The maximum smoothed number of sites identified over the 20 minutes is used as the number of amplification nucleation sites for that experiment. I refer to this method as the CHT (Circular Hough Transform) method. An alternative algorithm that relies on thresholding to identify the nucleation sites is also used. This algorithm (coded via ImageJ[235]) averages the pixel intensity over every 10 frames, and then performs a rolling-ball background subtraction. Thresholding of the resulting image-stack is performed using Otsu's method, followed by a watershed transformation to separate merged nucleation sites, and then analysis via an edge-finding algorithm to identify distinct nucleation sites. I refer to this method as the TAP (Threshold Analyze Particles) method. Both codes are available in the Appendix (A.4 and A.5).

I also use a mobile phone to image RPA nucleation sites to demonstrate the potential use of this method in point-of-care environments. I use a Pixel 4A mobile phone (Google, USA), bandpass excitation filter (FF01-466/40-25, Semrock, USA), bandpass emission filter (FF01-550/49-25, Semrock, USA), and plano-convex macro lens (37-784, Edmund Optics, USA). The excitation and emissions bandpass filters are centered at 466 nm and 550 nm, respectively, for use with the FAM fluorophore family. The plano-

convex lens is positioned such that it is directly adjacent to the mobile phone's camera, while the excitation and emission filters are positioned underneath the mobile phone flash and camera, respectively. These are held in position by a 3D-printed fixture (S3, Ultimaker, NLD), as shown in Figure 3-2B. The experiments were conducted in a darkroom to avoid any ambient light. Images were acquired with a fixed setting of ISO 55 and an exposure of 4 seconds.

I analyze a single frame recorded at 750 seconds into an experiment with a custom Android app written in Python 3.8.10 using the OpenCV library and run via Python for Android.[236] The algorithm first employs an auto-cropping function to define the square region of interest containing the amplification pad. A contrast limited adaptive histogram equalization adjusts the contrast of the image, and a bilateral filter smooths the image while also removing pixel noise. The image is binarized via an adaptive Gaussian binary threshold, and a Hough circle transform then identifies and quantifies the discrete nucleation sites. The user interface displays a results screen featuring the experimental image with nucleation sites highlighted, determination of HIV status, number nucleation sites identified, and corresponding nucleic acid copies (Figure 3-2C).

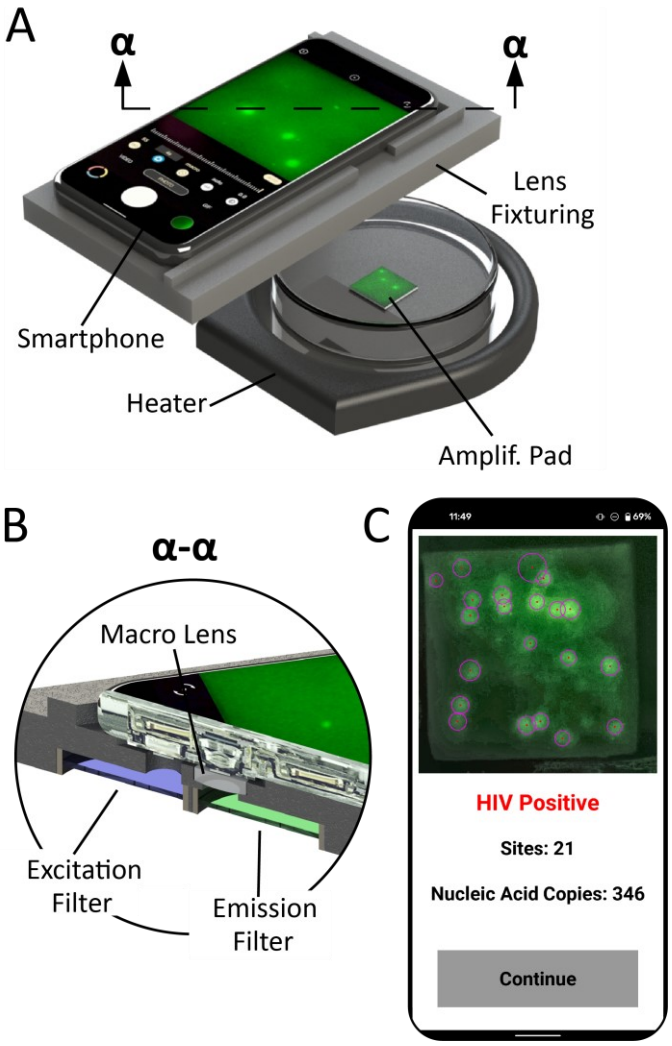

Figure 3-2: Smartphone setup for nucleation site analysis, showing smartphone, Petri dish containing the amplification membrane, heater, and 3D-printed fixturing, which holds the excitation and emission filters, as well as the plano-convex macro lens.

3.3 Results and Discussion

I perform RPA and RT-RPA on GF/DVA membranes for a range of target concentrations (30-100,000 cps/rxn and 50-3,000 cps/rxn for DNA and RNA, respectively). At target concentrations of 30-3,000 cps/rxn of DNA and RNA, I observe spatially separated and distinct fluorescent amplification nucleation sites dispersed on the amplification pad that grow in diameter over the course of the experiment, as shown in Figure 3-3. At higher concentrations (>10,000+ cps/rxn), there are many closely packed

nucleation sites that merge, resulting in splotchy heterogenous fluorescence over the amplification pad and making individual site identification more challenging. To my knowledge, this is the first instance that individual amplification nucleation sites in paper membranes have been described in the literature. I did not evaluate other amplification chemistries, though other publications that use these methods (e.g. LAMP, iSDA, etc. on paper membranes) exhibit homogenous fluorescence increase and not discrete amplification nucleation sites.[99,226,232,237,238] I hypothesize that the nucleation sites are a result of amplification reactants (e.g. recombinase-primer filaments) or products (i.e. duplicated amplicons) diffusing slowly in and out of the amplification nucleation sites. RPA's high viscosity reaction buffer likely impedes diffusion of reactants and products, limiting the reaction to individual nucleation sites. RPA relies on viscous crowding agents such as polyethylene glycol (PEG) to increase enzyme catalytic efficiency,[142] which traditionally necessitates a mixing step halfway through tube-based RPA assay protocols.[142,239] Previously, cast-gel amplification systems, including in-gel LAMP or in-gel PCR, have been leveraged in a similar application.[240,241] In these systems, native amplification chemistries are mixed with cross-linking polymers (e.g. polyacrylamide gels) resulting in discrete amplification zones. In the work presented here, the highly viscous RPA amplification chemistry in the porous membrane micron scale geometries dampen fluid flow[242,243] resulting in a diffusion-limited transport and formation of discrete amplification sites.

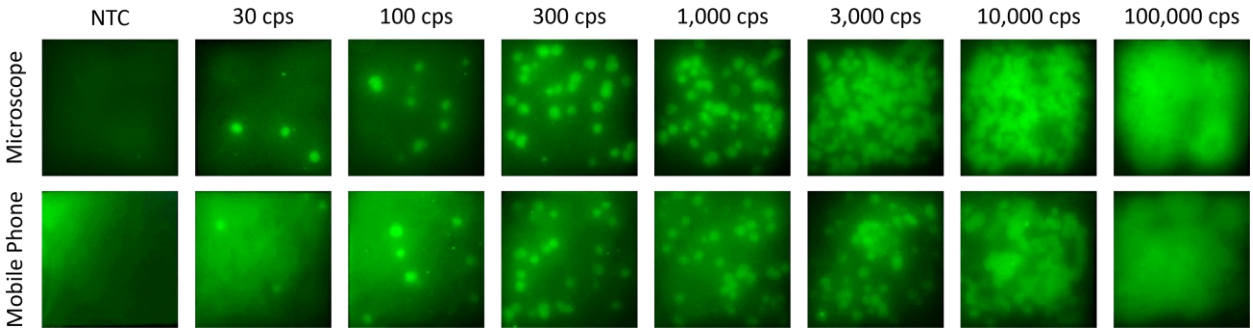

Figure 3-3: Representative fluorescence images of RPA amplification of HIV DNA on GF/DVA membrane captured via microscope and smartphone imaging setup, with copy number ranging from 30 to 100,000 cps/rxn. Images were taken at t = 750 s. At lower copy numbers (30-3,000 cps/rxn), I observe discrete amplification nucleation sites, with a positive relationship between number of nucleation sites and input copy number. At high copy numbers (10,000 and 100,000 cps/rxn), the nucleation sites are so numerous that they merge, making quantification difficult.

I briefly investigated the effects of polyethylene glycol on amplification nucleation site analysis by increasing its concentration in the reaction mixture. In order to better visualize the nucleation sites, I developed a glass-slide system, not unlike in-situ PCR platforms. Briefly, I adhere transfer tape (467MP, 3M, USA) on to a 2" x 3" glass slide (CA6101, Premiere) to form a border around the slide. The transfer tape is cut with the CO_2 laser cutter to form a 5 mm wide border immediately interior to the edges of glass slide. An RPA reaction is prepared as described above and then pipetted into the center of the glass slide. A matching glass slide is then placed over the RPA reaction, ensuring a good seal with the transfer tape. Three layers of transfer tape are used to create a gap between the glass slides of roughly 170 μm. This setup is shown in Figure 3-4A. The glass slides are then placed onto the heater set to 39°C and imaged in the same process as described above. RPA reactions are also supplemented with additional PEG. While it is unknown exactly how much PEG is present in the TwistDx RPA rehydration buffer and/or lyophilized RPA pellets, additional PEG experiments increased the final PEG concentration by 5% (w/v).

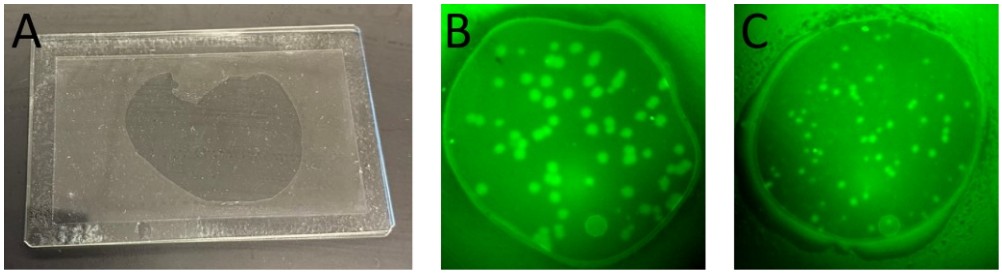

Figure 3-4: Amplification nucleation sites on glass slides. (A) RPA reaction sandwiched between two glass slides with transfer tape border. (B) 1,000 copies of HIV gBlocks DNA with baseline RPA chemistry. Nucleation sites that are similar to paper-based amplifications are visible. (C) 1,000 copies of HIV gBlocks DNA with an additional 5% (w/v) PEG. Nucleation sites are significantly smaller. Both images are taken at 850 seconds.

In experiments with additional PEG, I observe significantly smaller amplification nucleation sites, though this does not significantly affect the number of nucleation sites present. This does not entirely explain the presence of discrete amplification zones, though it suggests that the viscosity of the reaction plays an important role in their formation and evolution over time.

I find significant differences between the RPA reactions in the various membranes tested. For my initial comparison tests, I use 1,000 cps HIV DNA per reaction as the target. Both the GF041 and GF/DVA membranes show robust amplification, with 34-50 amplification nucleation sites visible. The Fusion 5 only results in 1-2 amplification nucleation sites and marginal increase in overall fluorescence. The PES GPWP04700 membrane supports successful amplification, in agreement with previous studies.[147,244] I find that both the GF041 and PES membranes exhibit lower contrast between the background and amplification fluorescence in comparison to the GF/DVA membrane. Due to the robust amplification and superior contrast, all subsequent experiments were carried out using the Whatman GF/DVA membrane. Representative images of comparison RPA reactions on the various membranes are shown in Figure 3-5.

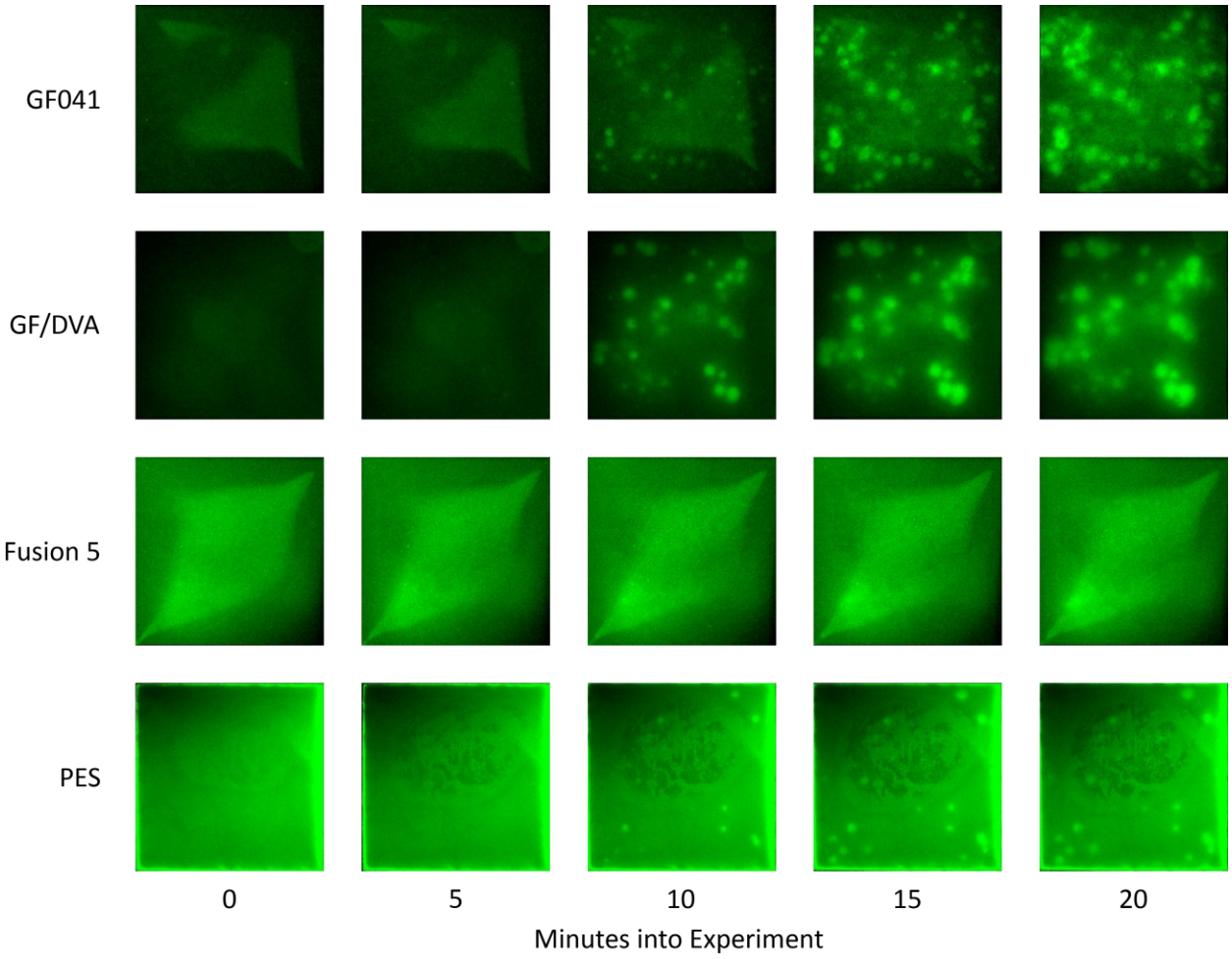

Figure 3-5: Representative amplification reactions on various membranes. From top to bottom: Millipore GF041, Whatman GF/DVA, Whatman Fusion 5, Millipore PES GPWP04700. All experiments are at 1,000 cps DNA per rxn. Due to the low water absorbency (~ 14 µL/cm^2) of the polyethersulfone (PES) membrane, a pad to hold the full 50 µL RPA mastermix volume would be too large for the imaging set up. Consequently, only 25 µL mastermix was used for the PES experiments. Strong amplification is seen in both the Millipore GF041 and the Whatman GF/DVA, with many distinct amplification nucleation sites visible. However, the Millipore GF041 exhibits brighter background fluorescence, reducing the contrast of the amplification nucleation sites compared to the Whatman GF/DVA membrane. Amplification within the Whatman Fusion 5 is relatively poor, with only one nucleation site appearing after 20 minutes and high background signal. The Millipore PES membrane supports amplification, though air bubbles (visible in the center of the pad) would consistently form, obscuring amplification nucleation sites.

Figure 3-6A shows example images captured via fluorescent microscope and processed with the CHT method, including the raw image, resampled image, multi-frame averaged image, background subtraction, and identified sites. I plot the number of nucleation sites counted for the algorithms I tested compared to the number of sites counted manually. I find that CHT, TAP, and manual count methods agree well at low copy numbers (<300 cps/rxn), where there are relatively few (<50) amplification nucleation sites. At higher DNA copy numbers (1,000 – 3,000 cps/rxn), there are differences between the algorithmic counts and manual counts, though this disagreement is scattered. At higher copy number (10,000 cps/rxn), both algorithms significantly undercount the number of sites relative to the manual count. I believe this deviation is due to the algorithms being unable to robustly identify individual nucleation sites prior to the sites merging at higher input copy numbers. This is supported by plots of identified amplification nucleation sites over time of a single experiment, shown in Figure 3-6C. Often, the number of nucleation sites will peak halfway through an experiment (I use the maximum as the recorded value for each respective experiment) and then begin to decrease as the sites merge, revealing this weakness in the algorithms (additional nucleation sites vs. time plots are shown in Figure 3-7. In all subsequent microscope-based experiments, I use the CHT algorithm for nucleation site quantification.

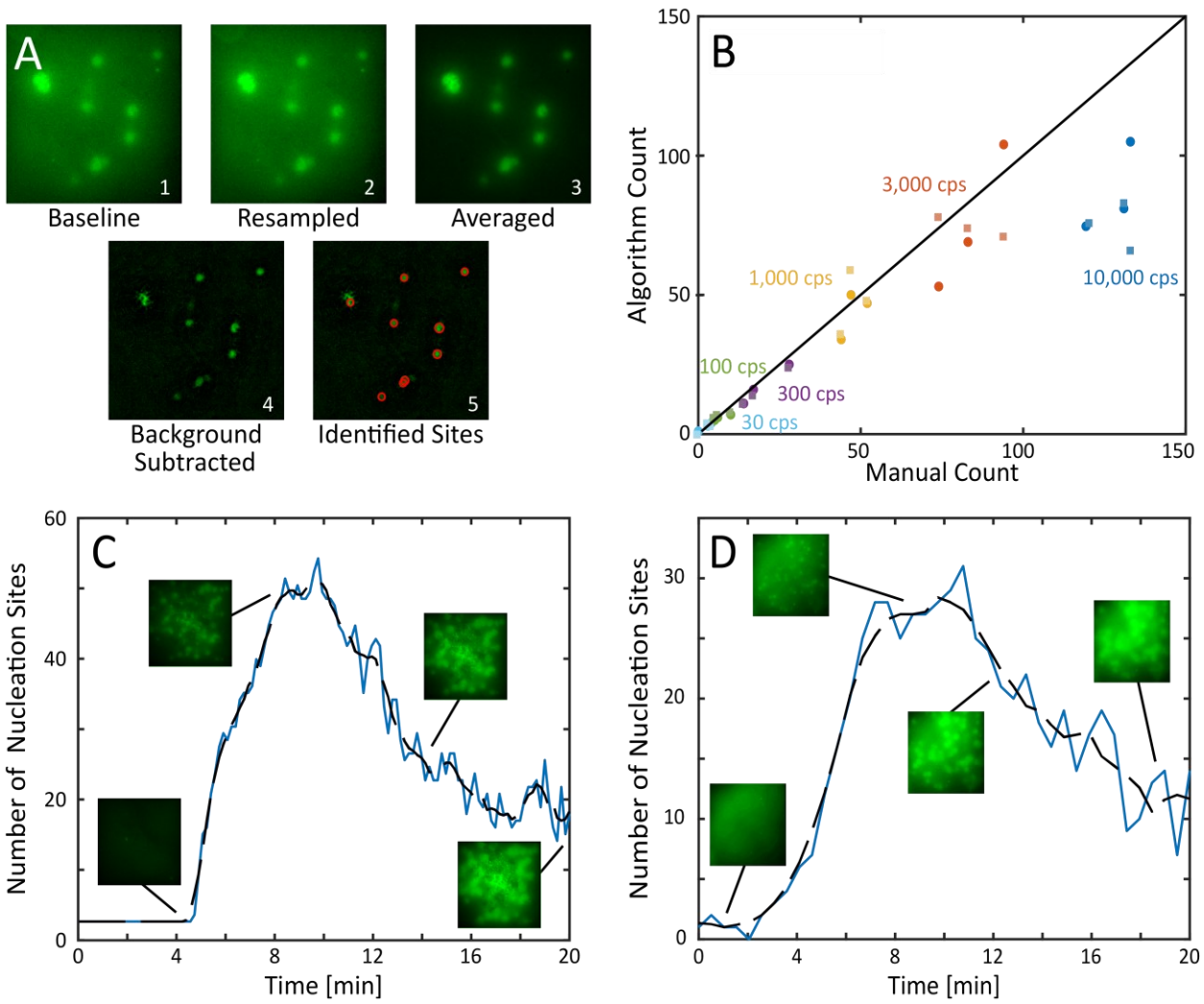

Figure 3-6: Results of algorithmic nucleation site identification and counting. (A) Circular Hough Transform (CHT) algorithm process. The raw data (1) is first resampled to increase pixel density (2) with the pixel intensity averaged over 10 frames (3). I perform background subtraction (4), subtracting the average of the first two minutes' frames on a pixel-by-pixel basis with the resulting amplification nucleation sites then identified and quantified via a circle counting algorithm (5). (B) Comparison of the CHT (○) and TAP (□) algorithms against a manual count of RPA amplification nucleation sites with DNA target copy numbers of 30 – 10,000 cps/rxn. At lower copy numbers (≤ 3,000 cps/rxn), there is good agreement between the manual count and both algorithms. In this regime, the number of amplification nucleation sites is relatively low and there is sufficient separation between the sites for successful algorithmic quantification. At higher copy numbers (10,000 cps/rxn), the nucleation sites begin to merge, making algorithmic quantification more difficult and resulting in an undercount relative to the manual count. This is observed for both algorithms, though it is more pronounced in the TAP algorithm. (C) Representative experiment of 1,000 cps/rxn DNA on Whatman GF/DVA membrane, showing the number of amplification nucleation sites as a function of experiment time, quantified via the CHT image analysis algorithm. A sharp increase in number of nucleation sites occurs near 4-10 minutes, followed by a decrease in number of identified sites as the sites begin to grow and merge. The dashed line represents the moving-mean smoothing function used. (D) Representative experiment of 1,000 cps/rxn DNA on Whatman GF/DVA membrane captured by the smartphone imaging system, showing the number of amplification nucleation sites as a function of experiment time.

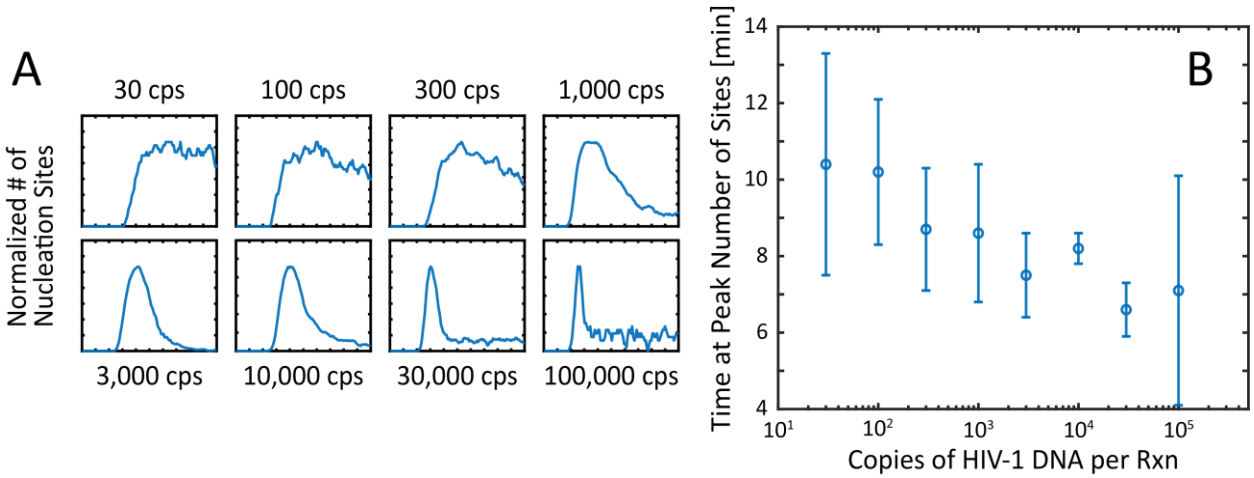

Figure 3-7: Representative normalized number of nucleation sites over the course of 20-minute experiments using HIV DNA copy numbers 30 – 100,000 cps/rxn, captured via the microscope setup. Number of nucleation sites is normalized by the maximum number of nucleation sites. At very low copy numbers, the nucleation sites are spatially separated such that there is little site merging, and consequently, I do not observe any distinguishable peak of number of quantified nucleation sites. As the copy number increases, I observe gradually more pronounced peaks, as the increase in number of sites leads to more site merging. At very high copy numbers, the number of quantified nucleation sites increases rapidly, then decreases very quickly as site merging dominates very soon after the nucleation sites become visible.

In Figure 3-8 I plot the number of nucleation sites as a function of the number of nucleic acid copies per reaction for HIV DNA and RNA using both the microscope and mobile phone imaging systems. The data shows that the number of amplification nucleation sites is proportional (log-log) to the number of input target copies. For RPA experiments with DNA target, input copy numbers of 30-100,000 cps/rxn were tested in triplicates and all experiments showed positive amplification except for one trial at 30 cps/rxn. No template controls (NTCs) did not show any amplification. I estimate the limit of detection (LoD) of this method via Probit analysis[245] as copies DNA per reaction. I find that the number of amplification nucleation sites as a function of copies of DNA per reaction follows power-law relationship in the form of $y = b * x^m$, where b = 0.184 and m = 0.766. This relationship holds well up to 3,000 cps/rxn, after which the number of identified amplification nucleation sites reaches a maximum and then decreases with increasing

number of copies. The measured decrease in amplification sites is due to merging of sites at high copy numbers (10,000-100,000 cps/rxn) and the inability of the algorithms to capture and record all the nucleation sites. With my methodology, I report the dynamic range to be 67-3,000 copies of HIV DNA per reaction (equivalent to 1,300-60,000 cps/mL). I show a comparison plot with a manual count in Figure 3-8, showing an extended dynamic range of up to 10,000 cps/rxn, suggesting that algorithm optimization can likely extend the reported dynamic range. Note that it is difficult to perform manual counts at copy numbers upwards of 10,000 cps/rxn, as the nucleation sites have already merged once they become sufficiently bright to distinguish from the background. These results suggest that alternative algorithm methodologies, such as pattern recognition or machine learning, may be useful in extending the dynamic range. While this site merging behavior limits the current dynamic range, I am still able to determine successful amplification in high copy number experiments using bulk fluorescence values.

Similar discrete amplification nucleation sites are observed in the RT-RPA experiments with HIV RNA target. The concentrations of viral RNA tested included 50-3,000 cps/rxn. I fit a similar power law model to the data ($y = b * x^m$), where b = 1.047 and m = 0.551.

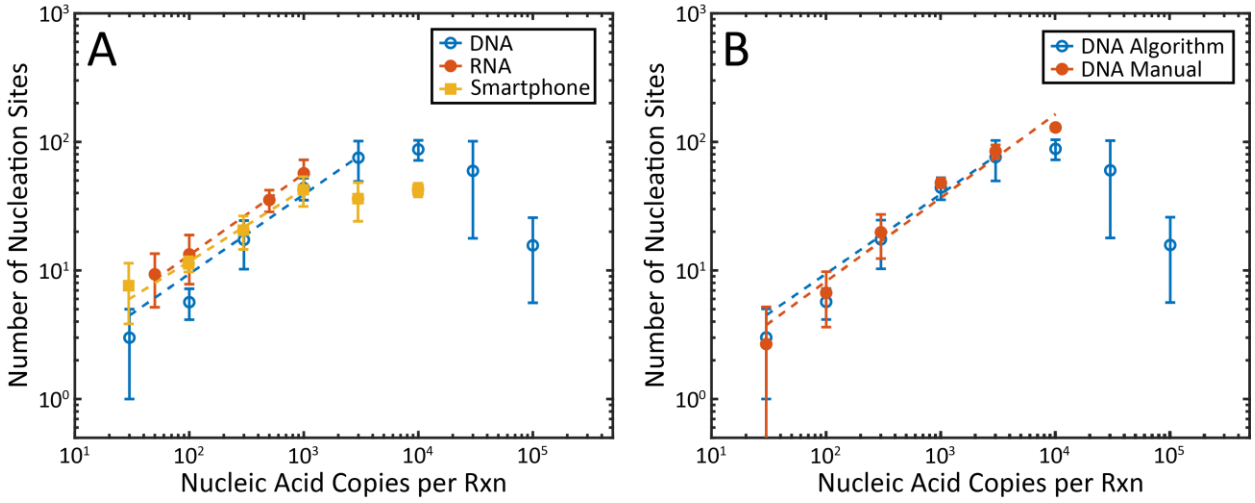

Figure 3-8: Log-log plots of quantification of amplification nucleation sites. (A) HIV DNA (blue open circles) and RNA (red filled circles) on GF/DVA membrane captured via microscope setup compared to HIV DNA data captured via smartphone setup (yellow filled squares). Data points represent the average and standard deviations (n=3) for each target copy number tested and quantified via CHT algorithms. Dashed lines represent fitted power models in the form of $y = m * x^b$. In all cases, I observe a strong relationship between nucleic acid input copy number and number of amplification nucleation sites. At high copy numbers (10,000+ cps/rxn), I observe a decrease in number of nucleation sites due to merging of amplification sites and inability of the experimental methodology to resolve and quantify the numerous nucleation sites. (B) Comparison of HIV DNA quantified via CHT algorithm to a manual hand count.

The mobile phone-based imaging and processing method demonstrates similar performance to microscope-based image capture for 30-1,000 cps/rxn; however, the performance of this system degrades at roughly 3,000 cps/rxn, significantly lower than the microscope-based system. This reduction in the dynamic range is due to the reduced sharpness and signal-to-noise of the mobile phone-based images and the associated challenges in counting the sites. The power law model fit to the data, ranging from 30 – 1,000 cps/rxn, is in the form $y = b * x^m$, where $b = 0.215$ and $m = 0.731$. The fit parameters are remarkably close to the fit calculated for the microscope-acquired data. In this work, I use a designated dark room to exclude ambient light. In a point-of-care setting, a specially constructed enclosure or dark box would be required

and interface directly with the smart phone while holding the necessary optics, similar to previously used dark boxes for epifluorescence imaging.[246]

I compare the LOD, dynamic range, time, cost, and complexity of amplification nucleation site analysis to ddPCR and various other isothermal amplification techniques in Table 3-1. ddPCR has the lowest limit-of-detection (1 copy per 20 μL reaction volume) and the largest dynamic range of the digital methods reviewed here (5 orders of magnitude), though requires multiple devices (droplet generator, thermocycler, and droplet reader) which cost upwards of $100,000. Other digital methods, such as the SlipChip[221] have marginally poorer performance than ddPCR, with LODs in the range of 1,000 to 10,000 cps/mL and similar high end dynamic range. While some of these chip-based platforms may ultimately be less expensive than commercially available ddPCR systems, they are manufactured via photolithography, complicating widespread POC applications. Publications using bulk fluorescence magnitudes of isothermal amplification for quantification report dynamic ranges of 3 to 4 orders of magnitude and 20-30 minute test time. Here, I report a minimally instrumented isothermal amplification which can quantify input copies over a dynamic range of 1.5 orders of magnitude.

While this method in its current form has smaller dynamic range compared to other digital methods, bulk fluorescence measurements of the amplification pad can be used to determine positive amplification at input concentrations above the quantifiable levels. Serial dilution of the target sample may be used with multiple concurrent amplification reactions (on separate amplification pads) to extend the dynamic range, with the only limitation being space and sample volume limits. This parallel processing of several target sample dilutions is routinely employed with ddPCR, which also suffers from signal saturation at the upper end of its dynamic range. Additional image processing methods, such as convolutional neural networks or similar image analysis machine learning algorithms might be employed to increase the dynamic range as well, potentially taking advantage of nucleation site cluster formation visible at higher input copy numbers, as opposed to individual nucleation site counting.[240]

Table 3-1: Comparison of amplification methods to quantify pathogen concentration

Publication	Description	Reported Range	Manufacturing	Time to Results	Quantification Scheme	Notes
Bio-RAD QX200	ddPCR	5E1 to 6E6 cps/mL		120 minutes	Digital Poisson statistics	Requires separate droplet generator, thermocycler, and reader, $100,000 cost
Shen *et al.*[221]	Digital RPA performed on SlipChip microfluidic chip	1.4E3 to 1E6 cps/mL	Photolithography	60 minutes	Digital Poisson statistics	Used 1,550 nanoliter-sized wells with automatic filling
Li *et al.*[223]	Digital RPA performed on microfluidic chip	1.3E4 to 2.9E6 cps/mL	Photolithography	20 minutes	Digital Poisson statistics	Used 27,000 picoliter-sized wells, rather complicated loading procedure
Lin *et al.*[222]	Digital LAMP on track-etched membrane	1.1E4 to 1.1E8 cps/mL	LAMP mastermix added directly to polycarbonate membrane	40 minutes	Digital Poisson statistics	Leveraged membrane pore structure to discretize amplification reactions
Liu *et al*.[232]	Paper-based LAMP	1E6 to 1E10 cps/mL	Lyophilized reagents on glass fiber membrane	30 minutes	Time-to-threshold analysis	Developed separate reader to measure real-time fluorescence
Seok *et al.*[226]	Paper-based LAMP	5.9E3 to 5.9E6 cps/mL	Dried LAMP reagents on polyethersulfone membrane	60 minutes	Bulk fluorescence magnitude	Multiplexed detection via multiple amplification pads
Ahn *et al.*[147]	Paper-based RPA	1E2 to 1E5 cfu/mL	Dried RPA reagents on polyethersulfone membrane	20 minutes	Bulk fluorescence magnitude	Multiplexed detection via multiple amplification pads, able to distinguish orders of magnitude input CFU concentrations
This work	Paper-based RPA	1.3E3 to 6E4 cps/mL	RPA mastermix added directly to glass fiber membrane	20 minutes	Amplification nucleation site analysis	No alterations to the membrane required, smartphone-compatible

Amplification nucleation site analysis may provide sufficient precision and accuracy for some point-of-care nucleic acid quantification applications. For example, in HIV viral load monitoring the relevant quantification range of interest is 200-1,000,000 cps/mL (whereas the current dynamic range I show of 67-3,000 cps/rxn equates to 1,300-60,000 cps/mL).[78] In this work, I tested highly purified and simple samples and a complete POC diagnostic test may require significant sample preparation steps that impact the concentration of target in the reaction volume. Nucleation site counting may also provide greater precision and accuracy than tube-based RPA. As an estimate, I use the calculated calibration curve and determine the average predicted concentrations and associated standard deviations (n=3) for the collected data, similar to the process used by Crannell et al.[155] and shown in Table 3-2. Tube-based RPA is able to reasonably quantify both HIV subtype A DNA and RNA within 0.33 and 0.25 $\log_{10}$(copies per reaction) of the correct concentration on average for DNA and RNA respectively, within the dynamic range tested, in agreement with results shown in Crannell *et al*.[155] For the same concentrations, microscope-acquired amplification nucleation site analysis quantifies the samples within 0.14 and 0.16 $\log_{10}$(copies per reaction) of the correct concentration on average for subtype A DNA and RNA targets, respectively.

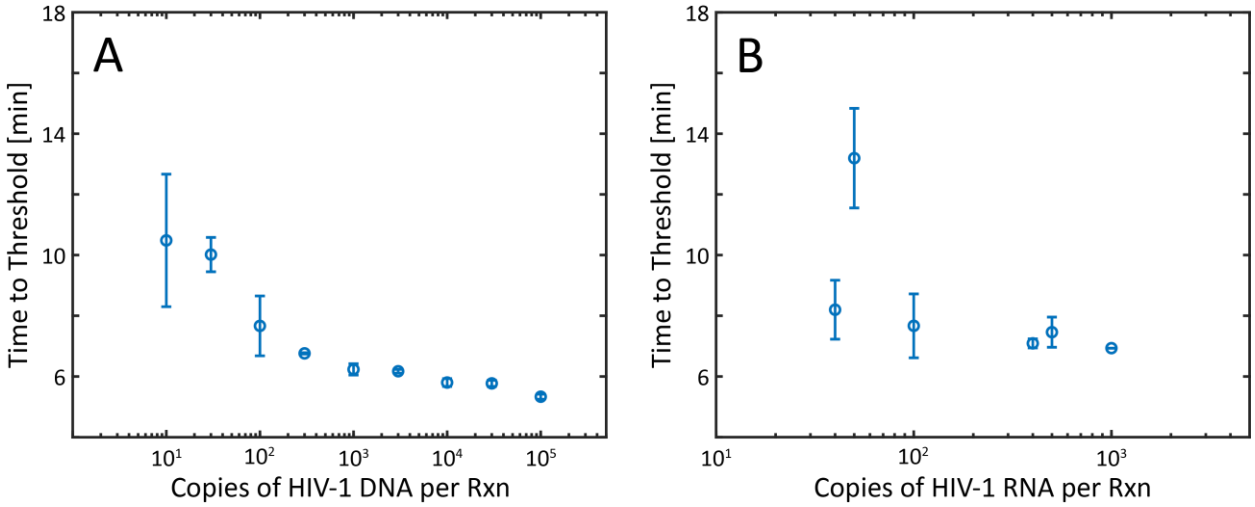

Figure 3-9: Time-to-threshold analysis of tube-based RPA experiments using HIV Subtype A RNA. Circles represent mean values with standard deviations shown. (A) HIV DNA targets 10-100,000 cps/rxn. Higher copy numbers take less time to reach the fluorescent threshold, though there is significant overlap when comparing various copy numbers, particularly at low copy numbers. (B) HIV RNA targets 40-1,000 cps/rxn. There is very little relationship between time-to-threshold and input copy number, making quantification difficult.

Table 3-2: Performance of amplification nucleation site analysis vs. tube-based RPA for HIV subtype A

	Log(Input Copies per Rxn)	**Average Predicted Concentration (Log)**	
		Tube-Based Time-to-Threshold Analysis	**Amplification Nucleation Site Analysis**
HIV DNA	3.48	3.18 (±0.05)	3.39 (±0.16)
	3	3.13 (±0.14)	3.09 (±0.10)
	2.48	2.76 (±0.01)	2.55 (±0.19)
	2	2.22 (±0.58)	1.93 (±0.13)
	Average Absolute Error	0.33 (±0.19)	0.14 (±0.09)
HIV RNA	3.48	3.36 (±0.03)	3.35 (±0.20)
	3	2.89 (±0.03)	3.03 (±0.07)
	2.7	2.83 (±0.08)	2.72 (±0.07)
	2	2.65 (±0.30)	1.95 (±0.32)
	Average Absolute Error	0.25 (±0.28)	0.16 (±0.13)

While RPA is well-known for its ability to robustly amply across genotypes and subtypes by withstanding primer mismatches,[148,172] mismatches can have a significant effect on amplification rate and time-to-threshold, such as that shown in Lillis *et al*.[154,247] This compounds challenges in tube-based quantification if exact target sequence is not known *a priori*, for example, when multiple genotypes and subtypes are detected with the same assay. To investigate this further, I compare the quantitative power of amplification nucleation site analysis to tube-based RPA across a range of HIV subtypes (A, B, and D) in a similar process to that shown in Table 3-2. I tested these viral RNA extracts over 60-3,000 cps/rxn in both tube-based RPA (using time-to-threshold analysis), amplification nucleation site analysis, and qPCR as a comparison. Resulting calibration curves for amplification nucleation site analysis, tube-based RPA, and qPCR are shown in Figure 3-10. As expected, qPCR has the tightest grouping across subtypes and ranges of HIV RNA. Both amplification nucleation site analysis and tube-based RPA show deviations based on subtype, with this differential amplification observed likely due to the nucleotide mismatches present between the primers and probe used and the respective subtypes, shown in Table 3-3.

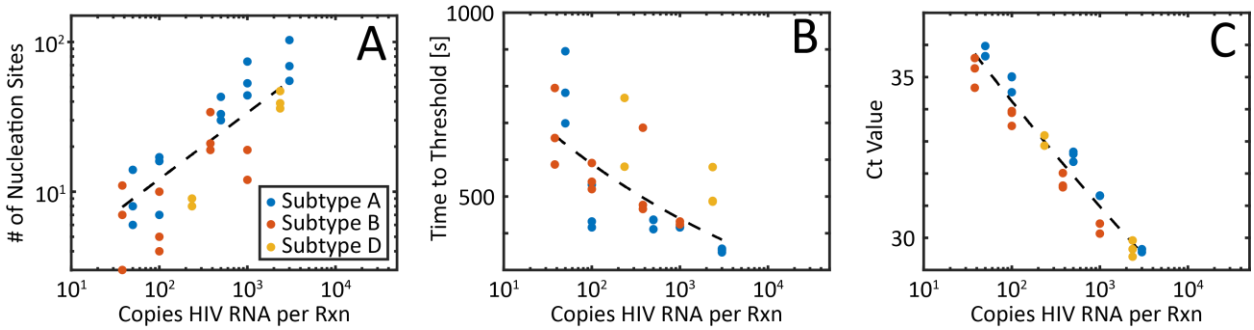

Figure 3-10: Comparison calibration curves across HIV subtypes for (A) Amplification nucleation site analysis (B) Tube-based RPA and (C) qPCR

Table 3-3: Number of nucleotide mismatches in primer and probe sequences by HIV subtype

	Number of Nucleotide Mismatches			
HIV Subtype	**Forward Primer**	**Reverse Primer**	**Probe**	**Total**
Subtype A	0	0	0	0
Subtype B	1	3	2	6
Subtype D	1	2	1	4

Interestingly, the subtype D supernatant used amplifies more poorly than the subtype B supernatant, though the subtype D genome has two fewer nucleotide mismatches. Previous studies have shown that the location of mismatches can greatly affect amplification performance.[171] In both amplification nucleation site analysis and tube-based RPA, subtypes B and D resulted in significantly lower fluorescence values than subtype A, with amplification nucleation site data shown in Figure 3-11.

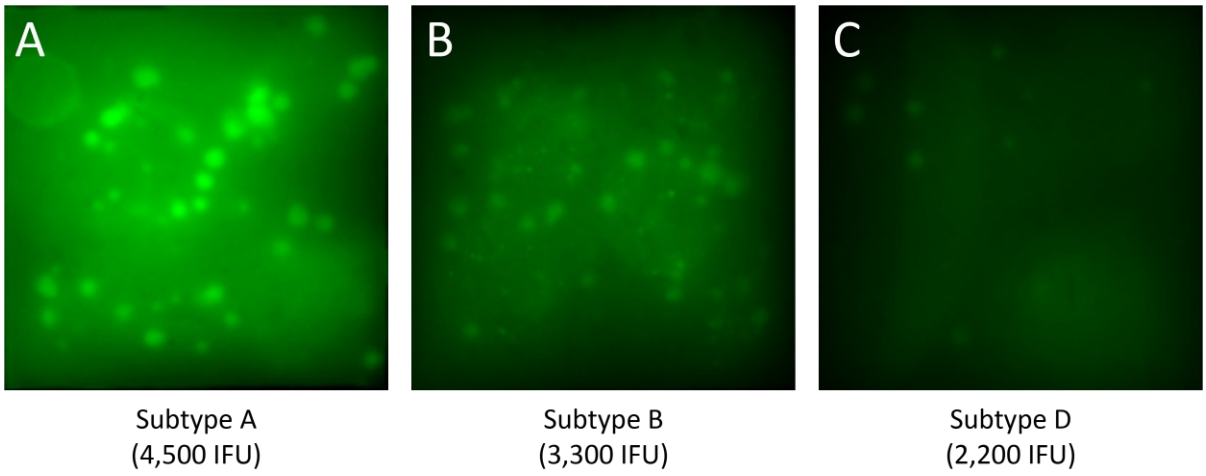

Figure 3-11: Comparison of fluorescence intensity observed in amplification nucleation site analysis between HIV RNA subtypes from subtypes A, B, and D, with average fluorescence intensities of several nucleation sites listed. Images are taken on the AZ100 microscope with identical settings at 750 seconds. Subtype A (0 mismatches) produces very bright nucleation sites. Subtype B (6 mismatches) produces dimmer nucleation sites, while subtype D (4 mismatches) produces the dimmest sites, though the sites are still are distinguishable from the background.

Across all subtypes (A, B and D) and RNA concentrations (30-3,000 cps/rxn) tested, amplification nucleation site analysis quantifies HIV RNA within an average of 0.35 (±0.22) $\log_{10}$(copies per reaction)

of the correct concentration, while tube-based RPA quantifies HIV RNA within of 0.53 (±0.38) $\log_{10}$(copies per reaction) of the correct concentration. qPCR, for comparison, quantifies HIV RNA within of 0.13 (±0.08) $\log_{10}$(copies per reaction) of the correct concentration. In this comparison, amplification nucleation site analysis is significantly more accurate than tube-based, time-to-threshold RPA ($p < 0.05$, via two-sided t-test). I hypothesize that this increase in accuracy is due to similar binomial classification of nucleation sites (i.e. present vs. not present) as done in traditional digital amplification methods; in this manner, individual amplification nucleation sites that may appear slowly or less brightly (in the case of subtypes with significant deviations in amplification efficiency) are counted the same as nucleation sites that appear very brightly. As there is very little time dependency in amplification nucleation site analysis, some of the inherent variation observed in traditional tube-based RPA is likely mitigated.

The recent target product profile (TPP) by Drain *et al*. states an ideal point-of-care HIV viral load test should have a quantitative precision of less than 0.3 $\log_{10}$ copies/mL.[78] While the metric used in the TPP represents an entire workflow's level of precision (e.g. sample preparation, amplification, and detection), it can roughly be applied to amplification and detection workflows on a per reaction basis as well. Amplification nucleation site analysis does not fully meet this requirement in its current form, though it is likely that slight adjustments to the workflow (e.g. larger amplification area to more accurately resolve nucleation sites) would further improve the level of precision. Multiple or degenerate primers may also aid in quantification across subtype.

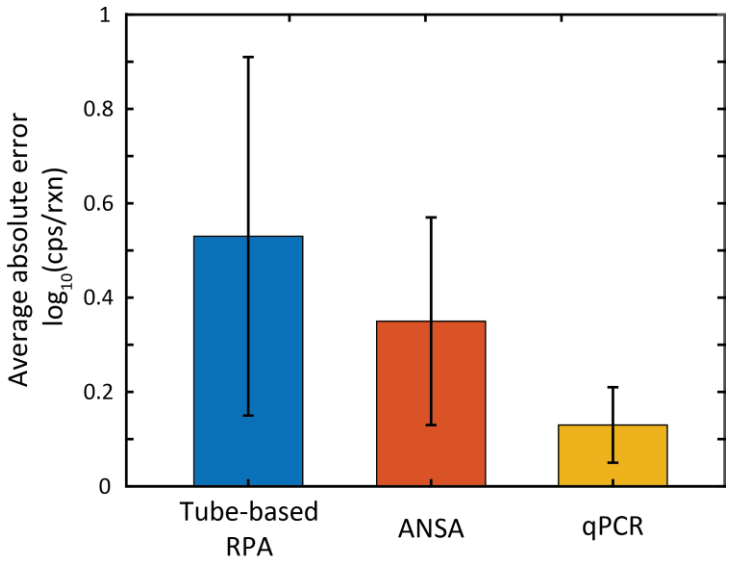

Figure 3-12: Average absolute quantification error of tube-based RPA, amplification nucleation site analysis (ANSA), and qPCR across 30-3,000 cps/rxn using extracted HIV RNA from subtypes A, B, and D (n = 31). Tube-based RPA (with traditional time-to-threshold analysis) is able to quantify the samples tested within 0.53 (±0.38) $\log_{10}$(cps/rxn) of the correct concentration on average, while amplification nucleation site analysis is able to quantify to within 0.35 (±0.22) $\log_{10}$(cps/rxn) of the correct concentration on average. qPCR quantifies the samples to within 0.13 (±0.08) $\log_{10}$(cps/rxn) of the correct concentration on average. All three methods are statistically different from each other ($p \leq 0.05$).

Crude sample preparation with remnant inhibitors/confounders can also adversely affect traditional amplification quantification, though it is not yet clear if this will impact the quantification accuracy of amplification nucleation site counting.

Smartphone- and inexpensive-based fluorescence readers have been used to detect and quantify isothermal amplification assays, typically using either endpoint fluorescence or time-to-threshold values.[237,246,248,249] Mobile phone or inexpensive optical component based readers may be appealing for a POC setting because they potentially result in lower costs and greater accessibility. However, it is well known that differences in phone components (i.e. camera quality and/or flash spectrum) can result in differing signals,[250,251] potentially confounding quantification if not properly calibrated. Amplification nucleation site analysis does not rely on relative fluorescence or precise pixel intensity values and may

prove to be a more robust and consistent method of quantification across inexpensive optics as well as mobile phone types and models.

3.4 Summary

I present a novel method for HIV DNA and RNA nucleic acid quantification using paper-based isothermal amplification and nucleation site amplification counting. I observe discrete fluorescent amplification nucleation sites when recombinase polymerase amplification is performed on porous fiber substrates and use an image analysis algorithm to count the sites. The number of amplification sites follows a power law relation to the number of input nucleic acid copies. Using DNA targets, I report a quantifiable range of 67-3,000 cps/rxn, as higher copy concentrations lead to significant amplification nucleation site merging and difficulty in site quantification using my algorithms. With HIV RNA targets, I show well-defined correlation between nucleation sites and input copies between 50-3,000 cps/rxn. This amplification nucleation site analysis method provides significantly more precise quantification than traditional tube-based time-to-threshold analysis across HIV supernatant subtypes A, B, and D. The amplification process takes less than 20 minutes at a single temperature with inexpensive materials and minimal user steps, and I believe that amplification nucleation site analysis could be leveraged in low-cost point-of-care nucleic acid amplification tests to provide more robust isothermal nucleic acid amplification quantification ability compared to current methods. I also present a mobile phone-based imaging system that is able to quantify amplification nucleation sites with a custom onboard processing app with similar performance to that of a microscope-based setup, suggesting that mobile phone-based amplification nucleation site analysis is a viable strategy for point-of-care applications.

I observe merging of nucleation sites at higher concentrations of target that limits the quantifiable range of my approach. There are several ways to improve the dynamic range. Improved image analysis algorithms, perhaps one using pattern recognition over time, may extend the quantifiable range by resolving

additional nucleation sites that are currently difficult to discern from site merging effects. The effective dynamic range of the system can be shifted by dilution of the sample, allowing for higher concentrations of target to be quantified. Using this dilution approach, multiple amplification pads could be used to extend the dynamic range, particularly if the expected copy number order of magnitude is not known *a priori*. This dilution scheme with multiple parallel experiments is frequently used in ddPCR. Several preliminary experiments have shown that increasing the area of the amplification pad (e.g. through tripling the reaction volume while keeping the nucleic acid copy number per reaction constant) can increase the dynamic range, as it effectively reduces the amplification nucleation site spatial density.

There is an inherent tradeoff in analytical techniques between reducing cost and complexity and decrease in performance. Amplification nucleation site analysis currently has a more limited dynamic range than qPCR or digital isothermal methods; however, the simplicity and potential for lower cost compared to other techniques may ultimately meet target product profiles. This is particularly true in an application spaces where pathogen concentrations are relatively low, such as in HIV viral load monitoring, where sample quantification is particularly valued near traditional cutoffs of 1,000 copies of HIV RNA per mL of plasma for antiretroviral efficacy determination.[78] Further optimization of membrane properties may also be useful in improving the limit-of-detection, as the important characteristics and properties of different membrane types in relation to their ability to sustain amplification reactions is still unclear.

I hypothesize that the RPA grouping agents, which increase the reaction fluid's bulk viscosity, are crucial in the formation of individual nucleation sites. For this reason, I do not expect this method will be possible with other native isothermal amplification chemistries; however, it may be possible to increase the viscosity of other amplification techniques (e.g. LAMP) through the addition of grouping agents with similar results.

The amplification nucleation site analysis method presented here can be integrated with most nucleic acid amplification sample preparation workflows to be used at the point-of-care. Each disease target has specific sample preparation requirements. For example, viral detection in blood samples, such as HIV,

requires viral envelope lysis, cell fractionation, RNase deactivation, and purification from amplification inhibitors (such as heme).[78] Viral detection in nasal and saliva samples, such as SARS-CoV-2 testing, can be accomplished at the POC with minimal sample preparation by direct addition of the sample into viral transport media with a lysis surfactant and reducing agent (such as DTT).[240,252,253] One potential challenge of integration of ANSA with various POC sample preparation methods is the requirement of homogenous distribution of target nucleic acids throughout the amplification pad. Many sample preparation methods purposefully concentrate target nucleic acids from larger initial sample volumes to improve limits-of-detection (such as the work discussed in Chapter 2: Without even distribution of nucleic acids throughout the amplification pad, the nucleation sites would likely be grouped closely together, further complicating quantification. While homogenous distribution of concentrated nucleic acids is trivial with the use of pipettes and tube-based manipulations, this becomes challenging in devices that rely on passive wicking to manipulate fluids, such as in paper-based diagnostics. It may be possible to use membranes with unique wicking properties to evenly distribute sample, such as that shown in Ahn *et al.*[147] They used a membrane with an asymmetric pore structure (Vivid plasma separation membrane) as a transfer membrane to which sample was added; the sample completely saturated the smaller pores of the asymmetric membrane first, resulting in a uniform distribution of sample across the membrane before wicking upwards through the larger pores and into overlaying amplification pads/zones. It is unclear how the flow dynamics of nucleic acids in these porous structures may affect nucleic acid distribution, though this is an ongoing area of research.

Chapter 4: Summary and Recommendations

4.1 Research Overview

There is an urgent, yet unmet need for sensitive and specific tests and devices for HIV viral load monitoring at the point-of-care. Molecular tests that target pathogenic nucleic acids are the gold standard for initial detection and subsequent monitoring of disease severity and are able to detect infection weeks before other available methods.[31,32] NAAT tests are mostly relegated to centralized laboratories due to the burdensome nature of these assays, requiring numerous pipetting, washing, and other fluid manipulation steps to progress through the three stages of (1) sample preparation, (2) amplification, and (3) detection. Automation has been extensively employed in large-format, high-throughput robotic platforms, alleviating many (otherwise) manual user steps. These machines are not readily accessible in low- and middle-income countries or settings where the burden of disease is often the highest, as requirements of controlled operating environment, stable electricity, and skilled technicians can be difficult to satisfy. In the context of HIV, there is a urgent need for more than 50 million viral load tests per year to meet World Health Organization 95-95-95 targets for controlling the ongoing HIV pandemic.[34] Near-point-of-care platforms have been developed for a number of bloodborne diseases, including HIV, though the costs of these platforms are prohibitive for more widespread, disseminated use, as they still rely on traditional robotics and automation which drives costs upwards.[80,81] Further research and development are needed to investigate new and novel techniques to address the specific needs of HIV viral load testing (and bloodborne nucleic acid testing in general) at the point-of-care.

In this dissertation, I describe novel methods for sample preparation, amplification, and detection, towards a point-of-care HIV viral load test device. I developed a paper-and-plastic device for nucleic acid sample preparation from human whole blood samples, integrating blood fractionation, proteolytic protein digestion, and isotachophoretic extraction of target DNA. The device uses low-cost materials and reagents and requires only the addition of several buffers and the removal of tape to produce purified, readily

amplifiable nucleic acids. The paper-based microfluidic device processes a 33 μL sample of undiluted whole blood by fractionating the blood into cell-free plasma (excluding WBCs which would theoretically harbor pro-viral HIV DNA), and electrokinetically separate and purify the target DNA using isotachophoresis for subsequent off-chip amplification via recombinase polymerase amplification. This process takes less than 30 minutes with minimal user interactions or steps. I am able to successfully extract and amplify at target concentrations as low as 100 cps/rxn, which corresponds to a concentration of 3 x 10^3 cps/mL of whole blood, within clinically relevant ranges of HIV, as well as that of HCV and HBV.[208,209,254]

I also show the development and integration of lyophilized RNase inactivation chemistries onto paper-like analytical membranes for point-of-care applications. This work builds off previously published work from our group, in which RNase inactivation chemistries were investigated for tube-based viral lysis and RNase inactivation of HIV+ plasma samples, though this work still required a number of fluid manipulation, pipetting, and mixing steps.[46,109] Rapid RNase inactivation is crucial in nucleic acid amplification tests that target RNA, including viral load monitoring. Methods for drying down these reagents onto paper-like analytical membranes such that they are stable and can be easily integrated into a point-of-care device were investigated, including simple air-drying and lyophilization. The RNase inactivation reagents consisted of sodium dodecyl sulfate (a strong detergent), proteinase K (a wide-spectrum protease) and dithiothreitol (a reducing agent). I show that these reagents retain their RNase inactivation properties after lyophilization onto a Fusion 5 glass-fiber membrane, eliminating endogenous RNase activity in human serum in less than 15 minutes. This is an important step towards integration into a point-of-care device for viral load testing, in which these reagents could be rehydrated by the sample, eliminating any user fluid manipulation or mixing steps.

I detail a novel method for the quantification of recombinase polymerase amplification reactions through amplification nucleation site analysis. While RPA is attractive for point-of-care applications due to its low incubation temperature (39 °C) and fast time to results (< 20 minutes), it is unclear whether traditional quantification metrics can be used in applications that require precise sample quantification (as

needed in HIV viral load monitoring) due to its lack of synchronized amplification, variable reaction initiation, and viscous reaction chemistry.[148] More common methods of quantification, such as tube-based time-to-threshold, can result in large quantification uncertainties, particularly across HIV subtypes.[154] I show that performing RPA on paper-like analytical membranes produces discrete fluorescent amplification nucleation sites. These amplification nucleation sites appear to grow over the course of a 20-minute incubation, with the number of nucleation sites correlating to the input DNA or RNA concentration in an almost pseudo-digital manner. I developed a site counting algorithm to quantify the number of nucleation sites per reaction and illustrate that this new method can quantify input copy numbers of both DNA and RNA between 67-3,000 cps/rxn across HIV subtypes A, B, and D significantly more accurately than traditional tube-based RPA with time-to-threshold quantification. This method can be performed with a smart phone and accompanying app, using inexpensive optics, showing great promise for low-cost applications.

The work presented in this dissertation represents steps towards the currently unmet need for technologies addressing sample preparation, amplification, and detection that are amenable to point-of-care settings. Novel methods are needed to meet challenging HIV viral load testing product profile targets for sensitivity and specificity, cost, and ease of use. I anticipate that the developments presented here can be further combined and integrated into a single device for viral load testing, such as envisioned in Figure 4-1. An ideal device must successfully integrate blood fractionation, viral lysis and RNase inactivation, ITP extraction of viral RNA, and amplification and detection. This will require significant engineering, as each step requires its own optimization and integration, though would represent a major step towards disseminated viral load testing.

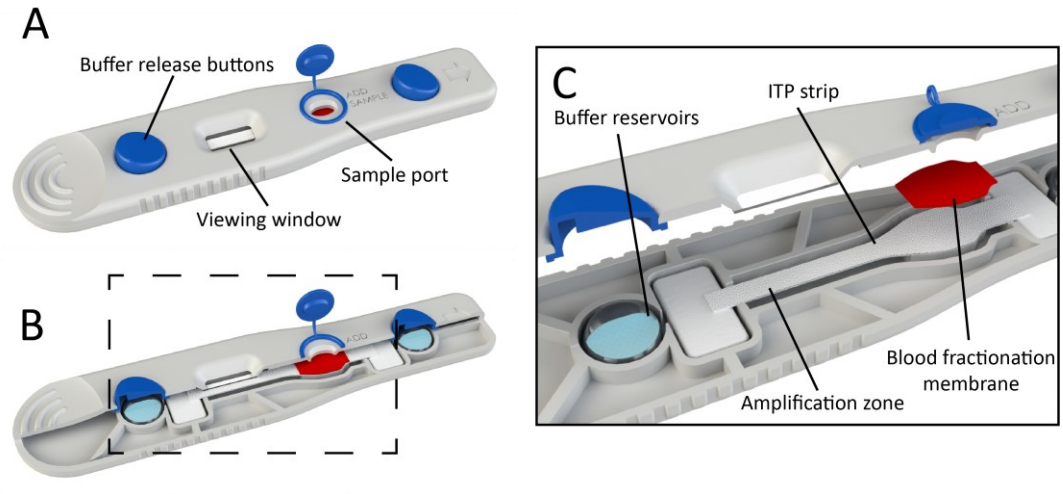

Figure 4-1: Renders of envisioned, theoretical point-of-care viral load test device with integrated blood fractionation, viral lysis and RNase inactivation, isotachophoretic extraction of viral RNA, and amplification. (A) Full device with sample port and user-activated buttons which release ITP buffers from on-device blister packs. (B), (C) Cut-away views, showing the blood fractionation membrane, ITP strip and amplification zones, and buffer reservoirs. A device such as this would likely be used with a separate reusable reader-unit, which may contain the more expensive components such as power supplies, heating, and/or optics.

4.2 Other Relevant Disease Targets

While HIV is the primary focus of this dissertation, many of the unmet clinical needs and technologies described here also apply to other bloodborne diseases for initial diagnosis or surveillance of diseases progression. These include hepatitis B and hepatitis C which have very similar characteristics to HIV (e.g. viral morphology, genetic diversity, and necessary limits of detection).

4.2.1 Hepatitis B

Hepatitis B is caused by small, enveloped virus with a partially double-stranded DNA genome.[255] It preferentially infects hepatocytes, with prolonged infection leading to chronic liver disease, cirrhosis, and/or liver cancer. The hepatitis B virus (HBV) can be spread through blood or sexual contact.[256] The World Health Organization estimates that in 2019, there were 296 million people living with chronic

hepatitis B infection and nearly 820,000 deaths annually. Initial hepatitis B diagnosis is primarily done via antigen or antibody tests with a blood sample, though only 10.5% of people living with hepatitis B are aware of their infection.[256,257] In low-resource settings, rapid diagnostic tests (RDTs) are often used for initial diagnosis. While preventative vaccination is highly effective, antivirals also exist for hepatitis B treatment (e.g. tenofovir or entecavir).[256,258] Routine viral load tests (i.e. quantitative nucleic acid amplification tests) are recommended to both initiate treatment and track efficacy, as well as for monitoring antiviral resistance.[259] Viral loads typically range from 300 to upwards of 10^6 cps/mL of serum in the case of uncontrolled infection.[67] HBV is genetically diverse as well, with at least eight identified genotypes (A-H).[260]

4.2.2 Hepatitis C

It is estimated that there are 58 million people living with chronic hepatitis C infection, with nearly 1.5 million new infections annually.[261] The hepatitis C virus (HCV) is spread primarily through blood contact (e.g. unsafe injection practices and/or injection drug use, unsafe healthcare, or unscreened blood transfusions) or sexual contact, though this is less common. HCV an enveloped, single-stranded RNA virus and is relatively genetically diverse, with seven separate genotypes identified.[262,263] While there is no preventative vaccine for hepatitis C, direct acting antiviral (DAA) treatments are available with cure rates of higher than 90%.[264,265] While pan-genomic DAA regimens are the standard-of-care, regimen decisions can be partially based on HCV genotype and previous treatment history, as the mutations between genotypes have led to various levels of specific DAA regimen susceptibility.[266,267]

Anti-HCV antibody tests are typically used for initial diagnosis of both acute and chronic HCV, with subsequent confirmation and quantification via HCV RNA nucleic acid amplification assays.[268] Rapid, point-of-care anti-HCV antibody tests exist (e.g. OraSure OraQuick HCV test[269]) and produce results in less than 20 minutes with finger prick blood samples, though antibody levels only become detectable 4-10

weeks post-infection.[262] HCV RNA, in contrast, is detectable 1-2 weeks after exposure. It is recommended that after DAA regimen completion, a follow-up HCV RNA quantification assay is performed to determine if sustained virological response (SVR) is achieved (defined by the absence of detectable HCV RNA 12 weeks after treatment completion).[262,268] The only currently available near-point-of-care solution for HCV RNA quantification is the Cepheid *GeneXpert*.

Two target product profiles have been published to guide development of HCV nucleic acid amplification tests for the diagnosis of active viremia in decentralized/low-resource settings.[270,271] The goals of the ideal tests are to (1) diagnose active HCV infection and (2) confirm cure upon treatment completion. These TPPs state that ideally, a test would be able to quantify HCV RNA with a sensitivity of 200 IU/mL, though a qualitative test with a sensitivity of 1,000-3,000 IU/mL would also be acceptable. The majority of individuals with chronic HCV infection have viral loads of 10^4-10^7 IU/mL with viral loads as low as 1,000 IU/mL in early-stage infection.[254] The tests should cost less than $15 per test (though instrumentation can be significantly more), should require less than two manual steps, and ideally operate with capillary whole blood.[270] These are ambitious targets to satisfy, but offer a roadmap to an acceptable POC HCV RNA test.

4.3 Reflections and Recommendations for Future Work

In this dissertation, I focus on separate elements of the nucleic acid amplification testing process: sample preparation, and amplification and detection. Significant further advancement and innovation are required in each of these areas to bring low-cost, disseminated HIV viral load testing to the point-of-care. For instance, in work presented here, I was able to purify, extract, and amplify target DNA from whole blood samples in concentrations as low as 3×10^3 cps/mL of whole blood, which equates to roughly 5,000 cps/mL of plasma/serum. Current target product profiles recommend POC HIV viral load tests have an LoD of between 200-1,000 cps/mL of plasma/serum. Increasing both the volume of sample processed and the isotachophoretic extraction efficiency of the described device would allow for more sensitive detection.

Additionally, refinement of the user steps is likely necessary, further reducing the number of steps and actions necessary from the user; for instance, continuing to investigate strategies to eliminate the removal step of the blood fractionation module or the inclusion of blister packs would ease user steps. In the current process of amplification nucleation site analysis, the dynamic range is currently limited to 3,000 cps/rxn due to site merging behavior which makes discrete site identification challenging in high copy concentration regimes. While precise nucleic acid quantification at elevated viral loads is likely not critically necessary for HIV VL testing as a significant viral load (>1,000 cps/mL) is indicative of treatment failure regardless of exact quantification, extending this dynamic range to higher concentrations may be useful for other disease targets with higher typical viral concentrations. This range could likely be increased by enlarging the amplification pad size while decreasing its thickness, spatially separating the nucleation sites for improved quantification. Simultaneous testing of several serial dilutions of sample in a small microfluidic device would also extend the dynamic range of the system.

While there are many adjustments and advancements that could be made to these processes separately, integration has always been a significant hurdle for point-of-care devices. NAAT testing requires timed, sequential fluid manipulation steps that are typically performed via pipetting or valving, either manually or robotically. In an ideal point-of-care device, these processes would be performed without significant user steps. Various approaches for fluid control, such as wax valving or swelling membrane "switches" have been developed, though these methods have been largely limited to academic works thus far, with the Cue platform being the exception (which uses wax valves to sequentially release substrate and wash buffers).[272,273] Integration is particularly difficult in applications such as HIV viral load monitoring where the required limits of detection are demanding. Integration can require compromise between various device aspects and maintaining sufficient efficacy throughout a device to meet these stringent requirements can be challenging. This requires a holistic approach to device design and an understanding of how separate technologies might interface with each other. Design for manufacturing (DFM) concepts should also be

considered during device design; in many cases, costs of manufacturing can quickly outpace costs of materials due to specialized manufacturing, assembly, and/or pick-and-place operations.

The COVID-19 pandemic has resulted in significantly more attention, urgency, and resources dedicated towards the development of widely disseminated diagnostic tests and kits. Much of this has focused on RDTs or LFAs in various form factors, though sizeable investments have been made in the development of nucleic acid amplification tests. In 2020, the NIH launched the Rapid Acceleration of Diagnostics (RADx) program to facilitate the rapid development of COVID-19 diagnostics with over $1.5 billion in federal funding.[274] This has funded a number of companies and academic groups who have developed POC NAAT-enabling technologies, including DETECT, Quidel, and Cue. This is an example of the major divergence from historical interest and funding in point-of-care NAAT technologies, with this sudden influx of monetary support spurring significant advancements. This, in concert with the FDA's use of Emergency Use Authorization (EUA) regulatory approval, has greatly accelerated development and commercialization for COVID-19 NAAT diagnostics, providing useful case-studies in device design and user acceptance for the next generation of assay and device developers to learn from. I hope that this recent surge in interest in NAATs will continue, and that these advancements will have positive effects to the development of point-of-care NAAT diagnostics for other diseases.

Citations to Previously Published Works

Portions of this dissertation have appeared in the following articles

Chapter 2

Sullivan BP, Bender AT, Nguyen DN, Zhang JY, Posner JD. Nucleic acid sample preparation from whole blood in a paper microfluidic device using isotachophoresis. *Journal of Chromatography* B 1163, 122494 (2021).

Chapter 3

Sullivan BP, Chou Y, Bender AT, Martin CD, Kaputa ZG, March H, Song M, Posner JD. Quantitative isothermal amplification on paper membranes using amplification nucleation site analysis. *Lab on a Chip*, 22, 2352-2363 (2022).

Appendix

A.1 Vivid integration experiments – Heat pressing

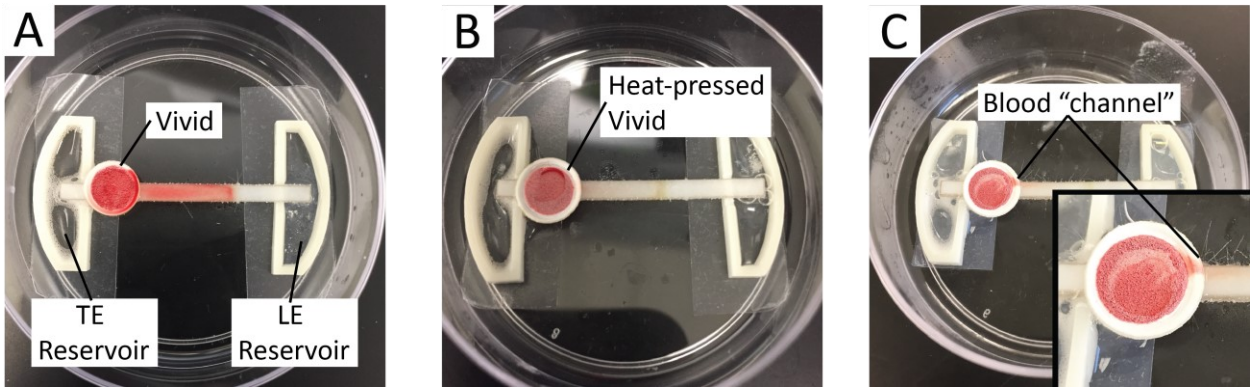

Figure A.1. Heat-pressed Vivid. Vivid circles were cut out to accommodate 20 µL blood volume (based on manufacturer's recommendations) and placed over a Fusion 5 ITP strip (with no blood fractionation fixturing). Whole blood (20 µL) was dispensed onto the Vivid, and after 3 minutes, the ITP buffers were added to their respective reservoirs and an electric potential was applied to the system, initiating ITP. (A) Using unprocessed Vivid, the red blood cells/hemoglobin migrate laterally off the Vivid and into the underlying Fusion 5 membrane during ITP, focusing in the ITP plug. (B) In Vivid that was heat pressed (performed by heating a metal annulus to ~150 °C and pressing by hand into the Vivid for 10 seconds), the pores near the edge of the Vivid membrane are fused/sintered together, providing a barrier for lateral flow. Here, the ITP plug is slightly visible on the Fusion 5 strip due to focused serum proteins, though no hemoglobin is visible. (C) In many experiments, the heat-pressing was not entirely complete, and small "channels" of RBCs/hemoglobin are visible wicking laterally through the Vivid and onto the underlying Fusion 5 membrane. While this method is promising for preventing lateral migration through the Vivid under ITP conditions, it is likely that significantly more precise temperature and pressure control are needed.

A.2 Vivid integration experiments – Wax printing

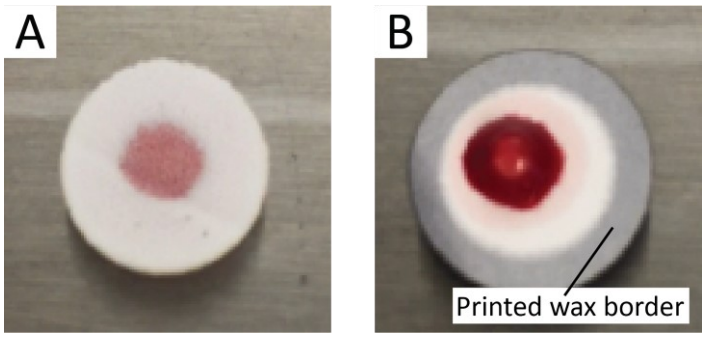

Figure A.2. Wax printed Vivid. A ColorQube 8570 (Xerox Corp., USA) printed a border of wax around a circle of Vivid membrane. The wax was then remelted at 150 °C for 5 minutes to completely fill the pore structure of the Vivid. A small amount of blood was then dispensed onto the Vivid and the wicking behavior was observed. (A) Using unprocessed Vivid, the whole blood immediately wicks through the larger pores and into the smaller pores on the underside of the membrane. (B) Using Vivid that had been printed upon and reheated, the blood does not wick well into the membrane, instead sitting on top of the membrane. I hypothesize that the membrane has been contaminated with oil from the printing process (likely from the transfer drum), affecting the hydrophilicity of the membrane. Both images are taken 2 minutes after blood dispensing.

A.3 Vivid integration experiments – Lysis reagents

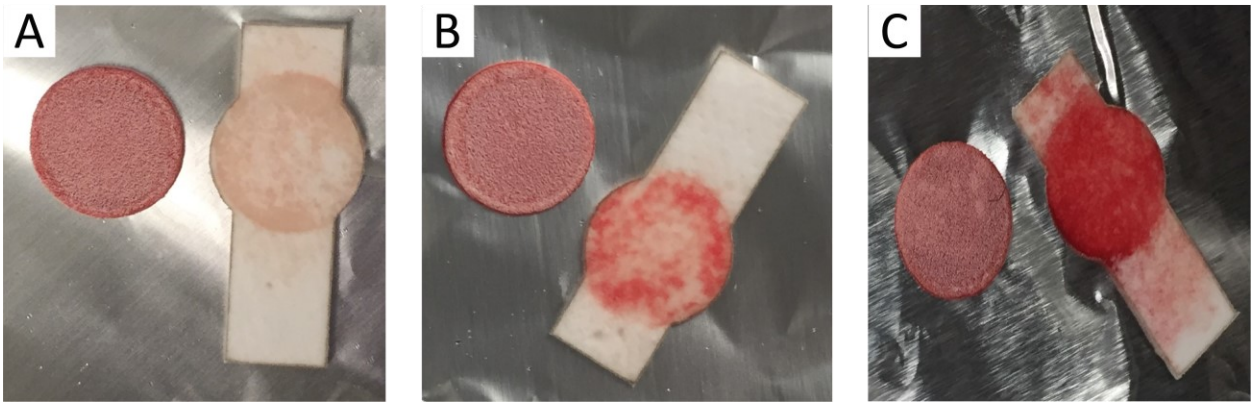

Figure A.3. Vivid experiments with potential lytic reagents dried down onto Fusion 5 membranes. A small circle of Vivid was placed on top of a Fusion 5 membrane, and whole blood was added to the Vivid (according to manufacturer's recommended volumes). After 4 minutes, the Vivid membrane is removed, and the system is imaged. Various potential lytic agents were dried down onto the Fusion 5 membrane previously. These included (A) 300 µg/mL proteinase K, (B) 10% (w/v) Triton-X 100 and 300 µg/mL proteinase K, and (C) 20% (w/v) Triton-X 100 and 300 µg/mL proteinase K. In all cases, the lytic agents were deposited onto the Fusion 5 membrane and air-dried at room temperature. With increasing Triton-X concentrations, significantly more hemolysis is visible in the underlying Fusion 5 membrane. This is likely due to the reagents diffusing upwards and interacting with the trapped red blood cells in the Vivid membrane. While these experiments are not indicative of other potential lytic agents (as proteinase K exhibits very little hemolysis), they signify that this is an area of necessary further investigation.

A.4 Circular Hough Transform (CHT) Method Algorithm – MATLAB Based

```
clear all; close all; clc;

%% User Inputs
namefile = uigetfile('*tif');

%% Crop Image
figure(1)
preview=imread(namefile,1200);
imshow(preview,[0 max(max(preview))])
draw = drawrectangle('Color','b','FaceAlpha',0.01); % Select region of interest
rect = customWait(draw);
xmin = double(rect(1));
ymin = double(rect(2));
height = double(rect(4));
L = double(rect(3));

%% Compile Image Data

k = length(imfinfo(namefile)); %number of frames in data stack
for j=1:k
 Image=imread(namefile,j); % read in multiple image tiff file
 imcell=imcrop(Image,[xmin ymin L height]);

 %Resample to higher pixel density
 sz = size(imcell);
 xg = 1:sz(1);
 yg = 1:sz(2);
 F = griddedInterpolant({xg,yg},double(imcell));
 xq = (0:1/3:sz(1))';
 yq = (0:1/3:sz(2))';
 vq = F({xq,yq});

 X(:,j) = vertcat(vq(:));
end

%% Smooth Data - Average Every N Frames
[m1,n1] = size(X);
aveint = 10;
X_aveint = reshape(X, m1, aveint, n1/aveint);
X_smooth = squeeze(mean(X_aveint,2));

[m2,n2] = size(vq);
[m3,n3] = size(X_smooth);

%% Subtract Background - ATB Method

fr = 0.1*n3; %Frame that is 0.1 way through image stack
X_back = mean(X_smooth(:,1:fr),2);

X_new = bsxfun(@minus,X_smooth,X_back);
[m2,n2] = size(vq);
se = strel('disk',15);

for i = 1:k/aveint
 new = reshape(X_new(:,i),m2,n2);
 new = mat2gray(new);
 new_all(:,:,i)=new;
 background = imopen(new,se);
 newback = (new - background);
```

```
J1 = newback;
 J1_all(:,:,i) = J1;
 [centers, radii, metric] = imfindcircles(J1,...
 [8 20],'objectpolarity','bright');... % Alter for performance boost!
 radii_all{i} = radii;
 metric_all{i} = metric;
 centers_all{i} = centers;
 dots(i) = length(radii);
 % Visualize dot size increase over time
 metricbest = metric(metric>0.2);
 averad(i) = mean(radii(1:length(metricbest)));
 averad(isnan(averad))=0;


 figure(2)
 imshow(J1)

 if isempty(centers) == 0
 figure(3)
 plot(centers(:,1),-centers(:,2),'k.','MarkerSize',15)
 hold on
 end
clc
end
%% Visualize Nucleation Sites
figure(2)
imshow(new_all(:,:,k/aveint/2))
for i = 1:k/aveint
 viscircles(centers_all{i},radii_all{i},'EdgeColor','b');
end

figure(4)
imshow(new_all(:,:,k/aveint/2))
viscircles(centers_all{k/aveint/2},radii_all{k/aveint/2},'EdgeColor','b');

%% Number of Nucleation Sites Over Time
smoothdots = smoothdata(dots,'movmean',5);
round(max(smoothdots))
figure(5)
set(gcf,'Units','inches');
time = linspace(0,20,length(dots));
plot(time,dots)
hold on
plot(time,smoothdots)
ylabel('Number of Amplification Nucleation Sites')
xlabel('Time [min]')

Count = ans
```

A.5 Threshold Analyze Particles (TAP) Method Algorithm – ImageJ Based

```
run("Grouped Z Project...", "projection=[Average Intensity] group=10");
run("Subtract Background...", "rolling=10 stack");
setSlice(48)
run("Make Binary", "method=Otsu background=Dark calculate");
run("Median...", "radius=2 stack");
run("Watershed", "stack");
run("Analyze Particles...", "size=20-Infinity exclude summarize stack");
```

Bibliography

1. Hymes KB, Cheung T, Greene JB, Prose NS, Marcus A, Ballard H, et al. Kaposi's sarcoma in homosexual men-a report of eight cases. Lancet. 1981 Sep 19;2(8247):598–600.

2. Global HIV & AIDS statistics — Fact sheet [Internet]. [cited 2021 Nov 11]. Available from: https://www.unaids.org/en/resources/fact-sheet

3. WHO | HIV/AIDS [Internet]. WHO. [cited 2019 Oct 9]. Available from: http://www.who.int/gho/hiv/en/

4. del Rio C. The Global HIV epidemic: What the pathologist needs to know. Semin Diagn Pathol. 2017 Jul;34(4):314–7.

5. Roser M, Ritchie H. HIV / AIDS. Our World in Data [Internet]. 2018 Apr 3 [cited 2019 Oct 9]; Available from: https://ourworldindata.org/hiv-aids

6. Becerra JC, Bildstein LS, Gach JS. Recent Insights into the HIV/AIDS Pandemic. Microb Cell. 3(9):451–75.

7. The Biology and Evolution of HIV | Annual Review of Anthropology [Internet]. [cited 2021 Nov 11]. Available from: https://www-annualreviews-org.offcampus.lib.washington.edu/doi/10.1146/annurev.anthro.30.1.85

8. Okoye AA, Picker LJ. CD4+ T cell depletion in HIV infection: mechanisms of immunological failure. Immunol Rev. 2013 Jul;254(1):54–64.

9. Craigie R. The molecular biology of HIV integrase. Future Virology. 2012 Jul;7(7):679–86.

10. Cummins NW, Badley AD. Making sense of how HIV kills infected CD4 T cells: implications for HIV cure. Mol Cell Ther. 2014 Jul 3;2:20.

11. Hernandez-Vargas EA, Middleton RH. Modeling the three stages in HIV infection. Journal of Theoretical Biology. 2013 Mar 7;320:33–40.

12. Robertson DL, Anderson JP, Bradac JA, Carr JK, Foley B, Funkhouser RK, et al. HIV-1 nomenclature proposal. Science. 2000 Apr 7;288(5463):55–6.

13. Bbosa N, Kaleebu P, Ssemwanga D. HIV subtype diversity worldwide. Current Opinion in HIV and AIDS. 2019 May;14(3):153–60.

14. Hemelaar J, Gouws E, Ghys PD, Osmanov S. Global and regional distribution of HIV-1 genetic subtypes and recombinants in 2004. AIDS. 2006 Oct 24;20(16):W13.

15. Hemelaar J, Elangovan R, Yun J, Dickson-Tetteh L, Fleminger I, Kirtley S, et al. Global and regional molecular epidemiology of HIV-1, 1990–2015: a systematic review, global survey, and trend analysis. The Lancet Infectious Diseases. 2019 Feb;19(2):143–55.

16. Antoniou T, Park-Wyllie LY, Tseng AL. Tenofovir: A Nucleotide Analog for The Management of Human Immunodeficiency Virus Infection. Pharmacotherapy: The Journal of Human Pharmacology and Drug Therapy. 2003;23(1):29–43.

17. Gallant J, Lazzarin A, Mills A, Orkin C, Podzamczer D, Tebas P, et al. Bictegravir, emtricitabine, and tenofovir alafenamide versus dolutegravir, abacavir, and lamivudine for initial treatment of HIV-1 infection (GS-US-380-1489): a double-blind, multicentre, phase 3, randomised controlled non-inferiority trial. The Lancet. 2017 Nov 4;390(10107):2063–72.

18. Updated recommendations on first-line and second-line antiretroviral regimens and post-exposure prophylaxis and recommendations on early infant diagnosis of HIV [Internet]. [cited 2021 Nov 12]. Available from: https://www.who.int/publications-detail-redirect/WHO-CDS-HIV-18.51

19. UNAIDS. UNAIDS Data. In 2019. p. 1–476.

20. Antiretroviral Therapy Cohort Collaboration. Survival of HIV-positive patients starting antiretroviral therapy between 1996 and 2013: a collaborative analysis of cohort studies. Lancet HIV. 2017;4(8):e349–56.

21. Rodger A, Bruun T, Cambiano V, Vernazza P, Estrada V, Lunzen JV, et al. 153LB HIV Transmission Risk Through Condomless Sex If HIV+ Partner On Suppressive ART: PARTNER Study. :1.

22. Baeten JM, Donnell D, Ndase P. Antiretroviral prophylaxis for HIV prevention in heterosexual men and women. N Engl J Med. 2012;367(5).

23. Donnell D, Baeten JM, Bumpus NN, Brantley J, Bangsberg DR, Haberer JE, et al. HIV Protective Efficacy and Correlates of Tenofovir Blood Concentrations in a Clinical Trial of PrEP for HIV Prevention. J Acquir Immune Defic Syndr. 2014 Jul 1;66(3):340–8.

24. Bangsberg DR. Preventing HIV Antiretroviral Resistance through Better Monitoring of Treatment Adherence. J Infect Dis. 2008 May 1;197(Supplement_3):S272–8.

25. 90-90-90: treatment for all [Internet]. [cited 2019 Oct 19]. Available from: https://www.unaids.org/en/resources/909090

26. UNAIDS. Prevailing Against Pandemics [Internet]. 2020 [cited 2022 Oct 22]. Available from: https://aidstargets2025.unaids.org/assets/images/prevailing-against-pandemics_en.pdf

27. Shroufi A, Van Cutsem G, Cambiano V, Bansi-Matharu L, Duncan K, Murphy RA, et al. Simplifying switch to second-line antiretroviral therapy in sub Saharan Africa: predicted effect of using a single viral load to define efavirenz-based first-line failure. AIDS. 2019 Aug 1;33(10):1635–44.

28. Usdin M, Guillerm M, Calmy A. Patient needs and point-of-care requirements for HIV load testing in resource-limited settings. J Infect Dis. 2010 Apr 15;201(Supplement_1):S73–7.

29. Eisinger RW, Dieffenbach CW, Fauci AS. HIV Viral Load and Transmissibility of HIV Infection: Undetectable Equals Untransmittable. JAMA. 2019 Feb 5;321(5):451–2.

30. Fiebig EW, Wright DJ, Rawal BD, Garrett PE, Schumacher RT, Peddada L, et al. Dynamics of HIV viremia and antibody seroconversion in plasma donors: implications for diagnosis and staging of primary HIV infection. AIDS. 2003 Sep 5;17(13):1871–9.

31. Branson BM, Stekler JD. Detection of Acute HIV Infection: We Can't Close the Window. The Journal of Infectious Diseases. 2012 Feb 15;205(4):521–4.

32. Cohen MS, Shaw GM, McMichael AJ, Haynes BF. Acute HIV-1 Infection. N Engl J Med. 2011 May 18;364(20):1943–54.

33. Calmy A, Ford N, Hirschel B, Reynolds SJ, Lynen L, Goemaere E, et al. HIV Viral Load Monitoring in Resource-Limited Regions: Optional or Necessary? Clin Infect Dis. 2007 Jan 1;44(1):128–34.

34. World Health Organization. HIV Molecular Diagnostics Toolkit to Improve Access to Viral Load Testing and Infant Diagnosis [Internet]. 3rd ed. Geneva: World Health Organization; 2020 [cited 2021 Nov 16]. Available from: https://apps.who.int/iris/handle/10665/336499

35. Core Concepts - Acute and Recent HIV Infection - Screening and Diagnosis - National HIV Curriculum [Internet]. [cited 2021 Nov 16]. Available from: https://www.hiv.uw.edu/go/screening-diagnosis/acute-recent-early-hiv/core-concept/all

36. Bloomfield MG, Balm MND, Blackmore TK. Molecular testing for viral and bacterial enteric pathogens: gold standard for viruses, but don't let culture go just yet? Pathology. 2015 Apr 1;47(3):227–33.

37. Price CP. Regular review: Point of care testing. BMJ: British Medical Journal. 2001;322(7297):1285.

38. Niemz A, Ferguson TM, Boyle DS. Point-of-care nucleic acid testing for infectious diseases. Trends in Biotechnology. 2011 May 1;29(5):240–50.

39. Anastassova Dineva M, Mahilum-Tapay L, Lee H. Sample preparation: a challenge in the development of point-of-care nucleic acid -based assays for resource-limited settings. Analyst. 2007;132(12):1193–9.

40. Heiniger EK, Buser JR, Mireles L, Zhang X, Ladd PD, Lutz BR, et al. Comparison of point-of-care-compatible lysis methods for bacteria and viruses. Journal of Microbiological Methods. 2016 Sep 1;128:80–7.

41. de Lange N, Tran TM, Abate AR. Electrical lysis of cells for detergent-free droplet assays. Biomicrofluidics [Internet]. 2016 Mar 22 [cited 2018 Oct 15];10(2). Available from: https://www.ncbi.nlm.nih.gov/pmc/articles/PMC4808063/

42. Gill C, Wijgert JHHM van de, Blow F, Darby AC. Evaluation of Lysis Methods for the Extraction of Bacterial DNA for Analysis of the Vaginal Microbiota. PLOS ONE. 2016 Sep 19;11(9):e0163148.

43. Boom R, Sol CJ, Salimans MM, Jansen CL, Wertheim-van Dillen PM, van der Noordaa J. Rapid and simple method for purification of nucleic acids. J Clin Microbiol. 1990 Mar;28(3):495–503.

44. Katevatis C, Fan A, Klapperich CM. Low concentration DNA extraction and recovery using a silica solid phase. PLOS ONE. 2017 May 5;12(5):e0176848.

45. Melzak KA, Sherwood CS, Turner RFB, Haynes CA. Driving Forces for DNA Adsorption to Silica in Perchlorate Solutions. Journal of Colloid and Interface Science. 1996 Aug 10;181(2):635–44.

46. Bender AT, Sullivan BP, Lillis L, Posner JD. Enzymatic and Chemical-Based Methods to Inactivate Endogenous Blood Ribonucleases for Nucleic Acid Diagnostics. The Journal of Molecular Diagnostics. 2020 Aug 1;22(8):1030–40.

47. Sambrook J, Russell DW. Purification of Nucleic Acids by Extraction with Phenol:Chloroform. Cold Spring Harb Protoc. 2006 Jun 1;2006(1):pdb.prot4455.

48. RNeasy Kits [Internet]. [cited 2021 Nov 16]. Available from: https://www.qiagen.com/us/products/discovery-and-translational-research/dna-rna-purification/rna-purification/total-rna/rneasy-kits/

49. Mullis KB, Erlich HA, Arnheim N, Horn GT, Saiki RK, Scharf SJ. Process for amplifying, detecting, and/or-cloning nucleic acid sequences [Internet]. US4683195A, 1987 [cited 2019 Oct 8]. Available from: https://patents.google.com/patent/US4683195/en

50. Real-time RT-PCR detection of 12 respiratory viral infections in four triplex reactions [Internet]. [cited 2021 Nov 16]. Available from: https://www.ncbi.nlm.nih.gov/pmc/articles/PMC7108440/

51. Pai NP. Multiplexed point-of-care assays for HIV and co-infections for resource constrained settings: a perspective. Future Microbiol. 2015 Sep;10:1393–6.

52. Multiplex PCR: Optimization and Application in Diagnostic Virology | Clinical Microbiology Reviews [Internet]. [cited 2021 Nov 16]. Available from: https://journals.asm.org/doi/full/10.1128/CMR.13.4.559

53. Forootan A, Sjöback R, Björkman J, Sjögreen B, Linz L, Kubista M. Methods to determine limit of detection and limit of quantification in quantitative real-time PCR (qPCR). Biomolecular Detection and Quantification. 2017 Jun 1;12:1–6.

54. Corman VM, Eckerle I, Bleicker T, Zaki A, Landt O, Eschbach-Bludau M, et al. Detection of a novel human coronavirus by real-time reverse-transcription polymerase chain reaction. Eurosurveillance. 2012 Sep 27;17(39):20285.

55. Emery SL, Erdman DD, Bowen MD, Newton BR, Winchell JM, Meyer RF, et al. Real-Time Reverse Transcription–Polymerase Chain Reaction Assay for SARS-associated Coronavirus. Emerg Infect Dis. 2004 Feb;10(2):311–6.

56. Gudnason H, Dufva M, Bang DD, Wolff A. Comparison of multiple DNA dyes for real-time PCR: effects of dye concentration and sequence composition on DNA amplification and melting temperature. Nucleic Acids Research. 2007 Oct 1;35(19):e127.

57. A quantitative PCR (TaqMan) assay for pathogenic Leptospira spp | BMC Infectious Diseases | Full Text [Internet]. [cited 2021 Nov 16]. Available from: https://bmcinfectdis.biomedcentral.com/articles/10.1186/1471-2334-2-13

58. Drummond TG, Hill MG, Barton JK. Electrochemical DNA sensors. Nature Biotechnology. 2003 Oct;21(10):1192–9.

59. Tomita N, Mori Y, Kanda H, Notomi T. Loop-mediated isothermal amplification (LAMP) of gene sequences and simple visual detection of products. Nature Protocols. 2008 Apr;3(5):877–82.

60. Uddin SM, Ibrahim F, Sayad AA, Thiha A, Pei KX, Mohktar MS, et al. A Portable Automatic Endpoint Detection System for Amplicons of Loop Mediated Isothermal Amplification on Microfluidic Compact Disk Platform. Sensors. 2015 Mar;15(3):5376–89.

61. Niesters HGM. Quantitation of Viral Load Using Real-Time Amplification Techniques. Methods. 2001 Dec 1;25(4):419–29.

62. Heid CA, Stevens J, Livak KJ, Williams PM. Real time quantitative PCR. Genome Res. 1996 Oct 1;6(10):986–94.

63. Vogelstein B, Kinzler KW. Digital PCR. PNAS. 1999 Aug 3;96(16):9236–41.

64. Singanayagam A, Patel M, Charlett A, Lopez Bernal J, Saliba V, Ellis J, et al. Duration of infectiousness and correlation with RT-PCR cycle threshold values in cases of COVID-19, England, January to May 2020. Euro Surveill [Internet]. 2020 Aug 13 [cited 2021 May 5];25(32). Available from: https://www.ncbi.nlm.nih.gov/pmc/articles/PMC7427302/

65. Jaafar R, Aherfi S, Wurtz N, Grimaldier C, Van Hoang T, Colson P, et al. Correlation Between 3790 Quantitative Polymerase Chain Reaction–Positives Samples and Positive Cell Cultures, Including 1941 Severe Acute Respiratory Syndrome Coronavirus 2 Isolates. Clinical Infectious Diseases [Internet]. 2020 Sep 28 [cited 2021 May 20];(ciaa1491). Available from: https://doi.org/10.1093/cid/ciaa1491

66. Hsu CS, Liu CJ, Liu CH, Wang CC, Chen CL, Lai MY, et al. High hepatitis C viral load is associated with insulin resistance in patients with chronic hepatitis C. Liver International. 2008;28(2):271–7.

67. Iloeje UH, Yang HI, Su J, Jen CL, You SL, Chen CJ, et al. Predicting cirrhosis risk based on the level of circulating hepatitis B viral load. Gastroenterology. 2006 Mar;130(3):678–86.

68. Chang J, Omuomo K, Anyango E, Kingwara L, Basiye F, Morwabe A, et al. Field evaluation of Abbott Real Time HIV-1 Qualitative test for early infant diagnosis using dried blood spots samples in comparison to Roche COBAS Ampliprep/COBAS TaqMan HIV-1 Qual Test in Kenya. Journal of Virological Methods. 2014 Aug 1;204:25–30.

69. Abel G. Current status and future prospects of point-of-care testing around the globe. Expert Review of Molecular Diagnostics. 2015 Jul 3;15(7):853–5.

70. Peeling RW, Holmes KK, Mabey D. Rapid tests for sexually transmitted infections (STIs): the way forward. Sex Transm Infect. 2006 Dec;82(Suppl 5):v1–6.

71. Land KJ, Boeras DI, Chen XS, Ramsay AR, Peeling RW. REASSURED diagnostics to inform disease control strategies, strengthen health systems and improve patient outcomes. Nat Microbiol. 2019 Jan;4(1):46–54.

72. Zhang JY, Bender AT, Boyle DS, Drain PK, Posner JD. Current state of commercial point-of-care nucleic acid tests for infectious diseases. Analyst. 2021 Apr 26;146(8):2449–62.

73. Gous N, Scott L, Berrie L, Stevens W. Options to Expand HIV Viral Load Testing in South Africa: Evaluation of the GeneXpert® HIV-1 Viral Load Assay. PLoS ONE. 2016;11(12):e0168244.

74. Ndlovu Z, Fajardo E, Mbofana E, Maparo T, Garone D, Metcalf C, et al. Multidisease testing for HIV and TB using the GeneXpert platform: A feasibility study in rural Zimbabwe. PLOS ONE. 2018 Mar 2;13(3):e0193577.

75. Meggi B, Bollinger T, Zitha A, Mudenyanga C, Vubil A, Mutsaka D, et al. Performance of a True Point-of-Care Assay for HIV-1/2 Viral Load Measurement at Antenatal and Postpartum Services. JAIDS Journal of Acquired Immune Deficiency Syndromes. 2021 May 1;87(1):693–9.

76. Cepheid. Xpert® Tests: Viral Load (3134-03) [Internet]. 2021 [cited 2021 Nov 17]. Available from: http://embed.widencdn.net/pdf/plus/cepheid/rjl98pdqrz/Cepheid-Viral-Load-Tests-Datasheet-CE-IVD-3134-English.pdf?u=zcezkx

77. Cepheid Corporate Menu Flyer US IVD [Internet]. [cited 2022 Oct 12]. Available from: https://cepheid.widen.net/content/6rod6rervw/pdf/Cepheid-Corporate-Menu-Flyer-US-IVD-0323-English.pdf?u=bk12mm

78. Paul Drain, Jienchi Dorward, Andrew Bender, Lorraine Lillis, Francesco Marinucci. Point-of-care HIV viral load testing: An essential tool for a sustainable global HIV/AIDS response. Clinical Microbiology Reviews: 2018 In Review.

79. WHO. WHO Prequalification of In Vitro Diagnostics - Product: m-PIMA HIV-1/2 VL [Internet]. 2019 [cited 2019 Oct 30]. Available from: https://www.who.int/diagnostics_laboratory/evaluations/pq-list/190408_pqdx_0359_032_00_pqpr_mpima.pdf

80. Drain PK, Dorward J, Bender A, Lillis L, Marinucci F, Sacks J, et al. Point-of-Care HIV Viral Load Testing: an Essential Tool for a Sustainable Global HIV/AIDS Response. Clinical Microbiology Reviews. 2019 Jun 19;32(3):e00097-18.

81. Mukherjee S, Cohn J, Ciaranello AL, Sacks E, Adetunji O, Chadambuka A, et al. Estimating the Cost of Point-of-Care Early Infant Diagnosis in a Program Setting: A Case Study Using Abbott m-PIMA and Cepheid GeneXpert IV in Zimbabwe. JAIDS Journal of Acquired Immune Deficiency Syndromes. 2020 Jul 1;84:S63.

82. In Vitro Diagnostics EUAs - Molecular Diagnostic Tests for SARS-CoV-2 [Internet]. U.S. Food and Drug Administration; 2021. Available from: https://www.fda.gov/medical-devices/coronavirus-disease-2019-covid-19-emergency-use-authorizations-medical-devices/in-vitro-diagnostics-euas-molecular-diagnostic-tests-sars-cov-2#individual-molecular

83. Lucira Health. Lucira™ COVID-19 All-In-One Test Kit Instructions for Use [Internet]. [cited 2022 Oct 24]. Report No.: INST011 Rev 1. Available from: https://www.fda.gov/media/143808/download

84. Chin CD, Linder V, Sia SK. Lab-on-a-chip devices for global health: Past studies and future opportunities. Lab Chip. 2007;7(1):41–57.

85. Mariella R. Sample preparation: the weak link in microfluidics-based biodetection. Biomedical Microdevices. 2008 Dec;10(6):777–84.

86. Merindol N, Pépin G, Marchand C, Rheault M, Peterson C, Poirier A, et al. SARS-CoV-2 detection by direct rRT-PCR without RNA extraction. Journal of Clinical Virology. 2020 Jul 1;128:104423.

87. Wee SK, Sivalingam SP, Yap EPH. Rapid Direct Nucleic Acid Amplification Test without RNA Extraction for SARS-CoV-2 Using a Portable PCR Thermocycler. Genes. 2020 Jun;11(6):664.

88. Al-Soud WA, Rådström P. Purification and Characterization of PCR-Inhibitory Components in Blood Cells. Journal of Clinical Microbiology. 2001 Feb 1;39(2):485–93.

89. Abu Al-Soud W, Rådström P. Effects of Amplification Facilitators on Diagnostic PCR in the Presence of Blood, Feces, and Meat. Journal of Clinical Microbiology. 2000 Dec 1;38(12):4463–70.

90. Liu C, Geva E, Mauk M, Qiu X, Abrams WR, Malamud D, et al. An isothermal amplification reactor with an integrated isolation membrane for point-of-care detection of infectious diseases. The Analyst. 2011;136(10):2069.

91. Liu C, Mauk M, Gross R, Bushman FD, Edelstein PH, Collman RG, et al. Membrane-based, sedimentation-assisted plasma separator for point-of-care applications. Anal Chem. 2013 Nov 5;85(21):10463–70.

92. Park BH, Oh SJ, Jung JH, Choi G, Seo JH, Kim DH, et al. An integrated rotary microfluidic system with DNA extraction, loop-mediated isothermal amplification, and lateral flow strip based detection for point-of-care pathogen diagnostics. Biosensors and Bioelectronics. 2017 May;91:334–40.

93. Zhang L, Zhang Y, Wang C, Feng Q, Fan F, Zhang G, et al. Integrated Microcapillary for Sample-to-Answer Nucleic Acid Pretreatment, Amplification, and Detection. Anal Chem. 2014 Oct 21;86(20):10461–6.

94. M. Berry S, T. Alarid E, J. Beebe D. One-step purification of nucleic acid for gene expression analysis via Immiscible Filtration Assisted by Surface Tension (IFAST). Lab on a Chip. 2011;11(10):1747–53.

95. Casavant BP, Guckenberger DJ, Beebe DJ, Berry SM. Efficient Sample Preparation from Complex Biological Samples Using a Sliding Lid for Immobilized Droplet Extractions. Anal Chem. 2014 Jul 1;86(13):6355–62.

96. Shin DJ, Trick AY, Hsieh YH, Thomas DL, Wang TH. Sample-to-Answer Droplet Magnetofluidic Platform for Point-of-Care Hepatitis C Viral Load Quantitation. Scientific Reports [Internet]. 2018 Dec [cited 2019 Oct 31];8(1). Available from: http://www.nature.com/articles/s41598-018-28124-3

97. Berensmeier S. Magnetic particles for the separation and purification of nucleic acids. Appl Microbiol Biotechnol. 2006 Dec 1;73(3):495–504.

98. Govindarajan AV, Ramachandran S, Vigil GD, Yager P, Böhringer KF. A low cost point-of-care viscous sample preparation device for molecular diagnosis in the developing world; an example of microfluidic origami. Lab Chip. 2011 Dec 1;12(1):174–81.

99. Connelly JT, Rolland JP, Whitesides GM. "Paper Machine" for Molecular Diagnostics. Analytical Chemistry. 2015 Aug 4;87(15):7595–601.

100. Jangam SR, Agarwal AK, Sur K, Kelso DM. A point-of-care PCR test for HIV-1 detection in resource-limitedsettings. Biosensors and Bioelectronics. 2013 Apr 15;42:69–75.

101. Byrnes SA, Bishop JD, Lafleur L, Buser JR, Lutz B, Yager P. One-step purification and concentration of DNA in porous membranes for point-of-care applications. Lab Chip. 2015;15(12):2647–59.

102. Zou Y, Mason MG, Wang Y, Wee E, Turni C, Blackall PJ, et al. Nucleic acid purification from plants, animals and microbes in under 30 seconds. Misteli T, editor. PLOS Biology. 2017 Nov 21;15(11):e2003916.

103. Rogacs A, Qu Y, Santiago JG. Bacterial RNA Extraction and Purification from Whole Human Blood Using Isotachophoresis. Anal Chem. 2012 Jul 17;84(14):5858–63.

104. Persat A, Marshall LA, Santiago JG. Purification of Nucleic Acids from Whole Blood Using Isotachophoresis. Anal Chem. 2009 Nov 15;81(22):9507–11.

105. Bender AT, Borysiak MD, Levenson AM, Lillis L, Boyle DS, Posner JD. Semiquantitative Nucleic Acid Test with Simultaneous Isotachophoretic Extraction and Amplification. Anal Chem. 2018 Jun 19;90(12):7221–9.

106. Kondratova V, Serd'uk O, Shelepov V, Lichtenstein A. Concentration and isolation of DNA from biological fluids by agarose gel isotachophoresis. BioTechniques. 2005 Nov;39(5):695–9.

107. Kondratova VN, Botezatu IV, Shelepov VP, Lichtenstein AV. Isotachophoresis of nucleic acids in agarose gel rods. Biochemistry (Moscow). 2009 Nov;74(11):1285–8.

108. Kendall J, Crittenden ED. The Separation of Isotopes. Proc Natl Acad Sci U S A. 1923 Mar;9(3):75–8.

109. Bender AT, Sullivan BP, Zhang JY, Juergens DC, Lillis L, Boyle DS, et al. HIV detection from human serum with paper-based isotachophoretic RNA extraction and reverse transcription recombinase polymerase amplification. Analyst. 2021 May 4;146(9):2851–61.

110. Rogacs A, Marshall LA, Santiago JG. Purification of nucleic acids using isotachophoresis. Journal of Chromatography A. 2014 Mar 28;1335:105–20.

111. Bottenus D, Jubery TZ, Ouyang Y, Dong WJ, Dutta P, Ivory CF. 10000-fold concentration increase of the biomarker cardiac troponin I in a reducing union microfluidic chip using cationic isotachophoresis. Lab on a Chip. 2011;11(5):890–8.

112. Bercovici M, Lele SK, Santiago JG. Open source simulation tool for electrophoretic stacking, focusing, and separation. Journal of Chromatography A. 2009 Feb 6;1216(6):1008–18.

113. Jung B, Bharadwaj R, Santiago JG. On-Chip Millionfold Sample Stacking Using Transient Isotachophoresis. Analytical Chemistry. 2006 Apr;78(7):2319–27.

114. Rosenfeld T, Bercovici M. 1,000-fold sample focusing on paper-based microfluidic devices. Lab Chip [Internet]. 2014 Sep 5 [cited 2014 Sep 13]; Available from: http://pubs.rsc.org/en/content/articlehtml/2014/lc/c4lc00734d

115. Kohlrausch F. Uber Concentrations-Verschiebungen durch Elektrolyse im Inneren von Losungen und Losungsgemischen. Ann Phys Chem (Leipzig). 1897;62:209–39.

116. Everaerts FM, Beckers JL, Verheggen ThPEM. Isotachophoresis: Theory, Instrumentation and applications. Elsevier; 1976.

117. Bocek P, Deml M, Gebauer P, Dolnik V. Analytical Isotachophoresis. VCH, Weinheim; 1988.

118. Ramachandran A, Santiago JG. Isotachophoresis: Theory and Microfluidic Applications. Chem Rev. 2022 Aug 10;122(15):12904–76.

119. Ramachandran A, Huyke DA, Sharma E, Sahoo MK, Huang C, Banaei N, et al. Electric field-driven microfluidics for rapid CRISPR-based diagnostics and its application to detection of SARS-CoV-2. Proceedings of the National Academy of Sciences. 2020 Nov 24;117(47):29518–25.

120. Avaro AS, Sun Y, Jiang K, Bahga SS, Santiago JG. Web-Based Open-Source Tool for Isotachophoresis. Anal Chem. 2021 Nov 30;93(47):15768–74.

121. Bercovici M, Lele SK, Santiago JG. Compact adaptive-grid scheme for high numerical resolution simulations of isotachophoresis. Journal of Chromatography A. 2010 Jan 22;1217(4):588–99.

122. Bercovici M, Kaigala GV, Mach KE, Han CM, Liao JC, Santiago JG. Rapid detection of urinary tract infections using isotachophoresis and molecular beacons. Anal Chem. 2011 Jun 1;83(11):4110–7.

123. Borysiak MD, Kimura KW, Posner JD. NAIL: Nucleic Acid detection using Isotachophoresis and Loop-mediated isothermal amplification. Lab Chip. 2015 Apr 7;15(7):1697–707.

124. Moghadam BY, Connelly KT, Posner JD. Isotachophoretic preconcenetration on paper-based microfluidic devices. Anal Chem. 2014 Jun 17;86(12):5829–37.

125. Li X, Luo L, Crooks RM. Low-voltage paper isotachophoresis device for DNA focusing. Lab Chip. 2015 Sep 29;15(20):4090–8.

126. Eid C, G. Santiago J. Assay for Listeria monocytogenes cells in whole blood using isotachophoresis and recombinase polymerase amplification. Analyst. 2017;142(1):48–54.

127. Marshall LA, Wu LL, Babikian S, Bachman M, Santiago JG. Integrated Printed Circuit Board Device for Cell Lysis and Nucleic Acid Extraction. Anal Chem. 2012 Nov 6;84(21):9640–5.

128. Singleton J, Osborn JL, Lillis L, Hawkins K, Guelig D, Price W, et al. Electricity-Free Amplification and Detection for Molecular Point-of-Care Diagnosis of HIV-1. PLOS ONE. 2014 Nov 26;9(11):e113693.

129. Notomi T, Okayama H, Masubuchi H, Yonekawa T, Watanabe K, Amino N, et al. Loop-mediated isothermal amplification of DNA. Nucleic Acids Research. 2000;28(12):e63.

130. Piepenburg O, Williams CH, Armes NA, Stemple DL. Recombinase polymerase amplification [Internet]. US7666598B2, 2010 [cited 2021 May 18]. Available from: https://patents.google.com/patent/US7666598B2/en

131. Vincent M, Xu Y, Kong H. Helicase-dependent isothermal DNA amplification. EMBO reports. 2004 Aug;5(8):795–800.

132. Toley BJ, Covelli I, Belousov Y, Ramachandran S, Kline E, Scarr N, et al. Isothermal strand displacement amplification (iSDA): a rapid and sensitive method of nucleic acid amplification for point-of-care diagnosis. The Analyst. 2015;140(22):7540–9.

133. Mori Y, Nagamine K, Tomita N, Notomi T. Detection of Loop-Mediated Isothermal Amplification Reaction by Turbidity Derived from Magnesium Pyrophosphate Formation. Biochemical and Biophysical Research Communications. 2001 Nov;289(1):150–4.

134. Tanner NA, Zhang Y, Evans TC. Visual detection of isothermal nucleic acid amplification using pH-sensitive dyes. BioTechniques. 2015 Feb 1;58(2):59–68.

135. Curtis KA, Morrison D, Rudolph DL, Shankar A, Bloomfield LSP, Switzer WM, et al. A multiplexed RT-LAMP assay for detection of group M HIV-1 in plasma or whole blood. Journal of Virological Methods. 2018 May 1;255:91–7.

136. Dao Thi VL, Herbst K, Boerner K, Meurer M, Kremer LP, Kirrmaier D, et al. A colorimetric RT-LAMP assay and LAMP-sequencing for detecting SARS-CoV-2 RNA in clinical samples. Science Translational Medicine. 2020 Aug 12;12(556):eabc7075.

137. Kargar M, Askari A, Doosti A, Ghorbani-Dalini S. Loop-Mediated Isothermal Amplification Assay for Rapid Detection of Hepatitis C virus. Indian J Virol. 2012 Jun;23(1):18–23.

138. Cai T, Lou G, Yang J, Xu D, Meng Z. Development and evaluation of real-time loop-mediated isothermal amplification for hepatitis B virus DNA quantification: A new tool for HBV management. Journal of Clinical Virology. 2008 Apr 1;41(4):270–6.

139. Mayboroda O, Katakis I, O'Sullivan CK. Multiplexed isothermal nucleic acid amplification. Analytical Biochemistry. 2018 Mar 15;545:20–30.

140. Kim JY, Lee JL. Development of a multiplex real-time recombinase polymerase amplification (RPA) assay for rapid quantitative detection of Campylobacter coli and jejuni from eggs and chicken products. Food Control. 2017 Mar 1;73:1247–55.

141. Crannell Z, Castellanos-Gonzalez A, Nair G, Mejia R, White AC. Multiplexed Recombinase Polymerase Amplification Assay To Detect Intestinal Protozoa. Anal Chem. 2016 Feb 2;88(3):1610–6.

142. Lillis L, Siverson J, Lee A, Cantera J, Parker M, Piepenburg O, et al. Factors influencing Recombinase polymerase amplification (RPA) assay outcomes at point of care. Molecular and Cellular Probes. 2016 Apr;30(2):74–8.

143. Kellogg DE, Rybalkin I, Chen S, Mukhamedova N, Vlasik T, Siebert PD, et al. TaqStart Antibody: "hot start" PCR facilitated by a neutralizing monoclonal antibody directed against Taq DNA polymerase. Biotechniques. 1994 Jun 1;16(6):1134–7.

144. Lobato IM, O'Sullivan CK. Recombinase polymerase amplification: Basics, applications and recent advances. TrAC Trends in Analytical Chemistry. 2018 Jan;98:19–35.

145. Rohrman BA, Richards-Kortum RR. A paper and plastic device for performing recombinase polymerase amplification of HIV DNA. Lab Chip. 2012 Jul 31;12(17):3082–8.

146. Crannell ZA, Rohrman B, Richards-Kortum R. Equipment-Free Incubation of Recombinase Polymerase Amplification Reactions Using Body Heat. PLOS ONE. 2014 Nov 5;9(11):e112146.

147. Ahn H, Batule BS, Seok Y, Kim MG. Single-Step Recombinase Polymerase Amplification Assay Based on a Paper Chip for Simultaneous Detection of Multiple Foodborne Pathogens. Anal Chem. 2018 Sep 4;90(17):10211–6.

148. Li J, Macdonald J, von Stetten F. Review: a comprehensive summary of a decade development of the recombinase polymerase amplification. Analyst. 2018 Dec 17;144(1):31–67.

149. Mori Y, Kitao M, Tomita N, Notomi T. Real-time turbidimetry of LAMP reaction for quantifying template DNA. Journal of Biochemical and Biophysical Methods. 2004 May 31;59(2):145–57.

150. Roy S, Mohd-Naim NF, Safavieh M, Ahmed MU. Colorimetric Nucleic Acid Detection on Paper Microchip Using Loop Mediated Isothermal Amplification and Crystal Violet Dye. ACS Sens. 2017 Nov 22;2(11):1713–20.

151. Wahed AAE, Patel P, Faye O, Thaloengsok S, Heidenreich D, Matangkasombut P, et al. Recombinase Polymerase Amplification Assay for Rapid Diagnostics of Dengue Infection. PLOS ONE. 2015 Jun 15;10(6):e0129682.

152. Euler M, Wang Y, Nentwich O, Piepenburg O, Hufert FT, Weidmann M. Recombinase polymerase amplification assay for rapid detection of Rift Valley fever virus. Journal of Clinical Virology. 2012 Aug;54(4):308–12.

153. Abd El Wahed A, Patel P, Heidenreich D, Hufert FT, Weidmann M. Reverse Transcription Recombinase Polymerase Amplification Assay for the Detection of Middle East Respiratory Syndrome Coronavirus. PLoS Curr [Internet]. 2013 Dec 12 [cited 2021 May 20];5. Available from: https://www.ncbi.nlm.nih.gov/pmc/articles/PMC3871419/

154. Lillis L, Lehman DA, Siverson JB, Weis J, Cantera J, Parker M, et al. Cross-subtype detection of HIV-1 using reverse transcription and recombinase polymerase amplification. Journal of Virological Methods. 2016 Apr 1;230:28–35.

155. Crannell ZA, Rohrman B, Richards-Kortum R. Quantification of HIV-1 DNA Using Real-Time Recombinase Polymerase Amplification. Analytical Chemistry. 2014 Jun 17;86(12):5615–9.

156. Koczula KM, Gallotta A. Lateral flow assays. In: Essays in biochemistry. 2016.

157. Rohrman BA, Leautaud V, Molyneux E, Richards-Kortum RR. A Lateral Flow Assay for Quantitative Detection of Amplified HIV-1 RNA. PLOS ONE. 2012 Sep 21;7(9):e45611.

158. Mao X, Wang W, Du TE. Dry-reagent nucleic acid biosensor based on blue dye doped latex beads and lateral flow strip. Talanta. 2013 Sep 30;114:248–53.

159. Boehringer H, Rowley G, Pronovost AD. Quantitative lateral flow assays and devices [Internet]. US7491551 B2, 2009 [cited 2014 Nov 5]. Available from: http://www.google.com/patents/US7491551

160. Hull IT, Kline EC, Gulati GK, Kotnik JH, Panpradist N, Shah KG, et al. Isothermal Amplification with a Target-Mimicking Internal Control and Quantitative Lateral Flow Readout for Rapid HIV Viral Load Testing in Low-Resource Settings. Anal Chem [Internet]. 2021 Dec 17 [cited 2022 Jan 3]; Available from: https://doi.org/10.1021/acs.analchem.1c03960

161. Mancuso CP, Lu ZX, Qian J, Boswell SA, Springer M. A Semi-Quantitative Isothermal Diagnostic Assay Utilizing Competitive Amplification. Anal Chem. 2021 Jun 28;acs.analchem.1c01576.

162. Rosenbohm JM, Klapperich CM, Cabodi M. Tunable Duplex Semiquantitative Detection of Nucleic Acids with a Visual Lateral Flow Immunoassay Readout. Anal Chem. 2022 Feb 24;acs.analchem.1c05039.

163. Smit PW, Sollis KA, Fiscus S, Ford N, Vitoria M, Essajee S, et al. Systematic Review of the Use of Dried Blood Spots for Monitoring HIV Viral Load and for Early Infant Diagnosis. PLOS ONE. 2014 Mar 6;9(3):e86461.

164. Im SB, Kim SC, Shim JS. A smart pipette for equipment-free separation and delivery of plasma for on-site whole blood analysis. Anal Bioanal Chem. 2016 Feb;408(5):1391–7.

165. Shamsi A, Shamloo A, Mohammadaliha N, Hajghassem H, Mehrabadi JF, Bazzaz M. High throughput blood plasma separation using a passive PMMA microfluidic device. Microsyst Technol. 2016 Oct 1;22(10):2447–54.

166. Liu C, Liao SC, Song J, Mauk MG, Li X, Wu G, et al. A high-efficiency superhydrophobic plasma separator. Lab Chip. 2016 Jan 26;16(3):553–60.

167. Tsui NBY, Ng EKO, Lo YMD. Stability of endogenous and added RNA in blood specimens, serum, and plasma. Clin Chem. 2002 Oct;48(10):1647–53.

168. Spackman DH, Stein WH, Moore S, Zamoyska W the assistance of AM. The Disulfide Bonds of Ribonuclease. J Biol Chem. 1960 Mar 1;235(3):648–59.

169. Instructions for Use: COBAS® AmpliPrep/COBAS® TaqMan® HIV-1 Test, version 2.0 05328276001-07EN [Internet]. [cited 2022 Oct 6]. Available from: https://www.aphl.org/programs/infectious_disease/Documents/IFU-COBASAmpliPrepCOBASTaqMan_HIV-1_Testversion2.pdf

170. Aptima HIV-1 Quant Dx assay package insert. General Information. :42.

171. Daher RK, Stewart G, Boissinot M, Boudreau DK, Bergeron MG. Influence of sequence mismatches on the specificity of recombinase polymerase amplification technology. Molecular and Cellular Probes. 2015 Apr;29(2):116–21.

172. Boyle DS, Lehman DA, Lillis L, Peterson D, Singhal M, Armes N, et al. Rapid Detection of HIV-1 Proviral DNA for Early Infant Diagnosis Using Recombinase Polymerase Amplification. mBio. 2013 May 1;4(2):e00135-13.

173. Curtis KA, Rudolph DL, Owen SM. Rapid detection of HIV-1 by reverse-transcription, loop-mediated isothermal amplification (RT-LAMP). Journal of Virological Methods. 2008 Aug;151(2):264–70.

174. van Kooten XF, Truman-Rosentsvit M, Kaigala GV, Bercovici M. Focusing analytes from 50 μL into 500 pL: On-chip focusing from large sample volumes using isotachophoresis. Sci Rep [Internet]. 2017 Sep 5 [cited 2017 Nov 30];7. Available from: https://www.ncbi.nlm.nih.gov/pmc/articles/PMC5585209/

175. Marshall LA, Rogacs A, Meinhart CD, Santiago JG. An injection molded microchip for nucleic acid purification from 25 microliter samples using isotachophoresis. Journal of Chromatography A. 2014;1331:139–42.

176. Taglia V, Lederer M. Isotachophoresis on paper Part I. Investigation of general conditions and separation of some inorganic anions. Journal of Chromatography A. 1973 Mar 28;77(2):467–71.

177. Abelev G, Karamova E. Counterflow immunoisotachophoresis on cellulose acetate membranes. Analytical biochemistry. 1984;142(2):437–44.

178. Schaumburg F, Kler PA, Carrell CS, Berli CLA, Henry CS. USB powered microfluidic paper-based analytical devices. Electrophoresis. 2019 Nov 2;

179. Rosenfeld T, Bercovici M. Amplification-free detection of DNA in a paper-based microfluidic device using electroosmotically balanced isotachophoresis. Lab on a Chip. 2018;18(6):861–8.

180. Moghadam BY, Connelly KT, Posner JD. Two Orders of Magnitude Improvement in Detection Limit of Lateral Flow Assays Using Isotachophoresis. Anal Chem. 2015 Jan 20;87(2):1009–17.

181. Rogacs A, Marshall LA, Santiago JG. Purification of nucleic acids using isotachophoresis. Journal of Chromatography A. 2014 Mar 28;1335:105–20.

182. Ebeling W, Hennrich N, Klockow M, Metz H, Orth HD, Lang H. Proteinase K from Tritirachium album Limber. Eur J Biochem. 1974 Aug;47(1):91–7.

183. Hin S, Loskyll M, Klein V, Keller M, Strohmeier O, von Stetten F, et al. Membrane-based sample inlet for centrifugal microfluidic cartridges. Microelectronic Engineering. 2018 Feb 5;187–188:78–83.

184. Harboe M. A Method for Determination of Hemoglobin in Plasma by Near-Ultraviolet Spectrophotometry. Scandinavian Journal of Clinical and Laboratory Investigation. 1959 Jan;11(1):66–70.

185. Han V, Serrano K, Devine DV. A comparative study of common techniques used to measure haemolysis in stored red cell concentrates. Vox Sanguinis. 2010 Feb;98(2):116–23.

186. Liu C, Liao SC, Song J, Mauk MG, Li X, Wu G, et al. A high-efficiency superhydrophobic plasma separator. Lab Chip. 2016 Jan 26;16(3):553–60.

187. Homsy A, van der Wal PD, Doll W, Schaller R, Korsatko S, Ratzer M, et al. Development and validation of a low cost blood filtration element separating plasma from undiluted whole blood. Biomicrofluidics. 2012 Mar 15;6(1):012804-012804–9.

188. Lu Z, Rey E, Vemulapati S, Srinivasan B, Mehta S, Erickson D. High-yield paper-based quantitative blood separation system. Lab Chip. 2018 Dec 4;18(24):3865–71.

189. Fairbanks VF, Ziesmer SC, O'brien PC. Methods for measuring plasma hemoglobin in micromolar concentration compared. Clinical chemistry. 1992;38(1):132–40.

190. Marshall LA, Han CM, Santiago JG. Extraction of DNA from Malaria-Infected Erythrocytes Using Isotachophoresis. Anal Chem. 2011 Dec 15;83(24):9715–8.

191. Qu Y, Marshall LA, Santiago JG. Simultaneous Purification and Fractionation of Nucleic Acids and Proteins from Complex Samples Using Bidirectional Isotachophoresis. Anal Chem. 2014 Aug 5;86(15):7264–8.

192. Bajorath J, Saenger W, Pal GP. Autolysis and inhibition of proteinase K, a subtilisin-related serine proteinase isolated from the fungus Tritirachium album Limber. Biochim Biophys Acta. 1988 May 18;954(2):176–82.

193. Kersting S, Rausch V, Bier FF, von Nickisch-Rosenegk M. Rapid detection of Plasmodium falciparum with isothermal recombinase polymerase amplification and lateral flow analysis. Malaria journal. 2014;13(1):1.

194. Crannell ZA, Rohrman B, Richards-Kortum R. Quantification of HIV-1 DNA Using Real-Time Recombinase Polymerase Amplification. Anal Chem. 2014 Jun 17;86(12):5615–9.

195. Gregory JB, Litaker RW, Noble RT. Rapid One-Step Quantitative Reverse Transcriptase PCR Assay with Competitive Internal Positive Control for Detection of Enteroviruses in Environmental Samples. Appl Environ Microbiol. 2006 Jun 1;72(6):3960–7.

196. Wang S, Kool ET. Origins of the Large Differences in Stability of DNA and RNA Helixes: C-5 Methyl and 2'-Hydroxyl Effects. Biochemistry. 1995 Mar 28;34(12):4125–32.

197. Lepinske M. Tips for Working with RNA and Troubleshooting Downstream Applications. :4.

198. Phillips EA, Moehling TJ, Ejendal KFK, Hoilett OS, Byers KM, Basing LA, et al. Microfluidic rapid and autonomous analytical device (microRAAD) to detect HIV from whole blood samples. Lab Chip [Internet]. 2019 Sep 20 [cited 2019 Oct 5]; Available from: http://pubs.rsc.org/en/content/articlelanding/2019/lc/c9lc00506d

199. Lafleur LK, Bishop JD, Heiniger EK, Gallagher RP, Wheeler MD, Kauffman P, et al. A rapid, instrument-free, sample-to-result nucleic acid amplification test. Lab Chip. 2016;16(19):3777–87.

200. Abdul-Fattah AM, Kalonia DS, Pikal MJ. The challenge of drying method selection for protein pharmaceuticals: Product quality implications. Journal of Pharmaceutical Sciences. 2007;96(8):1886–916.

201. Wang W. Lyophilization and development of solid protein pharmaceuticals. International Journal of Pharmaceutics. 2000 Aug 1;203(1):1–60.

202. Tang X (Charlie), Pikal MJ. Design of Freeze-Drying Processes for Pharmaceuticals: Practical Advice. Pharm Res. 2004 Feb 1;21(2):191–200.

203. Bhambere D, Gaidhani K, Harwalkar M, Nirgude P. LYOPHILIZATION / FREEZE DRYING – A REVIEW. World Journal of Pharmaceutical Research. 2015 Jul 19;4:516–43.

204. Kasper JC, Friess W. The freezing step in lyophilization: Physico-chemical fundamentals, freezing methods and consequences on process performance and quality attributes of biopharmaceuticals. European Journal of Pharmaceutics and Biopharmaceutics. 2011 Jun 1;78(2):248–63.

205. Patel SM, Doen T, Pikal MJ. Determination of End Point of Primary Drying in Freeze-Drying Process Control. AAPS PharmSciTech. 2010 Jan 8;11(1):73–84.

206. Williams NA, Polli GP. The Lyophilization of Pharmaceuticals: A Literature Review. PDA Journal of Pharmaceutical Science and Technology. 1984 Mar 1;38(2):48–60.

207. Jameel F, Alexeenko A, Bhambhani A, Sacha G, Zhu T, Tchessalov S, et al. Recommended Best Practices for Lyophilization Validation 2021 Part II: Process Qualification and Continued Process Verification. AAPS PharmSciTech. 2021 Nov 8;22(8):266.

208. Saag MS, Holodniy M, Kuritzkes DR, O'Brien WA, Coombs R, Poscher ME, et al. HIV viral load markers in clinical practice. Nature Medicine. 1996 Jun;2(6):625–9.

209. Iloeje UH, Yang HI, Su J, Jen CL, You SL, Chen CJ, et al. Predicting cirrhosis risk based on the level of circulating hepatitis B viral load. Gastroenterology. 2006 Mar;130(3):678–86.

210. Pilcher CD, Joaki G, Hoffman IF, Martinson FE, Mapanje C, Stewart PW, et al. Amplified transmission of HIV-1: comparison of HIV-1 concentrations in semen and blood during acute and chronic infection. AIDS. 2007 Aug 20;21(13):1723–30.

211. Martinot-Peignoux M, Le Breton V, Fritsch S, Le guludec G, Labouret N, Keller F, et al. Assessment of Viral Loads in Patients with Chronic Hepatitis C with AMPLICOR HCV MONITOR Version 1.0, COBAS HCV MONITOR Version 2.0, and QUANTIPLEX HCV RNA Version 2.0 Assays. J Clin Microbiol. 2000 Jul;38(7):2722–5.

212. Hadinedoushan H, Salmanroghani H, Amirbaigy MK, Akhondi-Meybodi M. Hepatitis C Virus Genotypes and Association With Viral Load in Yazd, Central Province of Iran [Internet]. Vol. 14, Hepatitis Monthly. Kowsar; 2014 [cited 2020 May 4]. Available from: http://hepatmon.com/en/articles/15297.html

213. Attia S, Egger M, Müller M, Zwahlen M, Low N. Sexual transmission of HIV according to viral load and antiretroviral therapy: systematic review and meta-analysis: AIDS. 2009 Jul;23(11):1397–404.

214. LeMessurier J, Traversy G, Varsaneux O, Weekes M, Avey MT, Niragira O, et al. Risk of sexual transmission of human immunodeficiency virus with antiretroviral therapy, suppressed viral load and condom use: a systematic review. CMAJ. 2018 Nov 19;190(46):E1350–60.

215. Antiretroviral Therapy Cohort Collaboration. Survival of HIV-positive patients starting antiretroviral therapy between 1996 and 2013: a collaborative analysis of cohort studies. Lancet HIV. 2017;4(8):e349–56.

216. Hindson BJ, Ness KD, Masquelier DA, Belgrader P, Heredia NJ, Makarewicz AJ, et al. High-Throughput Droplet Digital PCR System for Absolute Quantitation of DNA Copy Number. Anal Chem. 2011 Nov 15;83(22):8604–10.

217. QX200 Droplet Digital PCR System [Internet]. [cited 2021 Nov 18]. Available from: https://www.bio-rad.com/sites/default/files/webroot/web/pdf/lsr/literature/Bulletin_6311.pdf

218. Kojabad AA, Farzanehpour M, Galeh HEG, Dorostkar R, Jafarpour A, Bolandian M, et al. Droplet digital PCR of viral DNA/RNA, current progress, challenges, and future perspectives. Journal of Medical Virology. 2021;93(7):4182–97.

219. Drain PK, Hyle EP, Noubary F, Freedberg KA, Wilson D, Bishai WR, et al. Diagnostic point-of-care tests in resource-limited settings. The Lancet Infectious Diseases. 2014 Mar;14(3):239–49.

220. Peeling RW, Mabey D. Point-of-care tests for diagnosing infections in the developing world. Clinical Microbiology and Infection. 2010 Aug;16(8):1062–9.

221. Shen F, Davydova EK, Du W, Kreutz JE, Piepenburg O, Ismagilov RF. Digital Isothermal Quantification of Nucleic Acids via Simultaneous Chemical Initiation of Recombinase Polymerase Amplification Reactions on SlipChip. Anal Chem. 2011 May 1;83(9):3533–40.

222. Lin X, Huang X, Urmann K, Xie X, Hoffmann MR. Digital Loop-Mediated Isothermal Amplification on a Commercial Membrane. ACS Sens. 2019 Jan 25;4(1):242–9.

223. Li Z, Liu Y, Wei Q, Liu Y, Liu W, Zhang X, et al. Picoliter Well Array Chip-Based Digital Recombinase Polymerase Amplification for Absolute Quantification of Nucleic Acids. PLOS ONE. 2016 Apr 13;11(4):e0153359.

224. Mazutis L, Araghi AF, Miller OJ, Baret JC, Frenz L, Janoshazi A, et al. Droplet-Based Microfluidic Systems for High-Throughput Single DNA Molecule Isothermal Amplification and Analysis. Anal Chem. 2009 Jun 15;81(12):4813–21.

225. Gansen A, Herrick AM, Dimov IK, Lee LP, Chiu DT. Digital LAMP in a sample self-digitization (SD) chip. Lab Chip. 2012 May 22;12(12):2247–54.

226. Seok Y, Joung HA, Byun JY, Jeon HS, Shin SJ, Kim S, et al. A Paper-Based Device for Performing Loop-Mediated Isothermal Amplification with Real-Time Simultaneous Detection of Multiple DNA Targets. Theranostics. 2017 Jun 1;7(8):2220–30.

227. Magro L, Jacquelin B, Escadafal C, Garneret P, Kwasiborski A, Manuguerra JC, et al. Paper-based RNA detection and multiplexed analysis for Ebola virus diagnostics. Sci Rep. 2017 May 2;7:1347.

228. Lee D, Shin Y, Chung S, Hwang KS, Yoon DS, Lee JH. Simple and Highly Sensitive Molecular Diagnosis of Zika Virus by Lateral Flow Assays. Anal Chem. 2016 Dec 20;88(24):12272–8.

229. Choi JR, Hu J, Tang R, Gong Y, Feng S, Ren H, et al. An integrated paper-based sample-to-answer biosensor for nucleic acid testing at the point of care. Lab Chip. 2016 Jan 26;16(3):611–21.

230. Rodriguez NM, Linnes JC, Fan A, Ellenson CK, Pollock NR, Klapperich CM. Paper-Based RNA Extraction, *in Situ* Isothermal Amplification, and Lateral Flow Detection for Low-Cost, Rapid Diagnosis of Influenza A (H1N1) from Clinical Specimens. Analytical Chemistry. 2015 Aug 4;87(15):7872–9.

231. Seok Y, Batule BS, Kim MG. Lab-on-paper for all-in-one molecular diagnostics (LAMDA) of zika, dengue, and chikungunya virus from human serum. Biosensors and Bioelectronics. 2020 Oct 1;165:112400.

232. Liu M, Zhao Y, Monshat H, Tang Z, Wu Z, Zhang Q, et al. An IoT-enabled paper sensor platform for real-time analysis of isothermal nucleic acid amplification tests. Biosensors and Bioelectronics. 2020 Dec 1;169:112651.

233. Sanchez AM, DeMarco CT, Hora B, Keinonen S, Chen Y, Brinkley C, et al. Development of a contemporary globally diverse HIV viral panel by the EQAPOL program. J Immunol Methods. 2014 Jul;409:117–30.

234. Rouet F, Chaix ML, Nerrienet E, Ngo-Giang-Huong N, Plantier JC, Burgard M, et al. Impact of HIV-1 Genetic Diversity on Plasma HIV-1 RNA Quantification: Usefulness of the Agence Nationale de Recherches sur le SIDA Second-Generation Long Terminal Repeat-Based Real-Time Reverse Transcriptase Polymerase Chain Reaction Test. JAIDS Journal of Acquired Immune Deficiency Syndromes. 2007 Aug 1;45(4):380–8.

235. Schindelin J, Arganda-Carreras I, Frise E, Kaynig V, Longair M, Pietzsch T, et al. Fiji: an open-source platform for biological-image analysis. Nature Methods. 2012 Jul;9(7):676–82.

236. Bradski G. The OpenCV Library. Dr Dobb's Journal of Software Tools. 2000;

237. Kaur N, Michael JS, Toley BJ. A modular paper-and-plastic device for tuberculosis nucleic acid amplification testing in limited-resource settings. Scientific Reports. 2019 Oct 25;9(1):15367.

238. Xu G, Nolder D, Reboud J, Oguike MC, van Schalkwyk DA, Sutherland CJ, et al. Paper-Origami-Based Multiplexed Malaria Diagnostics from Whole Blood. Angewandte Chemie. 2016;128(49):15476–9.

239. Piepenburg O, Williams CH, Stemple DL, Armes NA. DNA Detection Using Recombination Proteins. PLOS Biology. 2006 Jun 13;4(7):e204.

240. Zhu Y, Wu X, Gu A, Dobelle L, Cid CA, Li J, et al. Membrane-Based In-Gel Loop-Mediated Isothermal Amplification (mgLAMP) System for SARS-CoV-2 Quantification in Environmental Waters. Environ Sci Technol. 2021 Dec 30;acs.est.1c04623.

241. Mitra RD, Church GM. In situ localized amplification and contact replication of many individual DNA molecules. Nucleic Acids Research. 1999 Dec 1;27(24):e34–9.

242. Lutz B, Liang T, Fu E, Ramachandran S, Kauffman P, Yager P. Dissolvable fluidic time delays for programming multi-step assays in instrument-free paper diagnostics. Lab Chip. 2013 Jun 18;13(14):2840–7.

243. Krishnan SR, Bal J, Putnam SA. A simple analytic model for predicting the wicking velocity in micropillar arrays. Sci Rep. 2019 Dec 27;9(1):20074.

244. Linnes JC, Rodriguez NM, Liu L, Klapperich CM. Polyethersulfone improves isothermal nucleic acid amplification compared to current paper-based diagnostics. Biomedical Microdevices [Internet]. 2016 Apr [cited 2017 Oct 18];18(2). Available from: http://link.springer.com/10.1007/s10544-016-0057-z

245. Burd EM. Validation of Laboratory-Developed Molecular Assays for Infectious Diseases. Clin Microbiol Rev. 2010 Jul;23(3):550–76.

246. Borysiak MD, Kimura KW, Posner JD. NAIL: Nucleic Acid detection using Isotachophoresis and Loop-mediated isothermal amplification. Lab Chip. 2015 Mar 17;15(7):1697–707.

247. Higgins M, Stringer OW, Ward D, Andrews JM, Forrest MS, Campino S, et al. Characterizing the Impact of Primer-Template Mismatches on Recombinase Polymerase Amplification. The Journal of Molecular Diagnostics. 2022 Nov 1;24(11):1207–16.

248. Song J, Mauk MG, Hackett BA, Cherry S, Bau HH, Liu C. Instrument-Free Point-of-Care Molecular Detection of Zika Virus. Analytical Chemistry. 2016 Jul 19;88(14):7289–94.

249. Damhorst GL, Duarte-Guevara C, Chen W, Ghonge T, Cunningham BT, Bashir R. Smartphone-Imaged HIV-1 Reverse-Transcription Loop-Mediated Isothermal Amplification (RT-LAMP) on a Chip from Whole Blood. Engineering (Beijing). 2015 Sep;1(3):324–35.

250. Shah KG, Kumar S, Singh V, Hansen L, Heiniger E, Bishop JD, et al. Two-Fluorophore Mobile Phone Imaging of Biplexed Real-Time NAATs Overcomes Optical Artifacts in Highly Scattering Porous Media. Anal Chem. 2020;7.

251. Lee D, Chou WP, Yeh SH, Chen PJ, Chen PH. DNA detection using commercial mobile phones. Biosensors and Bioelectronics. 2011 Jul 15;26(11):4349–54.

252. Ning B, Yu T, Zhang S, Huang Z, Tian D, Lin Z, et al. A smartphone-read ultrasensitive and quantitative saliva test for COVID-19. Science Advances. 7(2):eabe3703.

253. Xiong D, Dai W, Gong J, Li G, Liu N, Wu W, et al. Rapid detection of SARS-CoV-2 with CRISPR-Cas12a. PLOS Biology. 2020 Dec 15;18(12):e3000978.

254. Glynn SA, Wright DJ, Kleinman SH, Hirschkorn D, Tu Y, Heldebrant C, et al. Dynamics of viremia in early hepatitis C virus infection. Transfusion. 2005 Jun;45(6):994–1002.

255. Tiollais P, Pourcel C, Dejean A. The hepatitis B virus. Nature. 1985 Oct;317(6037):489–95.

256. Wilkins T, Zimmerman D, Schade RR. Hepatitis B: Diagnosis and Treatment. afp. 2010 Apr 15;81(8):965–72.

257. D'Souza R, Foster GR. Diagnosis and treatment of chronic hepatitis B. J R Soc Med. 2004 Jul;97(7):318–21.

258. Keating GM, Noble S. Recombinant Hepatitis B Vaccine (Engerix-B®). Drugs. 2003 May 1;63(10):1021–51.

259. World Health Organization, Global Hepatitis Programme. WHO guidelines on hepatitis B and C testing. [Internet]. 2017 [cited 2018 Nov 15]. Available from: http://apps.who.int/iris/bitstream/10665/254621/1/9789241549981-eng.pdf

260. Echevarría JM, Avellón A. Hepatitis B virus genetic diversity. Journal of Medical Virology. 2006 Jan 1;78(S1):S36–42.

261. Global progress report on HIV, viral hepatitis and sexually transmitted infections, 2021 [Internet]. [cited 2022 Oct 14]. Available from: https://www.who.int/publications-detail-redirect/9789240027077

262. Schillie S, Wester C, Osborne M, Wesolowski L, Ryerson AB. CDC Recommendations for Hepatitis C Screening Among Adults — United States, 2020. MMWR Recomm Rep. 2020 Apr 10;69(2):1–17.

263. Tang H, Grisé H. Cellular and molecular biology of HCV infection and hepatitis. Clinical Science. 2009 Jun 15;117(2):49–65.

264. Barber MJ, Gotham D, Khwairakpam G, Hill A. Price of a hepatitis C cure: Cost of production and current prices for direct-acting antivirals in 50 countries. Journal of Virus Eradication. 2020 Sep 1;6(3):100001.

265. Fierer DS, Wyles DL. Re-treatment of Hepatitis C Infection After Multiple Failures of Direct-Acting Antiviral Therapy. Open Forum Infect Dis. 2020 Mar 16;7(4):ofaa095.

266. Messina JP, Humphreys I, Flaxman A, Brown A, Cooke GS, Pybus OG, et al. Global distribution and prevalence of hepatitis C virus genotypes. Hepatology. 2015;61(1):77–87.

267. Guidelines for the Care and Treatment of Persons Diagnosed with Chronic Hepatitis C Virus Infection [Internet]. Guidelines for the Care and Treatment of Persons Diagnosed with Chronic Hepatitis C Virus Infection [Internet]. World Health Organization; 2018 [cited 2022 Dec 13]. Available from: https://www.ncbi.nlm.nih.gov/books/NBK531729/

268. Chevaliez S, Pawlotsky JM. Hepatitis C Virus Serologic and Virologic Tests and Clinical Diagnosis of HCV-Related Liver Disease. Int J Med Sci. 2006 Apr 1;3(2):35–40.

269. Gao F, Talbot EA, Loring CH, Power JJ, Dionne-Odom J, Alroy-Preis S, et al. Performance of the OraQuick HCV Rapid Antibody Test for Screening Exposed Patients in a Hepatitis C Outbreak Investigation. J Clin Microbiol. 2014 Jul;52(7):2650–2.

270. Ivanova Reipold E, Easterbrook P, Trianni A, Panneer N, Krakower D, Ongarello S, et al. Optimising diagnosis of viraemic hepatitis C infection: the development of a target product profile. BMC Infectious Diseases [Internet]. 2017 Nov [cited 2018 Nov 15];17(S1). Available from: http://bmcinfectdis.biomedcentral.com/articles/10.1186/s12879-017-2770-5

271. High-priority target product profile for hepatitis C diagnosis in decentralized settings: Report of a consensus meeting [Internet]. [cited 2022 Oct 14]. Available from: https://www.finddx.org/wp-content/uploads/2019/03/HCV-TPP-Report_FIND-2015.pdf

272. Phillips EA, Shen R, Zhao S, Linnes JC. Thermally actuated wax valves for paper-fluidic diagnostics. Lab Chip. 2016 Oct 18;16(21):4230–6.

273. J. Toley B, A. Wang J, Gupta M, R. Buser J, K. Lafleur L, R. Lutz B, et al. A versatile valving toolkit for automating fluidic operations in paper microfluidic devices. Lab on a Chip. 2015;15(6):1432–44.

274. NIH mobilizes national innovation initiative for COVID-19 diagnostics [Internet]. National Institutes of Health (NIH). 2020 [cited 2022 Oct 13]. Available from: https://www.nih.gov/news-events/news-releases/nih-mobilizes-national-innovation-initiative-covid-19-diagnostics